

Supporting Information

Ultra-thin films of amphiphilic lanthanide complexes: multi-colour emission from molecular monolayers

Alex T. O’Neil,^a John A. Harrison,^a and Jonathan A. Kitchen*^a

a. Chemistry, School of Natural and Computational Sciences, Massey, Auckland, NZ.

Table of Contents

Experimental	S3-S5
Ligand characterisation	S6-S15
Ligand crystal structure	S16
Lanthanide complex characterisation	S17-S25
Photophysical self-assembly titrations & non-linear regression analysis	S26-S27
Langmuir Blodgett	S28-S31
Lanthanide complex bulk and film characterisation	S32-S63
References	S64

General Experimental Details

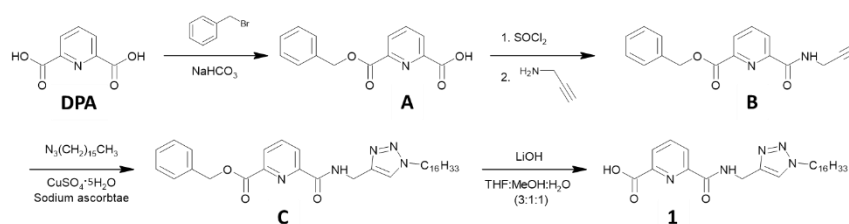
All reagents, solvents and starting materials were purchased from Sigma–Aldrich. Deuterated solvents [CDCl₃, CD₃OD] used for NMR analyses were purchased from Sigma-Aldrich. NMR spectra were recorded using a Bruker Ultrashield 300, with chemical shifts recorded in parts per million (ppm) downfield from the standard. UV/Vis was recorded on a Shimadzu UV-1800 or Shimadzu UV-2700 (for quantum measurements) using MeCN, CHCl₃ and MeOH solvents in a 3 mL quartz cuvette with a 1 cm path length. Mass spectroscopy of ligands was carried out in HPLC grade solvents, on a Shimadzu LCMS-2020 for ligands and a ThermoFisher QExactive Focus coupled to an Ultimate™ 3000 RSLC or a Bruker Daltonics MicrOTOF™ Spectrometer. Fourier-transform infrared spectroscopy (FT-IR) of solids were recorded on a Bruker Alpha platinum-ATR and FT-IR of LB films spectra were recorded on a ThermoFisher Scientific Nicolet iS50. Steady-state fluorescence measurements were recorded on a Shimadzu RF-6000 Spectrofluorophotometer, with MeCN, CHCl₃ and MeOH solvents in a capped 3.5 mL quartz cuvette with a 1 cm path length. Time-resolved measurements were carried out using an Agilent Technologies Cary Eclipse spectrophotometer. Refractive index measurements were carried out on a Bellingham + Stanley Abbe 5 optical refractometer. Melting points were obtained on an Electrothermal IA9000 Series Melting Point Apparatus. Langmuir-Blodgett measurements and film formation were measured on a Kibron G2 Microtrough. Single crystal X-ray diffraction data were collected at 123 K on a Bruker D8 Venture equipped with an I μ S DIAMOND microfocus with a Cu-K α ($\lambda = 1.54178$) X-ray source with a PHOTON III detector.¹ Unit cell parameters were refined against all data and an empirical absorption correction applied in APEX3. Structures were solved by direct methods using SHELXS-2013² and refined on Fo² by SHELXL-2013² using Olex2.³ H atoms were positioned geometrically and refined using a riding model. NH and OH were positioned manually and all non-H atoms were refined as anisotropic. The XPS data were collected on a Kratos Axis UltraDLD equipped with a hemispherical electron energy analyser. Spectra were excited using monochromatic Al K α X-rays (1486.69 eV) with the X-ray source operating at 150W. This instrument illuminates a large area on the surface and then using hybrid magnetic and electrostatic lenses collects photoelectrons from a desired location on the surface. In this case the analysis area was a 300 by 700 micron spot (=hybrid/slot). The measurements were carried out in a normal emission geometry. A charge neutralisation system was used to alleviate sample charge buildup, resulting in a shift of approximately 3eV to lower binding energy. Survey scans were collected with a 160eV pass energy, whilst core level scans were collected with a pass energy of 20eV. The analysis chamber was at pressures in the 10⁻⁹ torr range throughout the data collection. Data analysis was performed using CasaXPS (www.casaXPS.com). The binding energy scale was corrected for the neutraliser shift by using the

C 1s signal from saturated hydrocarbon at 285.0 eV as an internal standard. Synthesis of alkylazide was carried out according to reference 4, characterisation data matched that which was reported.

Safety & hazards

Sodium azide is very toxic and must be handled with appropriate precautions. Organic azides are potentially explosive and care must be taken during handling and preparation and they must be stored appropriately. This specific case of 1-azidohexadecane has an oxygen (O), carbon (C) and nitrogen (N) ratio of 5.3 which is much higher than the recommended safe $(C + O)/N > 3$ ratio. Any potential copper azides formed in solution are potentially explosive when dry, so they are removed during the washing stage with EDTA/NaOH (1 M).⁵

Full Ligand Synthesis



Scheme 1 - Synthetic pathway for synthesis of **1** starting from commercially available DPA.

Ligand **1** was synthesised in a six-step process (Scheme 1) from commercially available 2,6-pyridine dicarboxylic acid (dpa) and 1-bromohexadecane. Initially dpa was combined with NaHCO₃ in dry DMF and the solution was heated to 60 °C for 30 minutes under a nitrogen atmosphere. Benzyl bromide was then added, and the solution was further heated for 24 hours, where the off-white solution turned pale yellow. Acid-base workup yielded an off-white solid of mono ester protected **A** (72 %). **A** was then dissolved in dry DCM under a nitrogen atmosphere and thionyl chloride was then added to the solution, which was left to reflux for 5 hours. Solvent was removed by a stream of nitrogen yielding a pale-yellow solid containing the acid chloride. This was immediately dissolved in dry DCM and added dropwise to a cooled solution of propargyl amine and triethylamine in dry DCM. The resulting solution turned from a lime green to a dark burgundy and was left to stir for 24 hours. Acid-base workup resulted in a dark brown oil which eventually solidified to a light brown solid, containing mono-alkyne **B** (72 %). Intermediate **B** then underwent CuAAC reaction with 1-azidohexadecane. 1-Azidohexadecane was obtained by refluxing 1-bromohexadecane with NaN₃ in dry DMF for 24 hours and then extracted as a clear oil (88 %). **B** was combined with sodium ascorbate and the CuSO₄·5H₂O catalyst in DMF:H₂O (4:1) solution. This was then heated to 60 °C until the solid had dissolved. 1-Azidohexadecane was then added dropwise to the green solution, which over the course of 24 hours turned yellow, then to a light grey with visible solid precipitation. The solid precipitate was filtered yielding a light green solid which was then washed with 1 M NaOH/EDTA solution yielding an off-white solid **C** (75 %). **C** was then deprotected by stirring in a 3:1:1 solution of THF:MeOH:H₂O with LiOH, in which the solid slowly dissolved and the clear solution turned yellow. The solvent was removed until a yellow residue remained, 1 M HCl was added causing an off-white precipitate to form. This was filtered and washed with H₂O, yielding ligand **1** as an off-white solid (89 %). **1** was fully characterised, confirming the successful synthesis of **1**.

Ligand characterisation

¹H-NMR spectra of **1** shows the disappearances of the benzyl peaks 7.41 ppm (m) and ester link CH₂ 5.34 ppm (s), while maintaining the presence of the triazole singlet proton peak, although shifted downfield to 7.73 (s) compared to **C** (All other proton peaks are found in the expected locations). ¹³C-NMR also observed the disappearance of benzyl protons at 128.8-128.6 ppm, CH₂ ester link at 67.5 ppm and a downfield shift of the deprotected carbonyl 164.3 downfield to 166.2, indicating the shift from ester to carboxylic acid. LRMS further confirmed the successful synthesis of **1**, observing a peak at $m/z = 472.25$ [**1**+H], calculated for C₃₃H₄₈N₅O₃⁺, 472.33.

Experimental

Synthesis of 6-((benzyloxy)carbonyl)pyridine-2-carboxylic acid (A)

2,6-pyridinedicarboxylic acid (2.00 g, 11.97 mmol) was combined with dried NaHCO₃ (1.00 g, 11.90 mmol) in 100 mL of dried DMF. The solution was heated to 60 °C for 30 minutes under a N₂ atmosphere resulting in a cloudy, off-white solution. Benzyl bromide (1.4 mL, 12.61 mmol) was added to the solution and left stirring for 48 hours at 60 °C. The resulting pale-yellow solution was then diluted with 100 mL of H₂O and neutralised with a saturated solution of NaHCO₃ (pH ≈ 7). The diester side product was extracted by diethyl ether and then the aqueous layer was acidified to a pH ≈ 1, **A** was then extracted into ethyl acetate. The organic layer was dried with MgSO₄, filtered and solvent was removed by reduced pressure. This resulted in an off-white cloudy slurry which was dissolved in DCM and the organic layer was washed with H₂O and brine removing residue DMF. The organic layer was then dried with MgSO₄, filtered and then solvent was removed under reduced pressure resulting in an off-white solid (1.683 g, 6.54 mmol, 55 %). Melting point = 134.9 °C. LRMS *m/z* = 258.00 [**A** + H]⁺ (calc. for C₁₄H₁₂NO₄⁺, 258.25). ¹H NMR (300 MHz, CDCl₃, ppm), δ = 8.40 (dd, *J* = 10.0, 8.0 Hz, 2H, meta pyridine-H), 8.12 (t, *J* = 8.0 Hz, 1H, para pyridine-H), 7.44 (m, 5H, benzene), 5.47 (s, 2H, CH₂); ¹³C NMR (75 MHz, CDCl₃, ppm): δ = 163.6 (C=O), 163.5 (C=O), 146.9 (CN), 146.6 (CN), 139.9 (CH), 135.2 (C), 129.1-128.8 (3x CH), 127.0 (CH), 68.25 (CH₂). FTIR (ATR, cm⁻¹) 2879 -2615 (OH), 1737 (COOR), 1694 (COOH), 1575, 1499, 1467, 1416, 1376, 1329, 1288, 1242, 1151, 1083, 1006, 994, 955, 939, 855 796, 753, 728, 710, 690, 648, 554, 510, 457, 421.

Synthesis of N₂-(prop-2-ynyl)-O₆-((benzyloxy)carbonyl)pyridine-2-carboxamide-6-carboxylate (B)

A (2.00 g, 7.78 mmol) was dissolved in 20 mL of freshly dried DCM and placed under a nitrogen atmosphere. Thionyl chloride (1.5 mL, 20.56 mmol) was added to the clear solution, causing an off-white precipitate to form. The solution was then heated to 80 °C for 5 hours. The resulting yellow solution, solvent and excess thionyl chloride was removed by a stream of nitrogen resulting in a pale yellow solid (acid chloride product). Once the solid was dry it was then dissolved in 10 mL freshly dried DCM. A separate solution of propargyl amine (0.996 mL, 15.55 mmol) and triethylamine (5.746 mL, 41.23 mmol) in 30 mL of freshly dried DCM was cooled in an ice bath. While stirring the acid chloride solution was added dropwise to the (lime green) propargyl amine containing solution turning the solution a dark red with smoke extruding from the round bottom flask. The solution was left to stir overnight for 24 hours at room temperature. The organic layer was washed with 1 M HCl, saturated NaHCO₃, then dried with MgSO₄, filtered and then solvent was removed by reduced pressure resulting in a brown oil which solidified into a light brown solid (1.640 g, 5.57 mmol, 72 %). Melting point = 75.4 °C. LRMS *m/z* = 294.95 [**B** + H]⁺ (calc. for C₁₇H₁₅N₂O₃⁺, 295.11), *m/z* = 316.95 [**B** + H]⁺ (calc. for C₁₇H₁₅N₂O₃⁺, 317.19). ¹H NMR (300 MHz, CDCl₃, ppm), δ = 8.39 (dd, *J* = 7.79, 1.14 Hz, 1H, meta pyridine-H), 8.30 (m, 1H, NH), 8.25 (dd, *J* = 8.0, 1.0 Hz, 1H, meta pyridine-H), 8.00 (t, *J* = 8.0 Hz, 1H, para pyridine-H), 7.44 (m, 5H, benzene), 5.45 (s, 2H, CH₂-O), 4.28 (dd, *J* = 6.0, 2.5 Hz, 2H, CH₂-NH), 2.26 (t, *J* = 2.5 Hz, 1H, CH); ¹³C NMR (75 MHz, CDCl₃, ppm): δ = 164.3 (C=O), 163.4 (C=O), 149.9 (CN), 146.8 (CN), 138.8, 135.5 (C), 128.9, 128.8-128.6 (3x CH), 127.8, 125.7, 79.4, 71.8, 67.9 (CH₂), 29.3 (CH₂). FTIR (ATR, cm⁻¹) 3384, 3212, 1737 (COOR), 1682 (CONH), 1514, 1446, 1418, 1373, 1286, 1256, 1228, 1161, 1082, 1050, 1012, 998, 983, 912, 901,842, 747, 729, 692, 647, 617, 582, 546, 455, 421.

Synthesis of N₂-((1-(hexadecane)-1H-1,2,3-triazol-4-yl)methyl)-O₆-((benzyloxy)carbonyl)pyridine-2-carboxamide-6-carboxylate (C)

B (0.354 g, 1.20 mmol) was combined with sodium ascorbate (0.217 g, 1.10 mmol) and CuSO₄·5H₂O (0.137 g, 0.55 mmol) in 20 mL of DMF:H₂O (4:1). 1-Azidohexadecane (0.373 g, 1.09 mmol) was added to 4 mL DMF:H₂O (4:1) and then added dropwise to the alkyne solution, which was left to stir at 60 °C for 24 hours. The brown solution formed a grey precipitate overnight, which was filtered and dissolved in DCM. The organic layer was then washed with 1 M EDTA/NaOH solution, H₂O and brine before being dried by MgSO₄, filtered and then solvent was removed by reduced pressure resulting in white solid (0.507 g, 0.89 mmol, 75 %). If required, product was purified by silica column with a 8:2 hexane:MeOH gradient. Melting point = 128.4 °C. LRMS *m/z* = 562.35 [**C** + H]⁺ (calc. for C₃₃H₄₈N₅O₃⁺, 562.38), *m/z* = 584.25 [**C** + Na]⁺ (calc. for C₃₃H₄₇N₅O₃Na⁺, 584.36), *m/z* = 600.25 [**C** + K]⁺ (calc. for C₃₃H₄₇N₅O₃K⁺, 600.20). ¹H NMR (300 MHz, CDCl₃), δ = 8.62 (t, 1H, NH), 8.36 (dd, *J* = 8.0, 1.0 Hz, 1H, meta pyridine-H), 8.22 (dd, *J* = 8.0, 1.0 Hz, 1H, meta pyridine-H), 7.98 (t, *J* = 8.0 Hz, 1H, para pyridine-H), 7.56 (s, 1H, triazole), 7.41 (m, 5H, benzene), 5.43 (s, 2H, CH₂-O), 4.75 (d, *J* = 6.0 Hz, 2H, CH₂-NH), 4.29 (t, *J* = 7.0 Hz, 2H, CH₂-N), 1.86 (m, 2H, CH₂-CH₂N), 1.27 (m, 26H, 13 x CH₂), 0.86 (t, *J* = 7.0 Hz, 3H, CH₃); ¹³C NMR (75 MHz, CDCl₃, ppm): δ = 164.3 (CO), 163.7 (CO), 150.0 (CN), 146.8 (CN), 144.7 (C), 138.6, 135.4 (C), 128.8-128.7 (3x CH), 127.6, 125.5, 122.3, 67.8 (CH₂), 50.5 (CH₂), 35.2 (CH₂), 32.0 (CH₂), 30.4 (CH₂), 29.8-6 (CH₂ x 10), 29.5 (CH₂), 26.6 (CH₂), 22.8 (CH₂), 14.2. FTIR (ATR, cm⁻¹) 3263, 3065, 2955 (CH), 2915 (CH), 2848 (CH), 1740 (COOR), 1635 (CONH), 1587, 1537, 1499, 1470, 1456, 1422, 1373, 1344, 1287, 1248, 1220, 1153, 1089, 1049, 1029, 1009, 992, 971, 849, 830, 775, 756, 728, 717, 692, 665, 641, 588, 517, 458, 421.

Synthesis of N₂-(1-(hexadecane)-1H-1,2,3-triazol-4-yl)methyl)-2-carboxamide-6-carboxylic acid (**1**)

1 (1.116 g, 1.98 mmol) was combined with LiOH (0.190 g, 7.95 mmol) in 30 mL of THF:MeOH:H₂O (3:1:1) and was stirred at room temperature under a nitrogen atmosphere overnight. The solid slowly dissolved resulting in a clear yellow solution over the course of 24 hours. 50 mL of H₂O was added to the solution causing a white precipitate to form, which was filtered and washed with H₂O, yielding an off-white solid (0.834 g, 89 %). Melting point = 94.3 °C; LRMS m/z = 472.25 [**1** + H]⁺ (calc. for C₂₆H₄₂N₅O₃⁺, 472.33), m/z = 494.20 [**1** + Na]⁺ (calc. for C₂₆H₄₁N₅O₃Na⁺, 494.31) and m/z = 510.20 [**1** + K]⁺ (calc. for C₂₆H₄₁N₅O₃K⁺, 510.28). ¹H NMR (300 MHz, CDCl₃, ppm), δ = 9.83 (t, 1H, NH), 8.38 (t, J = 7.0 Hz, 2H, meta-pyridine-H), 8.04 (t, J = 8.0 Hz, 1H, para-pyridine-H), 7.73 (s, 1H, triazole), 4.85 (d, J = 5.0 Hz, 2H, CH₂-NH), 4.32 (t, J = 7.0 Hz, 2H, CH₂-N), 1.87 (m, 2H, CH₂-CH₂N), 1.23 (m, 26H, 13 x CH₂), 0.87 (t, J = 7.0, 3H, CH₃); ¹³C NMR (75 MHz, CDCl₃, ppm): δ = 166.2 (CO), 163.9 (CO), 149.9 (CN), 146.7 (CN), 139.0, 127.4, 125.8, 123.2, 51.0 (CH₂), 34.0 (CH₂), 32.0 (CH₂), 30.2 (CH₂), 29.8-5(11x CH₂), 26.6 (CH₂), 22.8 (CH₂), 14.2. FTIR (ATR, cm⁻¹) 3345, 2915 (CH), 2849 (CH), 1745 (COOH), 1669 (CONH), 1536, 1471, 1453, 1430, 1337, 1235, 1174, 1114, 1073, 1056, 999, 879, 849, 804, 785, 739, 716, 699, 659, 568, 520, 428.

Lanthanide complexation

General procedure for complexation of ligand **1** with trivalent lanthanide ions

Ligand **1** was combined with 0.33 equivalents of selected trivalent lanthanide ion (with either triflate or chloride anion) and 1 equivalent of triethylamine in 5 mL of DCM:MeOH:MeCN 1:1:0.5 ratio. The solution was refluxed under microwave irradiation for 30 minutes and then subjected to vapour diffusion of diethyl ether at room temperature until precipitation occurred and was then filtered.

Synthesis of Eu(**1**)₃

1 (0.0336 g, 0.071 mmol) was combined with Eu(Cl)₃·6H₂O (0.0078 g, 0.022 mmol) and 1 equivalent of triethylamine in 5 mL of DCM:MeOH:MeCN. The complex precipitated as a white powder, which was filtered giving Eu(**1**)₃ as a white solid (red emissive under short wave UV light) (0.0258 g, 77 %). HRMS m/z = 1564.8694 [Eu(**1**)₃ + H]⁺ (calc. for (C₇₈H₁₂₁N₁₅O₉Eu)⁺, 1564.8678), m/z = 1586.8340 [Eu(**1**)₃ + Na]⁺ (calc. for (C₇₈H₁₂₀N₁₅O₉EuNa)⁺, 1586.8511) and m/z = 804.9050 [Eu(**1**)₃ + 2Na]²⁺ (calc. for (C₇₈H₁₂₀N₁₅O₉EuNa)⁺, 1564.8678). FTIR (ATR, cm⁻¹) 2920, 2851, 1632, 1588, 1461, 1426, 1353, 1183, 1081, 1049, 1017, 889, 852, 802, 760, 722, 661, 521, 434, 409. Elemental analysis for C₇₈H₁₂₀N₁₅O₉Eu·2H₂O·0.5MeCN (1616.92 g mol⁻¹) Calculated: C 58.52, H 7.80, N 13.39 %. Found C 58.31, H 7.97, N 13.29 %.

Synthesis of Tb(**1**)₃

1 (0.0355 g, 0.071 mmol) was combined with Tb(CF₃SO₃)₃·5H₂O (0.0157 g, 0.023 mmol) and 1 equivalent of triethylamine in 5 mL of DCM:MeOH:MeCN. The complex precipitated as a white powder, which was filtered giving Tb(**1**)₃ as a white solid (green emissive under short wave UV light) (0.0235 g, 66 %). HRMS m/z = 1570.8715 [Tb(**1**)₃ + H]⁺ (calc. for (C₇₈H₁₂₁N₁₅O₉Tb)⁺, 1570.8720), m/z = 1592.8646 [Tb(**1**)₃ + Na]⁺ (calc. for (C₇₈H₁₂₀N₁₅O₉TbNa)⁺, 1592.8539) and m/z = 807.9306 [Tb(**1**)₃ + 2Na]²⁺ (calc. for (C₇₈H₁₂₀N₁₅O₉TbNa)⁺, 1592.8539). FTIR (ATR, cm⁻¹) 2920, 2851, 1032, 1592, 1567, 1464, 1430, 374, 1280, 1240, 1164, 1082, 1029, 889, 852, 760, 723, 661, 636, 574, 518, 437, 414. Elemental analysis for C₇₈H₁₂₀N₁₅O₉Tb·H₂O·2MeCN·2.5CH₂Cl₂ (1883.28 g mol⁻¹) Calculated: C 53.90, H 7.34, N 12.78 %. Found C 53.95, H 7.08, N 12.81 %.

Synthesis of Dy(**1**)₃

1 (0.0356 g, 0.076 mmol) was combined with Dy(CF₃SO₃)₃·8H₂O (0.0158 g, 0.023 mmol) and 1 equivalent of triethylamine in 5 mL of DCM:MeOH:MeCN. The complex precipitated as a white powder, which was filtered giving Dy(**1**)₃ as a white solid (yellow emissive under short wave UV light) (0.0210 g, 57 %). HRMS m/z = 1575.8769 [Dy(**1**)₃ + H]⁺ (calc. for (C₇₈H₁₂₁N₁₅O₉Dy)⁺, 1575.8769) and m/z = 810.4346 [Dy(**1**)₃ + 2Na]²⁺ (calc. for (C₇₈H₁₂₀N₁₅O₉DyNa)⁺, 810.4244). FTIR (ATR, cm⁻¹) 2920, 2851, 1636, 1590, 1562, 1461, 1428, 1375, 1278, 1244, 185, 1160, 1081, 1049, 1029, 891, 852, 761, 724, 661, 637, 573, 518, 460, 436, 414. Elemental analysis for C₇₈H₁₂₀N₁₅O₉Dy·4.5H₂O (1655.47 g mol⁻¹) Calculated: C 56.59, H 7.85, N 12.69 %. Found C 56.73, H 7.76, N 12.62 %.

Synthesis of Sm(**1**)₃

1 (0.0359 g, 0.076 mmol) was combined with Sm(Cl)₃·6H₂O (0.0083 g, 0.023 mmol) and 1 equivalent of triethylamine in 5 mL of DCM:MeOH:MeCN. This complex precipitated as a white powder, which was filtered giving Sm(**1**)₃ as a white solid (dim

red/orange emissive under short wave UV light) (0.0204 g, 56 %). HRMS $m/z = 1563.8838$ [$\text{Sm}(\mathbf{1})_3 + \text{H}]^+$ (calc. for $(\text{C}_{78}\text{H}_{121}\text{N}_{15}\text{O}_9\text{Sm})^+$, 1563.8672), $m/z = 1585.8727$ [$\text{Sm}(\mathbf{1})_3 + \text{Na}]^+$ (calc. for $(\text{C}_{78}\text{H}_{120}\text{N}_{15}\text{O}_9\text{SmNa})^+$, 1585.8491) and $m/z = 804.4482$ [$\text{La}(\mathbf{1})_3 + 2\text{Na}]^{2+}$ (calc. for $(\text{C}_{78}\text{H}_{120}\text{N}_{15}\text{O}_9\text{SmNa}_2)^{2+}$, 804.4192). FTIR (ATR, cm^{-1}) 2919, 2850, 1631, 1587, 1562, 1460, 1426, 1350, 1276, 1182, 1080, 1050, 1016, 890, 852, 760, 721, 661, 520, 463, 433, 409. Elemental analysis for $\text{C}_{78}\text{H}_{120}\text{N}_{15}\text{O}_9\text{Sm}\cdot 2\text{H}_2\text{O}$ (1598.30 g mol^{-1}) Calculated: C 58.62, H 7.82, N 13.15 %. Found C 58.43, H 7.89, N 13.38 %.

Synthesis of $\text{La}(\mathbf{1})_3$

1 (0.0285 g, 0.060 mmol) was combined with $\text{La}(\text{Cl})_3\cdot 7\text{H}_2\text{O}$ (0.0067 g, 0.018 mmol) and 1 equivalent of triethylamine in 5 mL of DCM:MeOH:MeCN. This complex precipitated as a white powder; this was filtered giving $\text{La}(\mathbf{1})_3$ as a white solid (0.0157 g, 51 %). HRMS $m/z = 1550.8528$ [$\text{La}(\mathbf{1})_3 + \text{H}]^+$ (calc. for $(\text{C}_{78}\text{H}_{121}\text{N}_{15}\text{O}_9\text{La})^+$, 1550.8530) and $m/z = 1572.8352$ [$\text{La}(\mathbf{1})_3 + \text{Na}]^+$ (calc. for $(\text{C}_{78}\text{H}_{120}\text{N}_{15}\text{O}_9\text{LaNa})^+$, 1572.8349). FTIR (ATR, cm^{-1}) 2920, 2851, 16227, 1586, 1563, 1463, 1425, 1371, 1276, 1183, 1051, 1030, 1014, 887, 853, 759, 721, 689, 659, 638, 517. ^1H NMR (300 MHz, CDCl_3 & CD_3OD) ppm, $\delta = 8.20$ (m, 2H, pyridine-H), 8.04 (m, 1H, pyridine-H), 7.66 (s, H, triazole-H), 0.88 (d, $J = 6.70$ Hz, 3H, CH_3), 1.77 (m, 2H, $\text{CH}_2\text{-CH}_2\text{N}$), 1.167 (m, 26H, 13 x CH_2), 0.80 (t, 3H, CH_3).

Photophysical measurements

Unless otherwise stated, all measurements were performed at room temperature in MeCN (HPLC grade). The stock solutions of ligand or complex were prepared using a (1:1) ratio of CH_2Cl_2 and MeOH (spectroscopic grade). Emission (steady-state, time-resolved, and excitation) spectra and lifetimes were recorded at room temperature.

Ligand characterisation

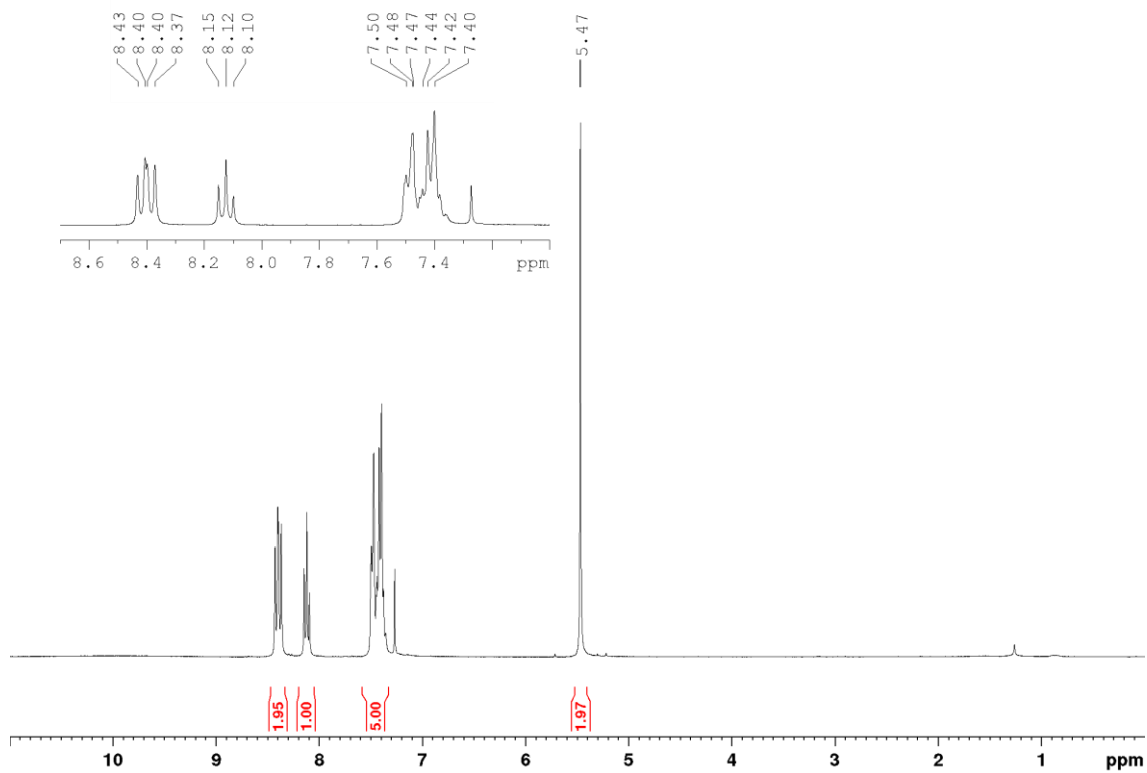


Figure S1. ^1H NMR spectrum (300 MHz, CDCl_3) of A.

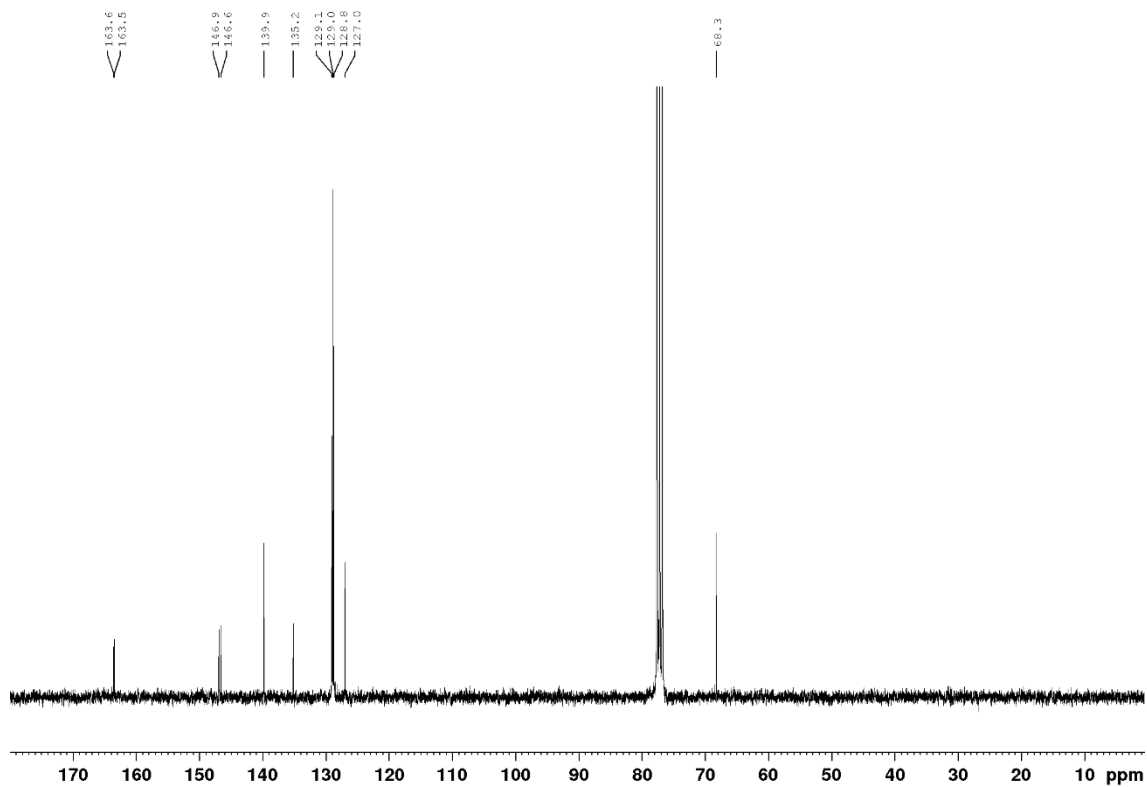


Figure S2. ^{13}C NMR spectrum (75 MHz, CDCl_3) of A.

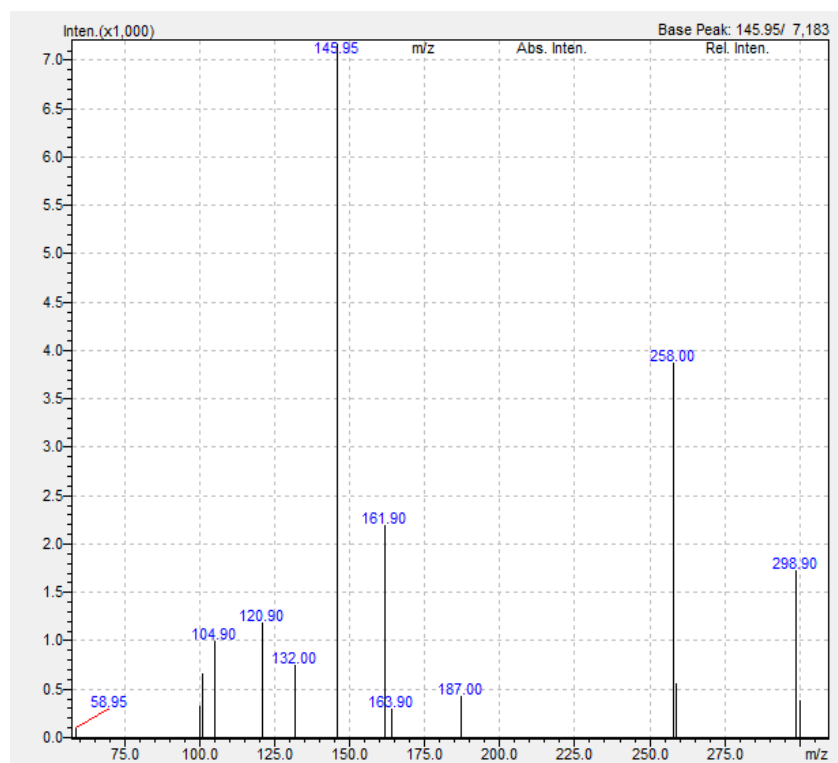


Figure S3. LRMS m/z= 258.00 [A + H]⁺ (calc. for C₁₄H₁₂NO₄⁺, 258.25).

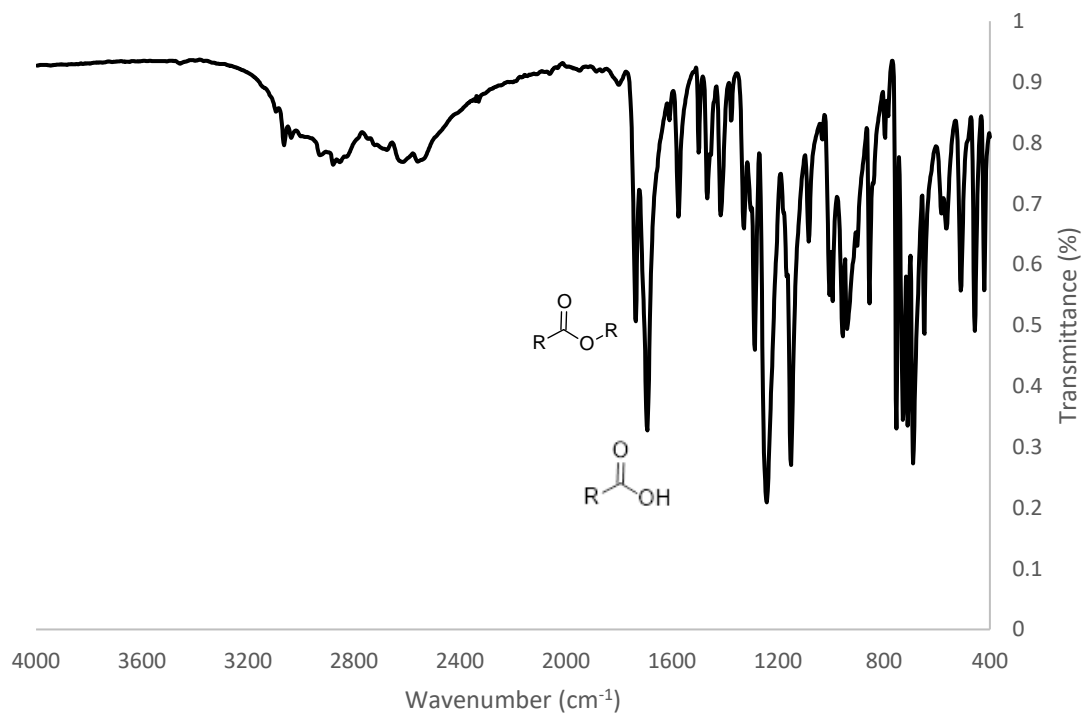


Figure S4. Infra-red spectrum of A.

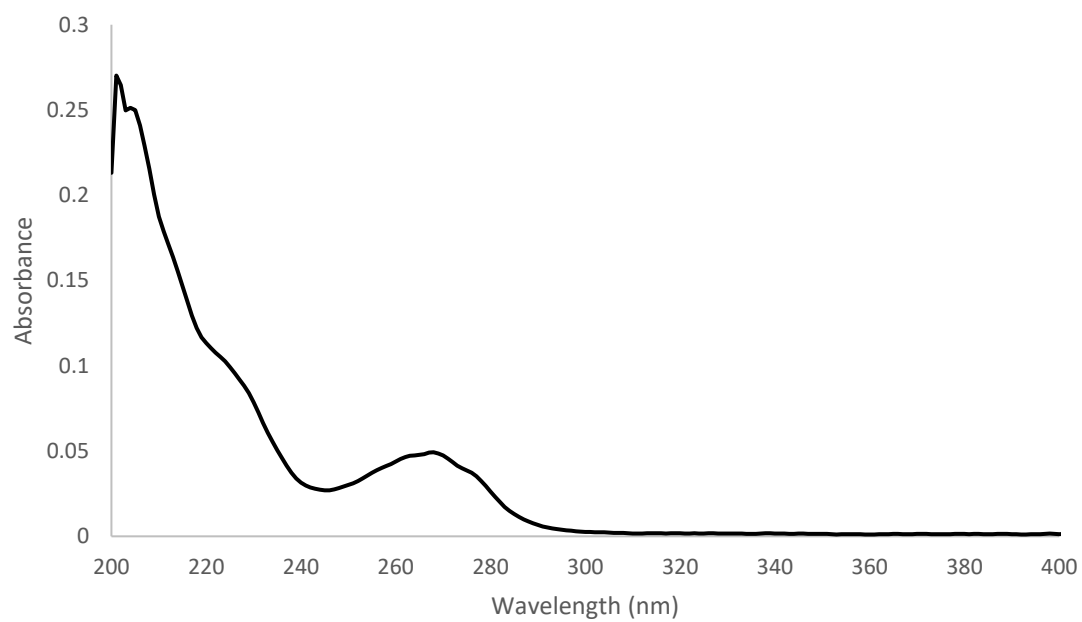


Figure S5. UV-visible absorption spectrum of **A**, in MeCN (0.01 mM).

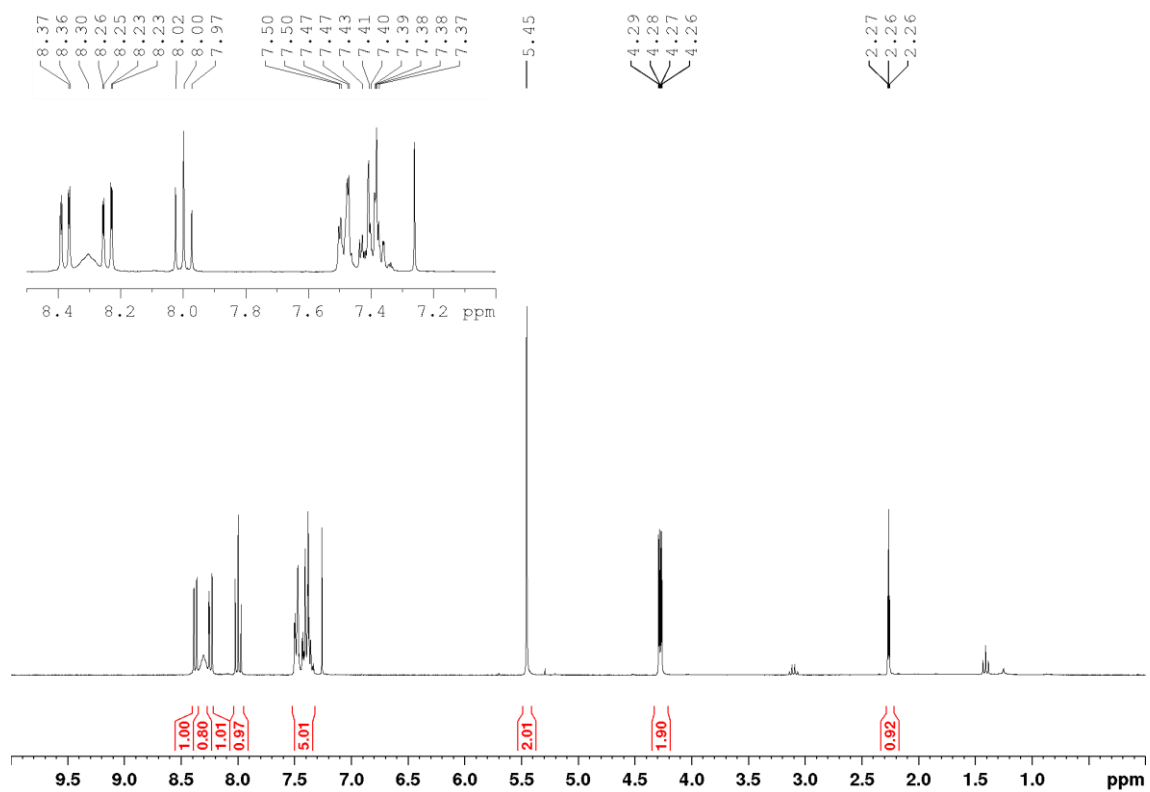


Figure S6. ^1H NMR spectrum (300 MHz, CDCl_3) of **B**.

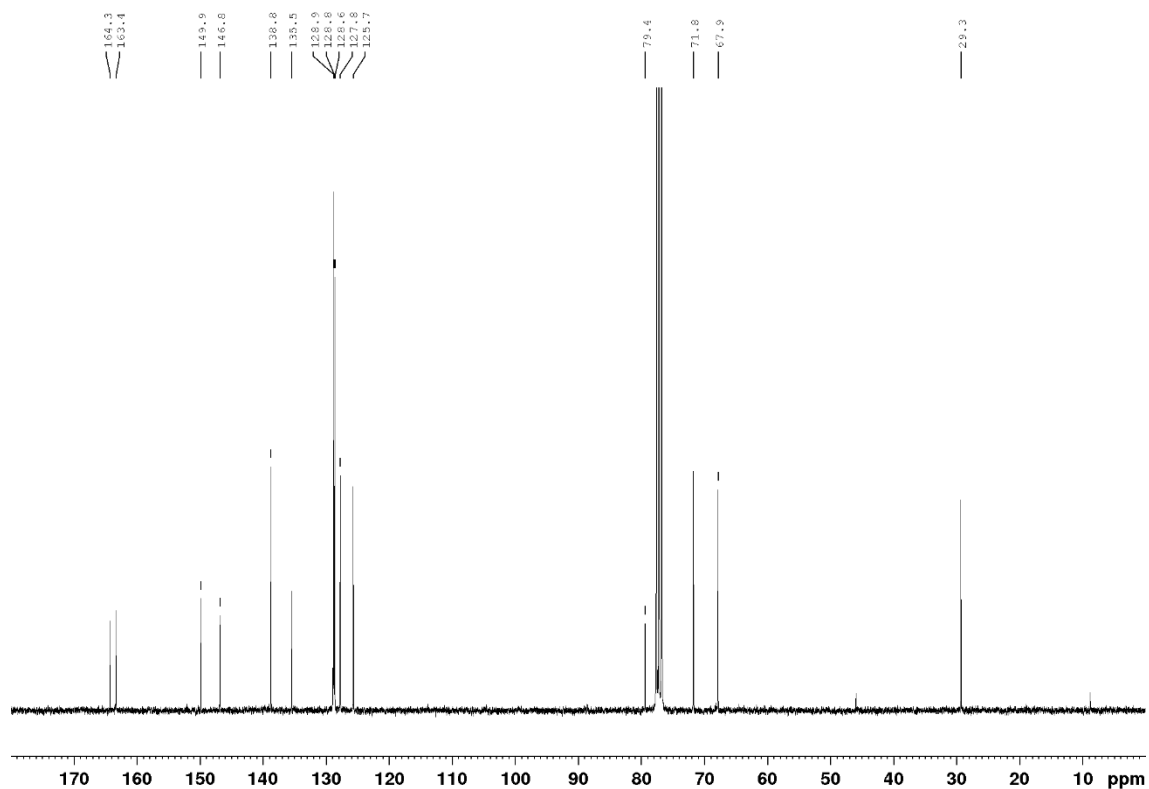


Figure S7. ^{13}C NMR spectrum (75 MHz, CDCl_3) of **B**.

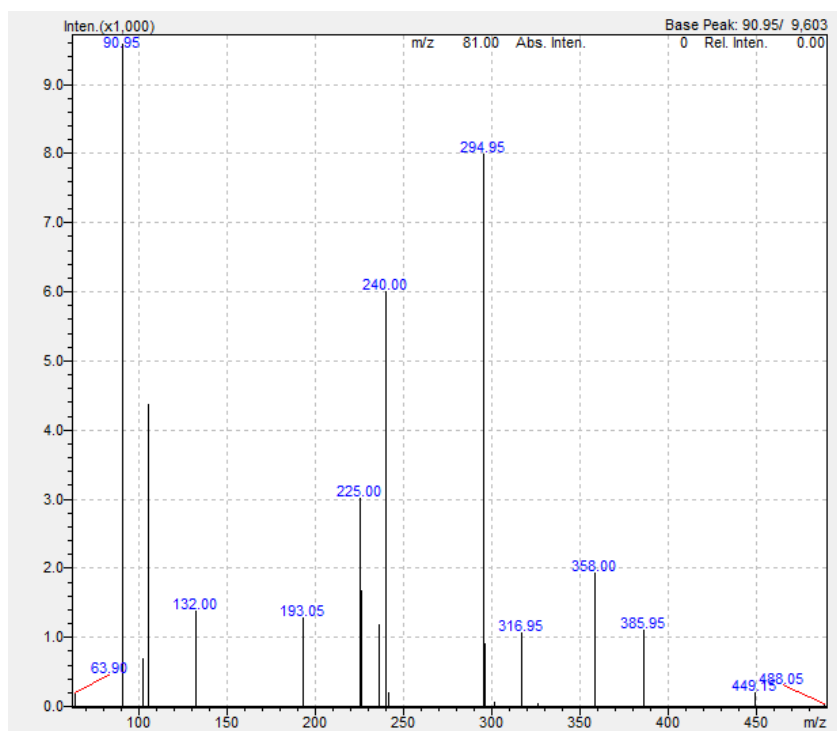


Figure S8. LRMS $m/z = 294.95$ $[\text{B} + \text{H}]^+$ (calc. for $\text{C}_{17}\text{H}_{15}\text{N}_2\text{O}_3^+$, 295.11), $m/z = 316.95$ $[\text{B} + \text{H}]^+$ (calc. for $\text{C}_{17}\text{H}_{15}\text{N}_2\text{O}_3^+$, 317.19).

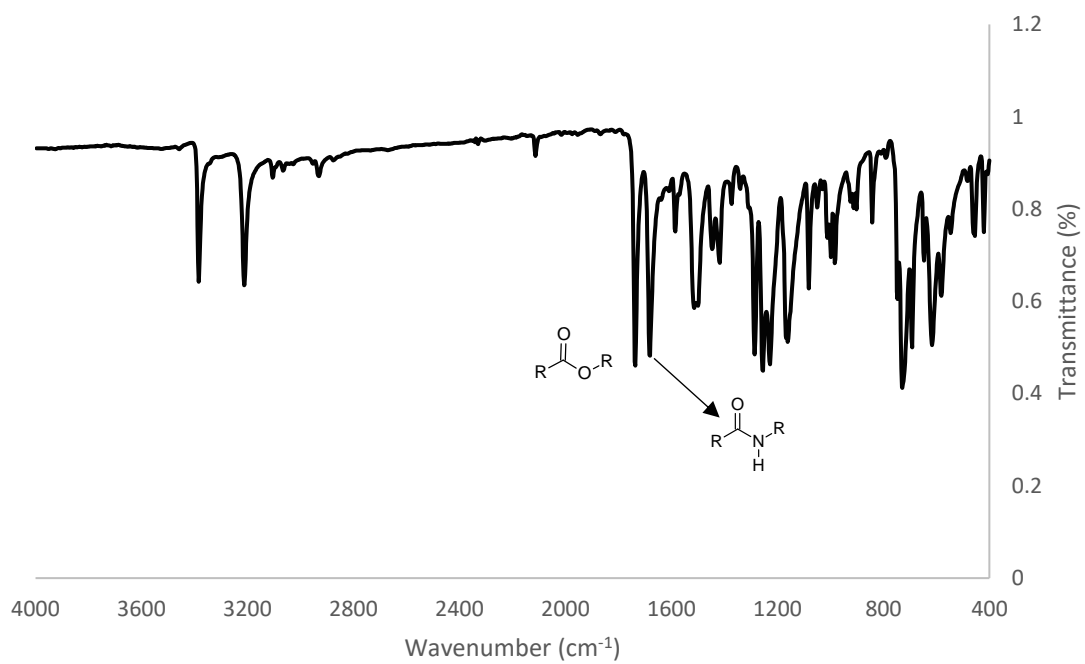


Figure S9. Infra-red spectrum of **B**.

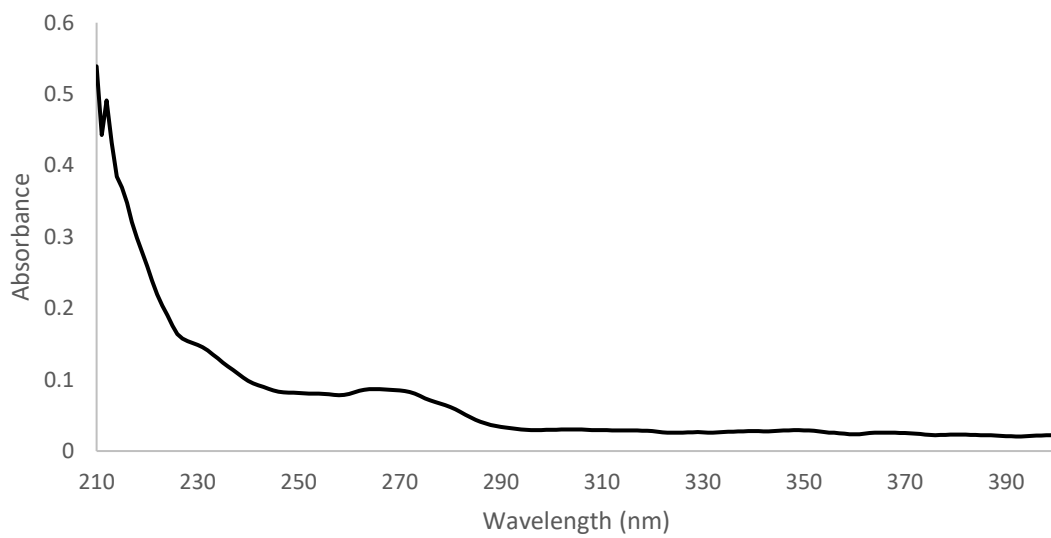


Figure S9. UV-visible absorption spectrum of **B**, in MeCN (0.01 mM).

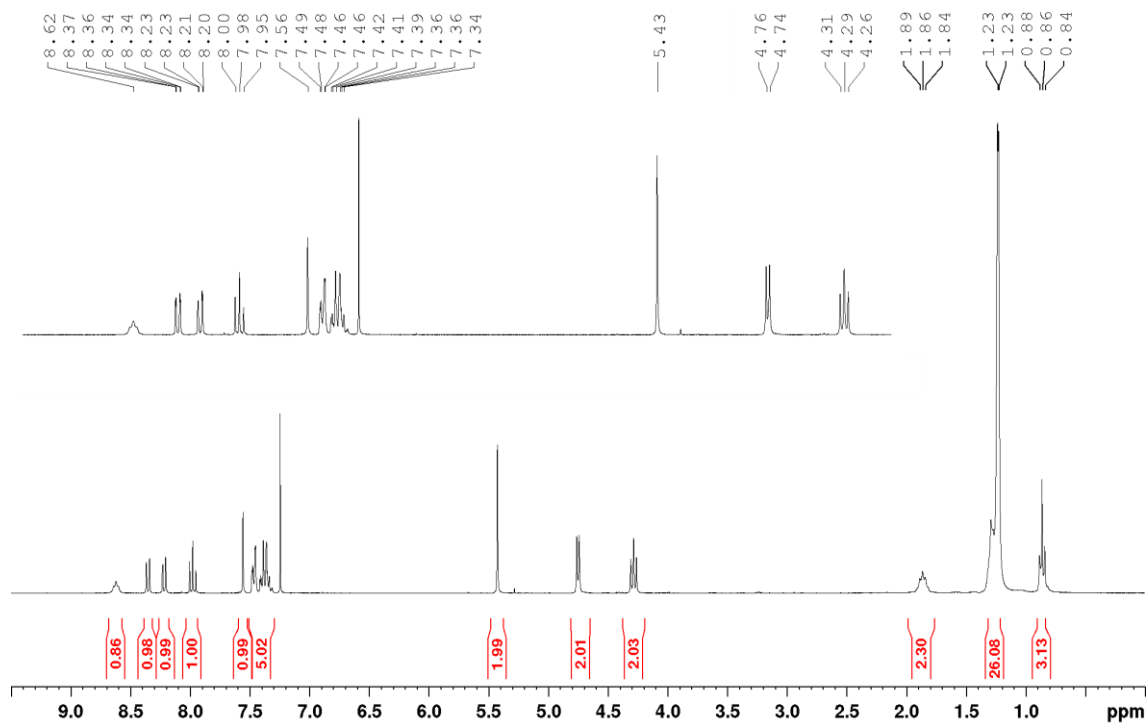


Figure S10. ^1H NMR spectrum (300 MHz, CDCl_3) of **C**.

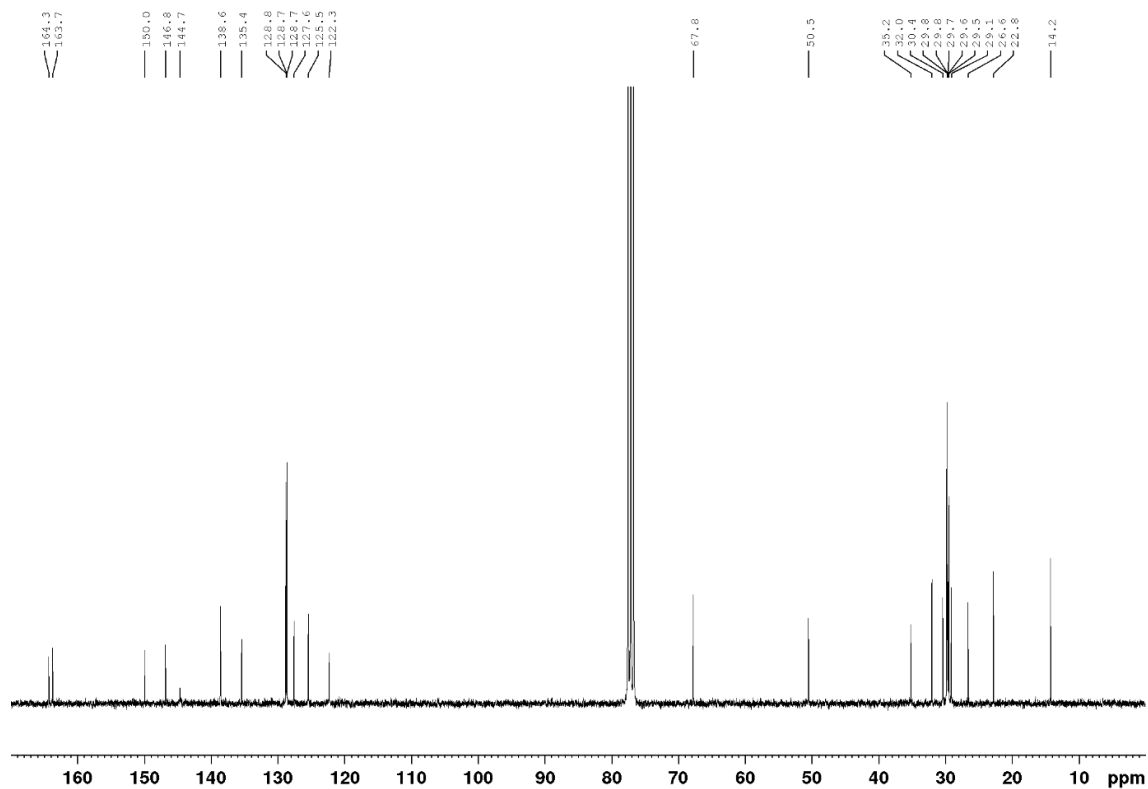


Figure S11. ^{13}C NMR spectrum (75 MHz, CDCl_3) of **C**.

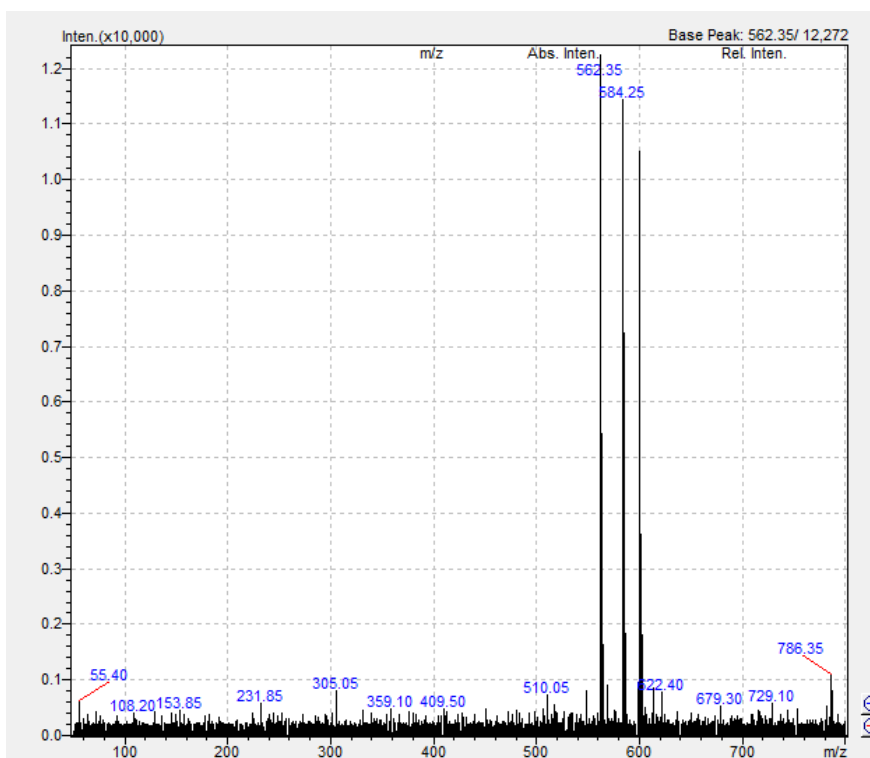


Figure S12. LRMS $m/z = 562.35$ $[C + H]^+$ (calc. for $C_{33}H_{48}N_5O_3^+$, 562.38), $m/z = 584.25$ $[C + Na]^+$ (calc. for $C_{33}H_{47}N_5O_3Na^+$, 584.36), $m/z = 600.25$ $[C + K]^+$ (calc. for $C_{33}H_{47}N_5O_3K^+$, 600.20).

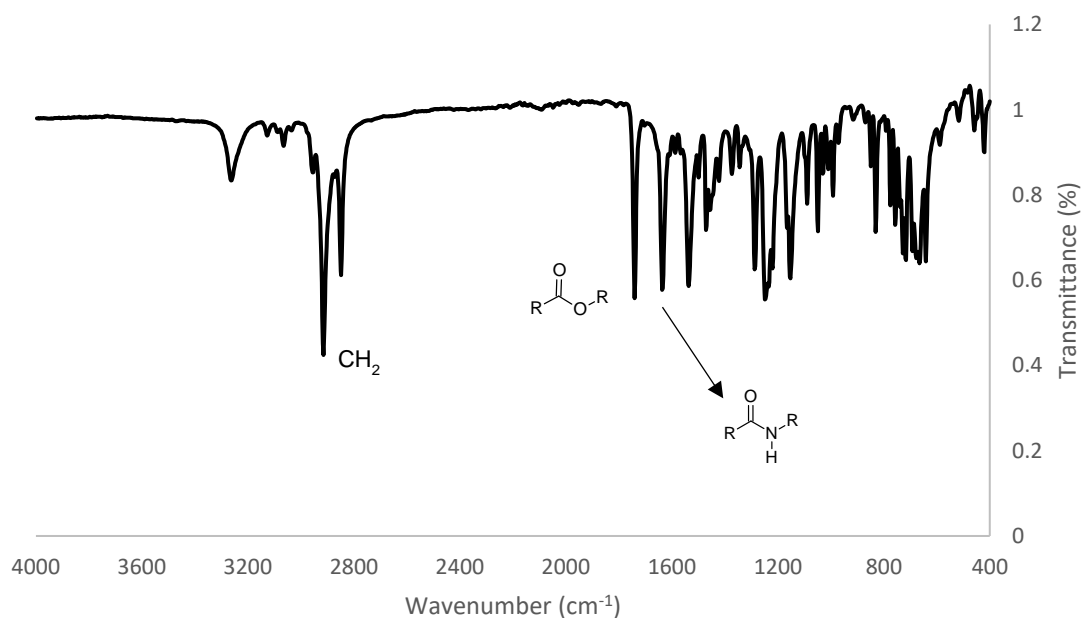


Figure S13. Infra-red spectrum of **C**.

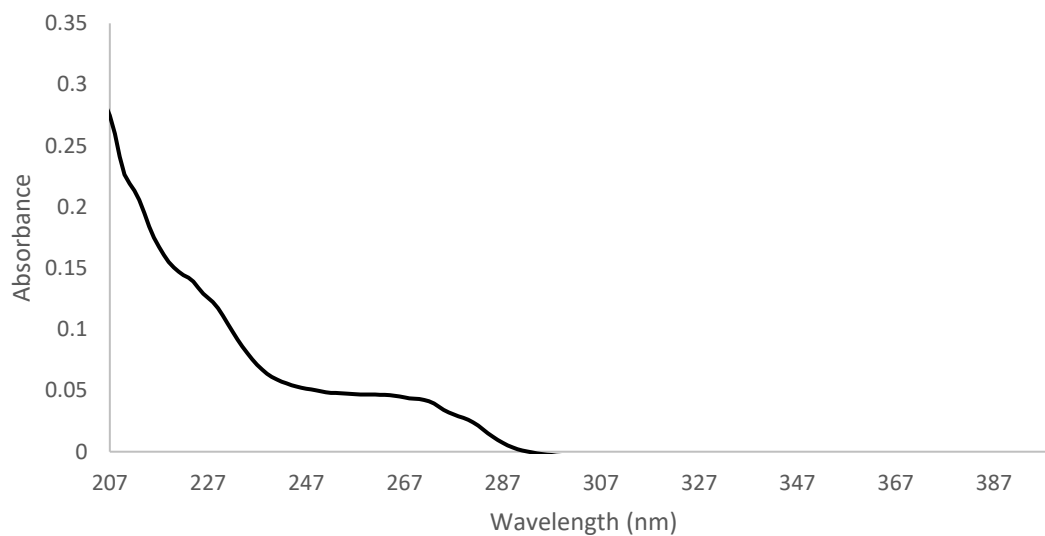


Figure S14. UV-visible absorption spectrum of **C**, in MeCN (0.01 mM).

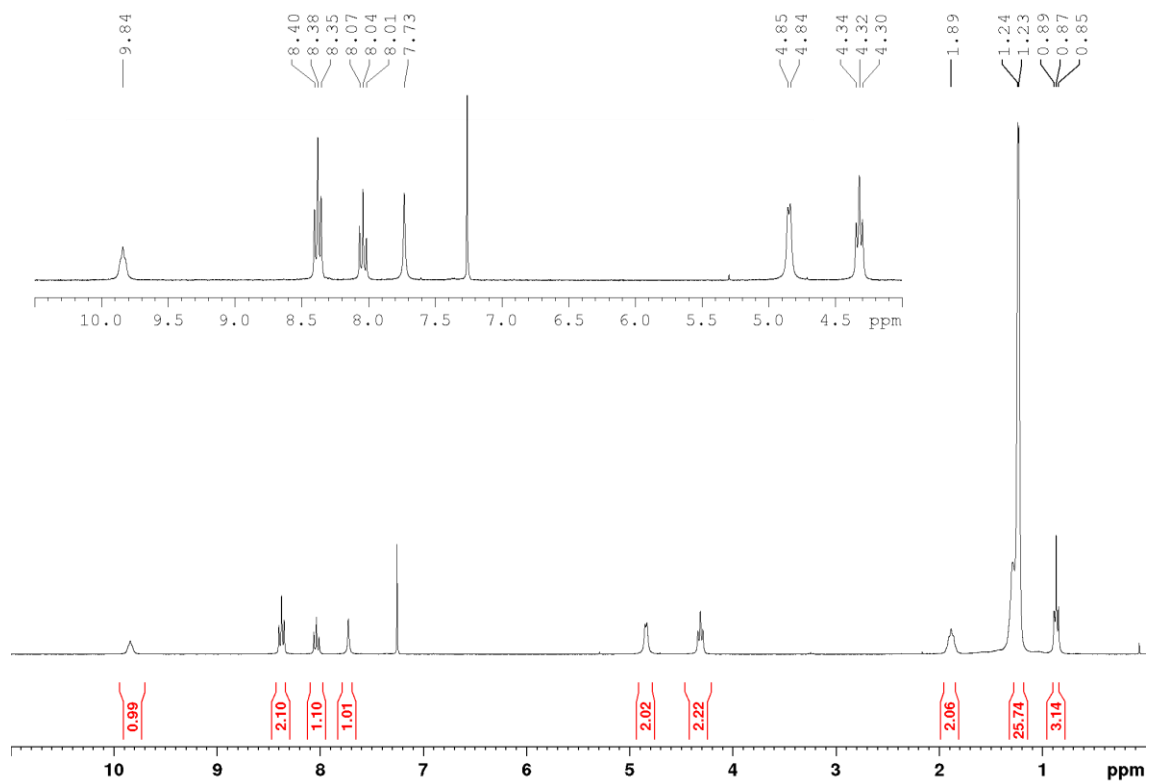


Figure S15. ^1H NMR spectrum (300 MHz, CDCl_3) of **1**.

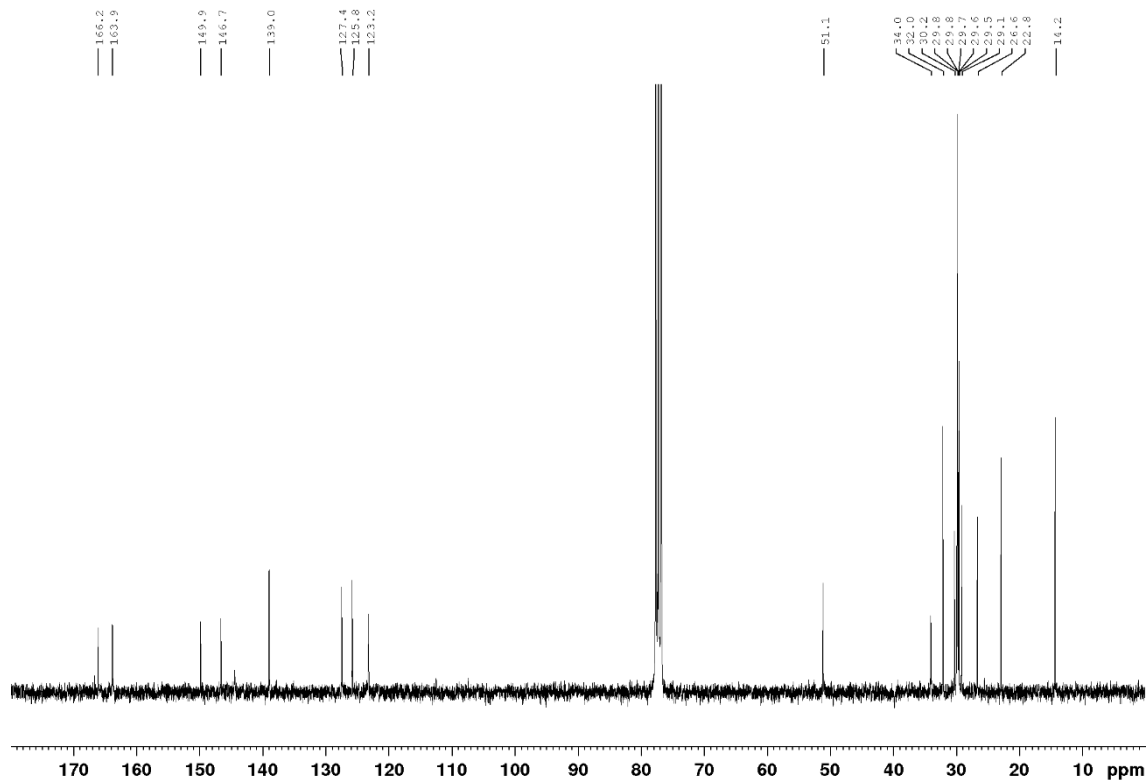


Figure S16. ^{13}C NMR spectrum (75 MHz, CDCl_3) of **1**.

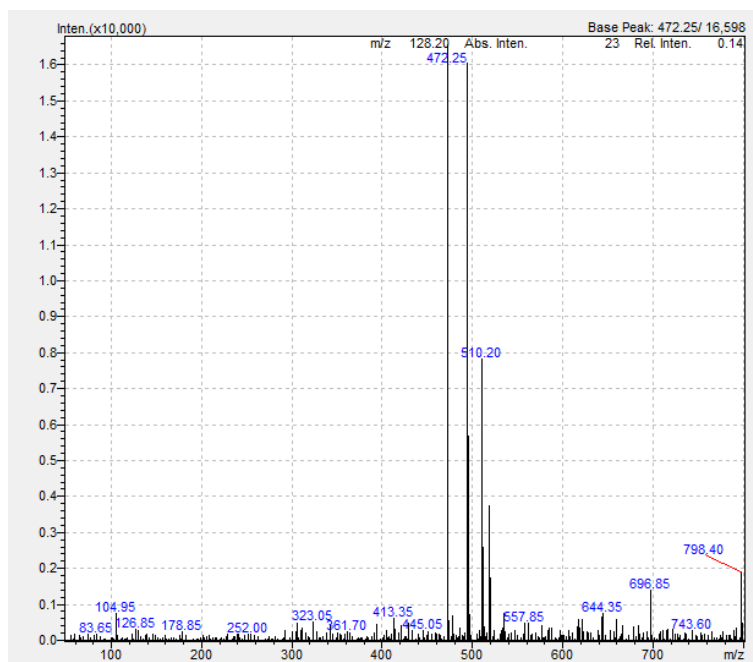


Figure 17. LRMS $m/z = 472.25$ [$\mathbf{1} + \text{H}$] $^+$ (calc. for $\text{C}_{26}\text{H}_{42}\text{N}_5\text{O}_3^+$, 472.33), $m/z = 494.20$ [$\mathbf{1} + \text{Na}$] $^+$ (calc. for $\text{C}_{26}\text{H}_{41}\text{N}_5\text{O}_3\text{Na}^+$, 494.31) and $m/z = 510.20$ [$\mathbf{1} + \text{K}$] $^+$ (calc. for $\text{C}_{26}\text{H}_{41}\text{N}_5\text{O}_3\text{K}^+$, 510.28).

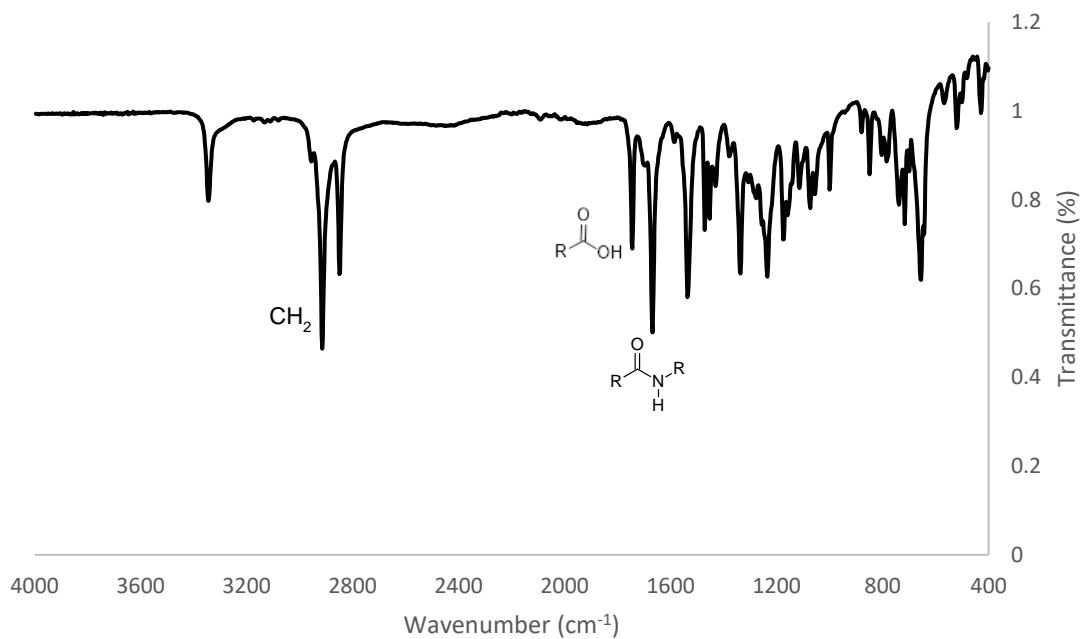


Figure S17. Infra-red spectrum of **1**.

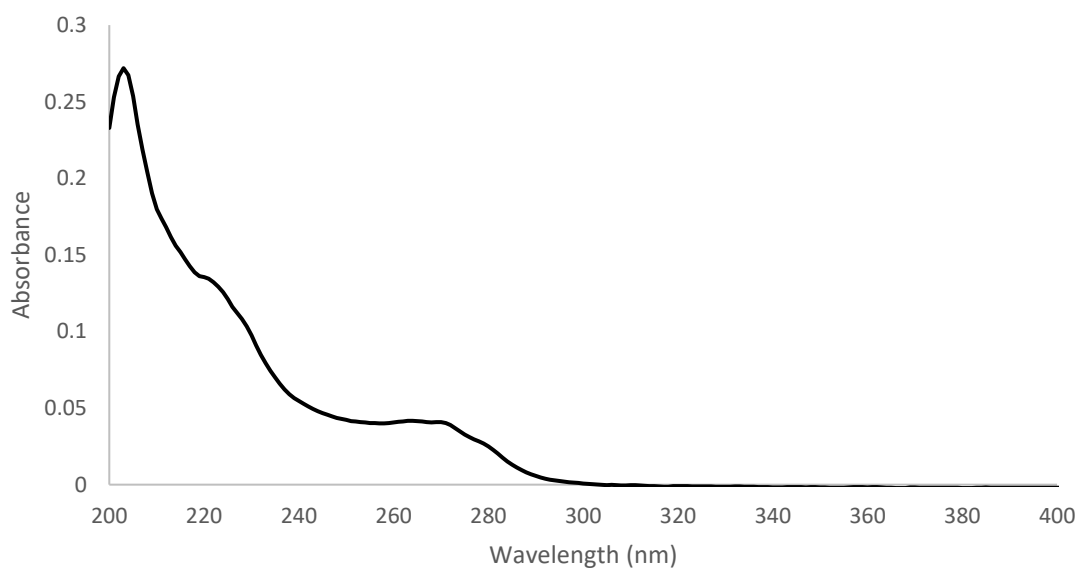


Figure S18. UV-visible absorption spectrum of **1**, in MeCN (0.01 mM).

Ligand crystal structure

1-DMSO crystallised in the triclinic space group P-1 and contained one molecule and an associated DMSO solvent molecule in the asymmetric unit. The structure shows the expected connectivity, with both the amide and carboxylate bonds oriented such that the NH and OH groups are pointing towards the central pyridyl nitrogen atom, forming a moderate strength hydrogen bonding pocket that contains the solvent DMSO molecule [$N2-H2\cdots O100' = 2.996(4)$ Å and $\angle(N2-H2\cdots O100') = 165(3)^\circ$]; [$O1-H1\cdots O100' = 2.696(4)$ and $\angle(O3-H3a\cdots O100') = 153(4)^\circ$]. Long range ordering showed the formation of “membrane” like bilayers, where the C_{16} chains interdigitate.

Crystal Data for $C_{28}H_{47}N_5O_4S$ ($M = 549.76$ g/mol): triclinic, space group P-1 (no. 2), $a = 5.4939(6)$ Å, $b = 9.5425(11)$ Å, $c = 29.273(4)$ Å, $\alpha = 82.514(6)^\circ$, $\beta = 87.742(6)^\circ$, $\gamma = 84.220(6)^\circ$, $V = 1513.3(3)$ Å³, $Z = 2$, $T = 123.0$ K, $\mu(\text{CuK}\alpha) = 1.269$ mm⁻¹, $D_{\text{calc}} = 1.206$ g/cm³, 25890 reflections measured ($6.092^\circ \leq 2\theta \leq 101.006^\circ$), 3130 unique ($R_{\text{int}} = 0.0478$, $R_{\text{sigma}} = 0.0293$) which were used in all calculations. The final R_1 was 0.0496 ($I > 2\sigma(I)$) and wR_2 was 0.1277 (all data). CCDC : 2046714

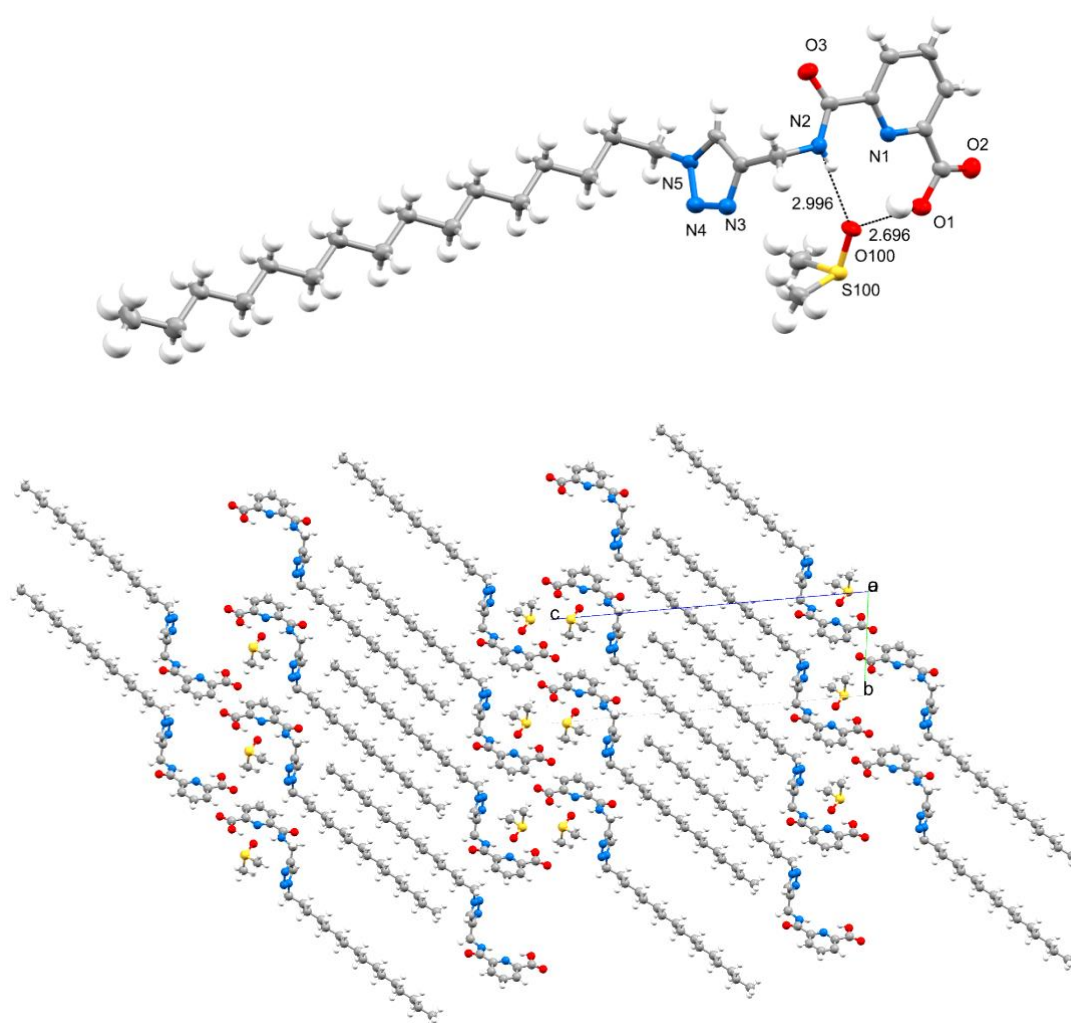


Figure S19. (Top) The crystallographically independent molecules of **1** in the asymmetric unit and associated hydrogen bonding with the singular DMSO solvent molecule. (Bottom) The overall result of the aforementioned interactions is the formation of sheet-like packing along the crystallographic a-axis.

Lanthanide complex characterisation

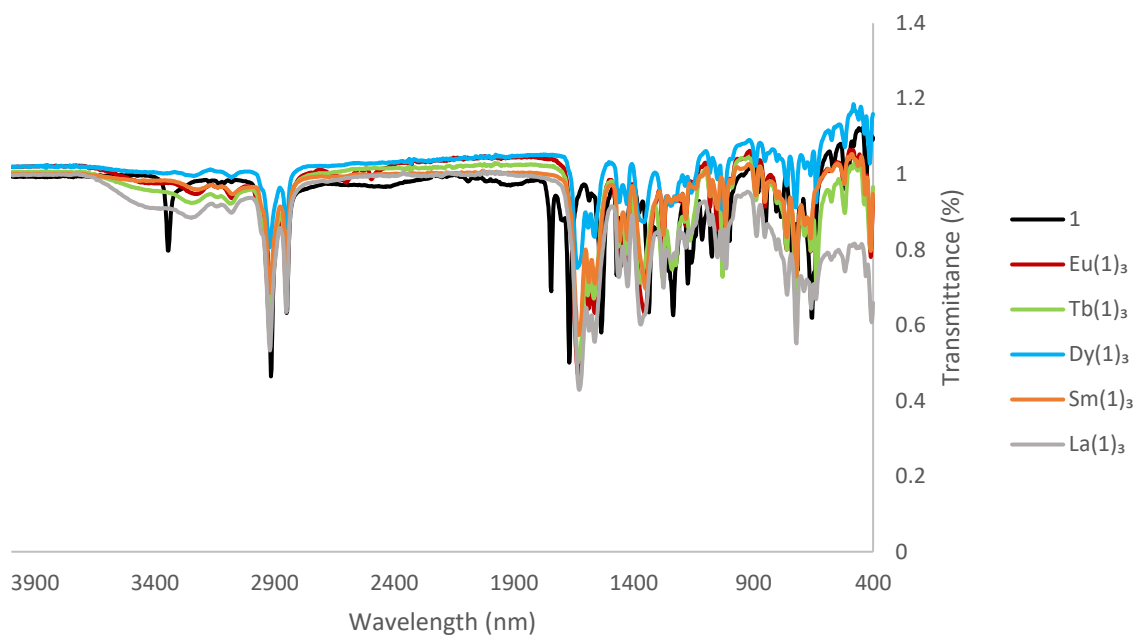


Figure S20. Infra-red spectra of **1** and Ln(**1**)₃ where Ln = Eu³⁺, Tb³⁺, Dy³⁺, Sm³⁺, and La³⁺.

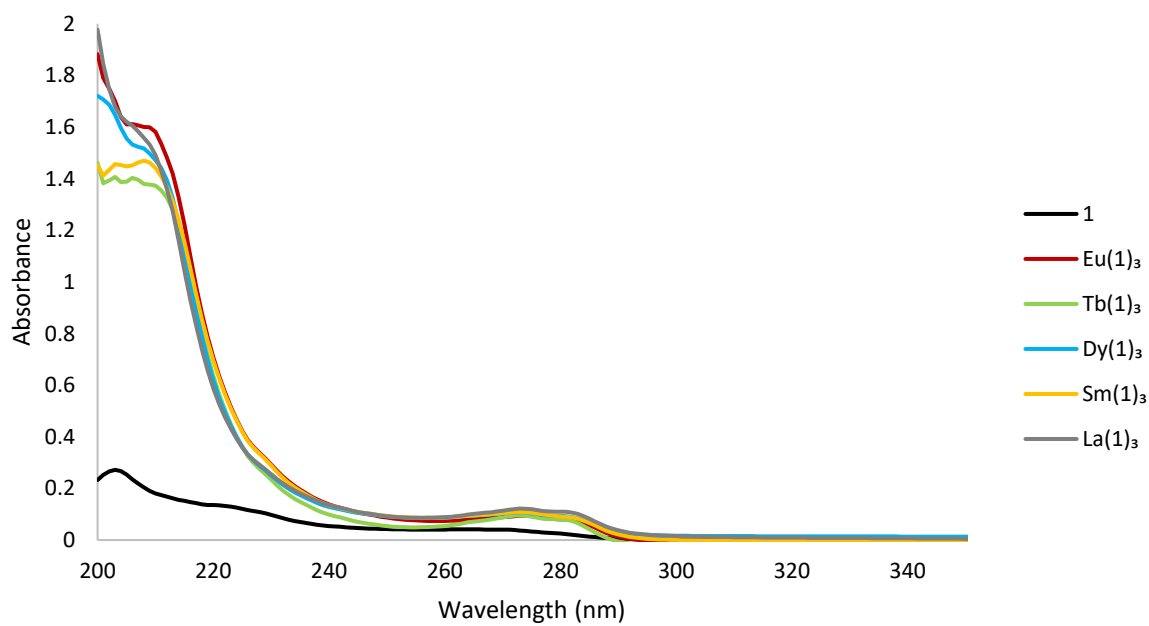


Figure S21. UV-visible absorption of **1** and Ln(**1**)₃ where Ln = Eu³⁺, Tb³⁺, Dy³⁺, Sm³⁺ and La³⁺ in MeCN (0.001 mM).

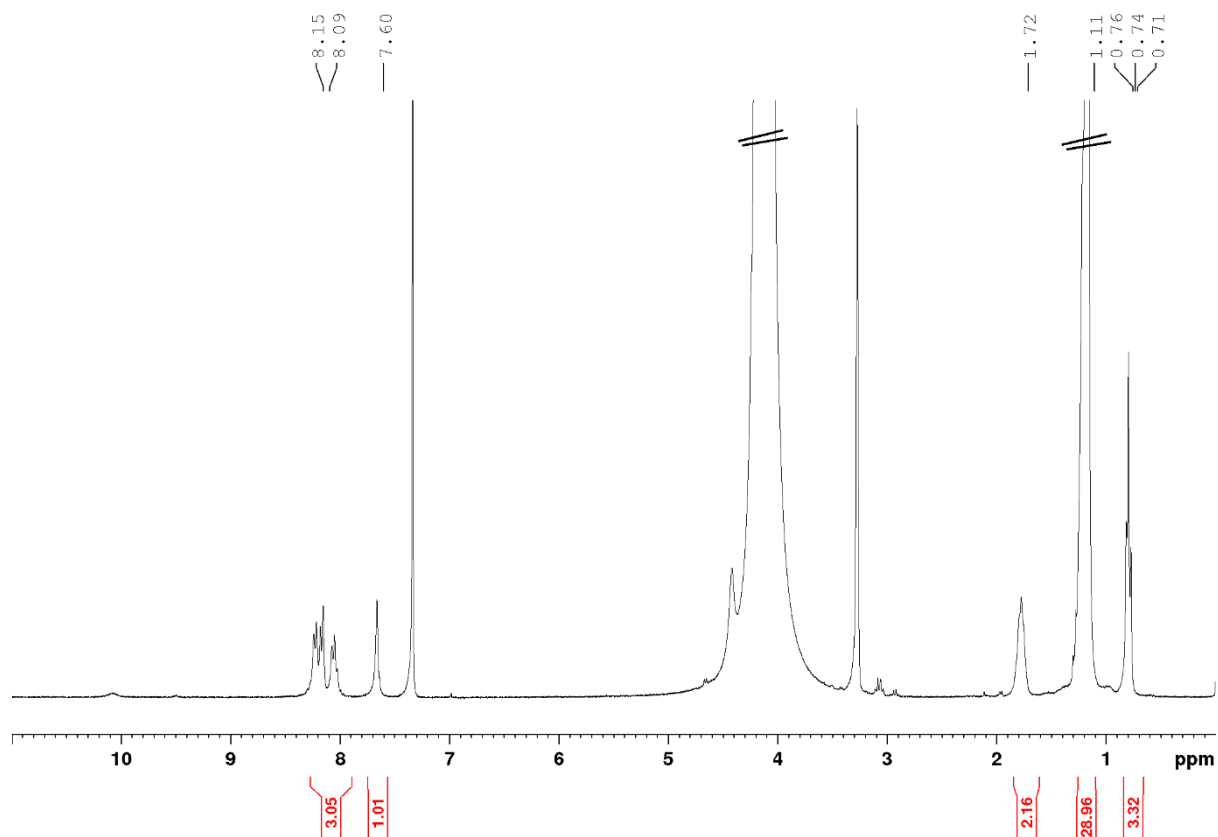


Figure S22. ^1H NMR spectrum (300 MHz, CDCl_3 & CD_3OD) of $\text{La}(\mathbf{1})_3$.

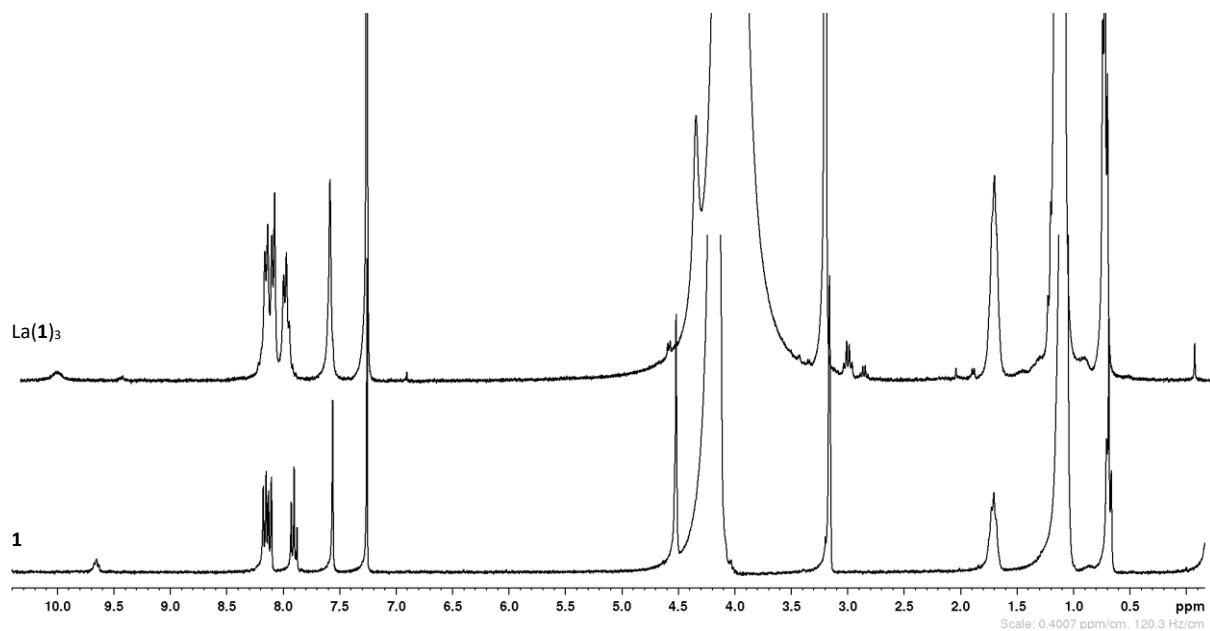


Figure S23. ^1H NMR spectrum (300 MHz, CDCl_3 & CD_3OD) of $\text{La}(\mathbf{1})_3$ (top) and $\mathbf{1}$ (bottom).

Mass Spectrometry carried out on ThermoFisher Q Exactive Focus coupled to an Ultimate™ 3000 RSLC

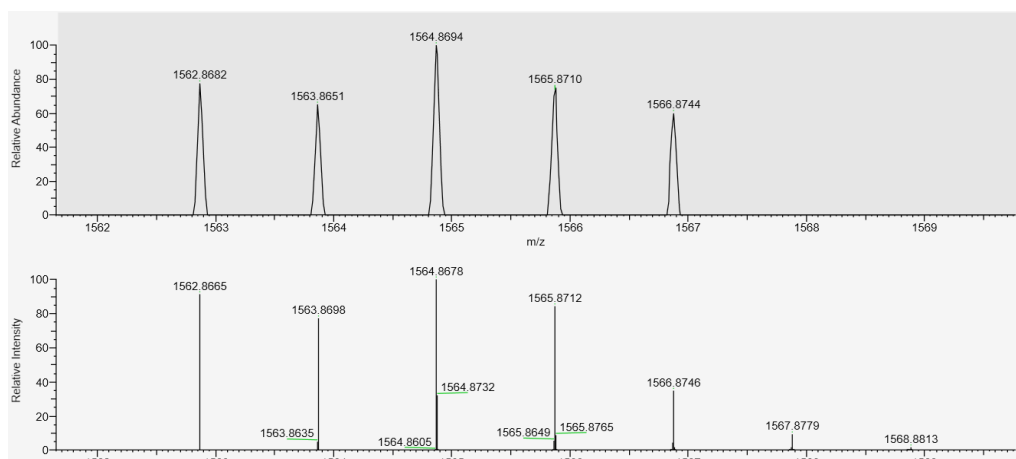


Figure S24. (Top) HRMS $m/z = 1564.8694 [Eu(1)_3 + H]^+$. (Bottom) Calc. for $(C_{78}H_{122}N_{15}O_9Eu)^+$, 1564.8678.

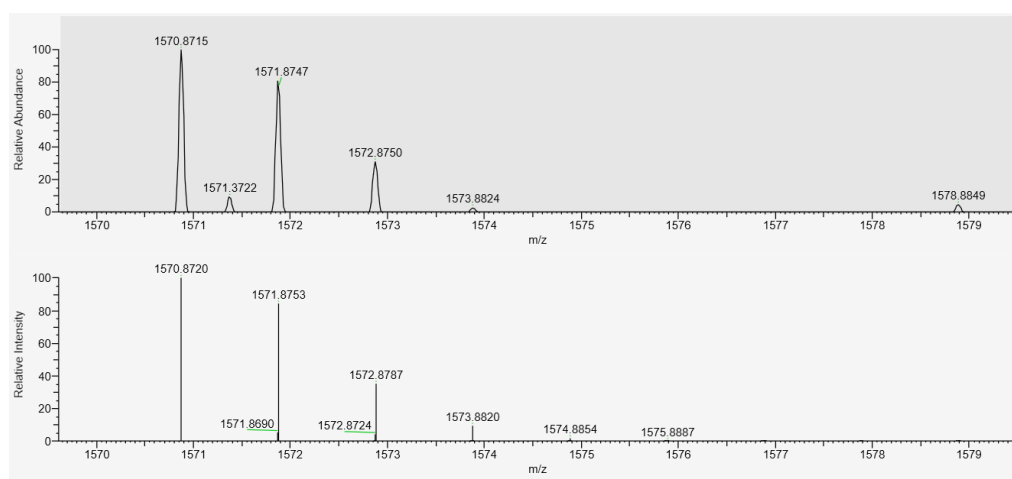


Figure S25. (Top) HRMS $m/z = 1570.8715 [Tb(1)_3 + H]^+$. (Bottom) Calc. for $(C_{78}H_{122}N_{15}O_9Tb)^+$, 1570.8720.

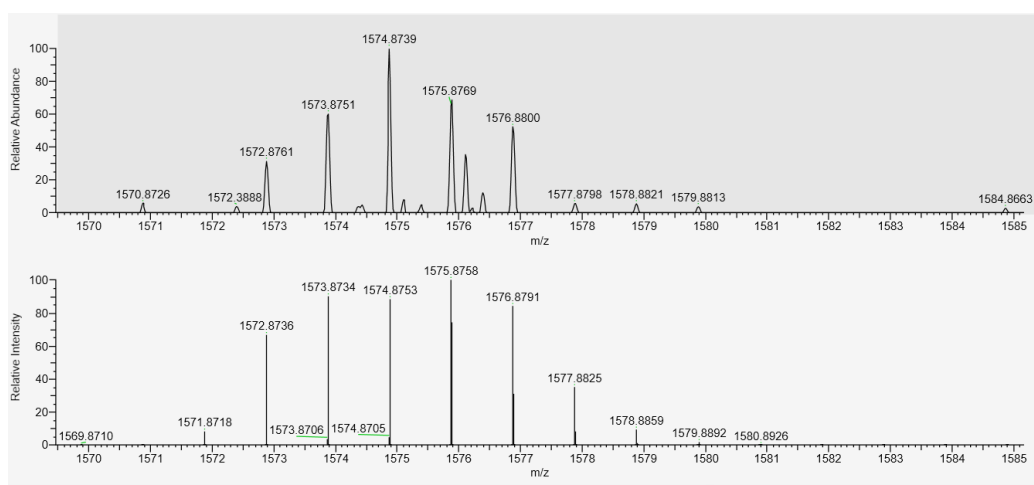


Figure S25. (Top) HRMS $m/z = 1575.8769 [Dy(1)_3 + H]^+$. (Bottom) Calc. for $(C_{78}H_{122}N_{15}O_9Dy)^+$, 1575.8769.

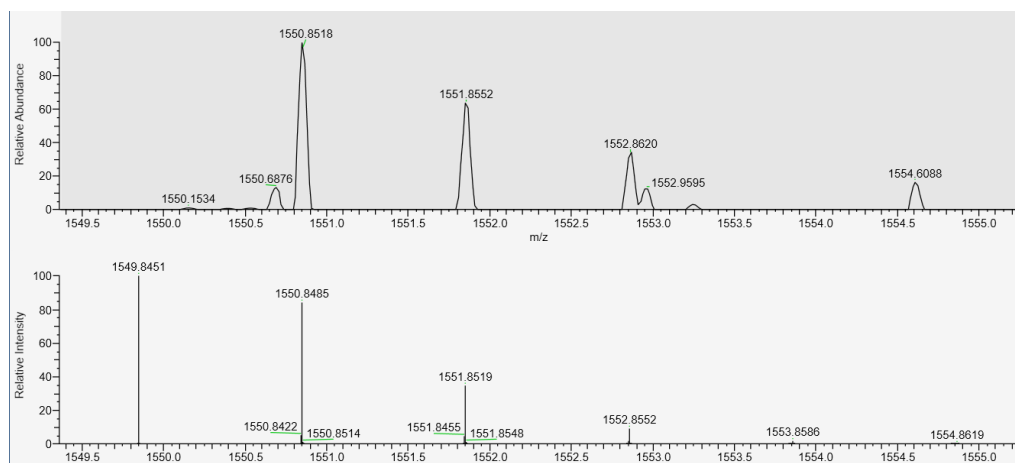


Figure S26. (Top) HRMS $m/z = 1550.8528 [La(1)_3 + H]^+$. (Bottom) Calc. for $(C_{78}H_{121}N_{15}O_9La)^+$, 1550.8530.

Mass Spectrometry carried out on Bruker Daltonics MicrOTOF™ Spectrometer

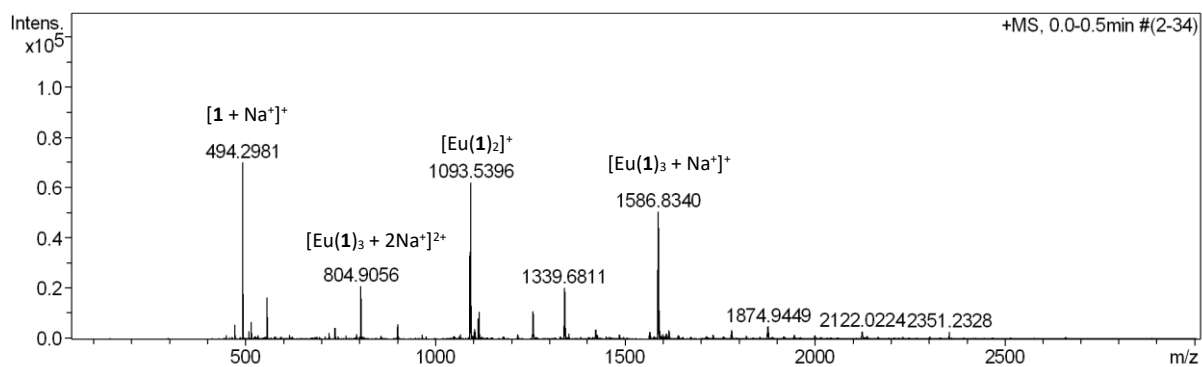


Figure S27. HRMS $Eu(1)_3$.

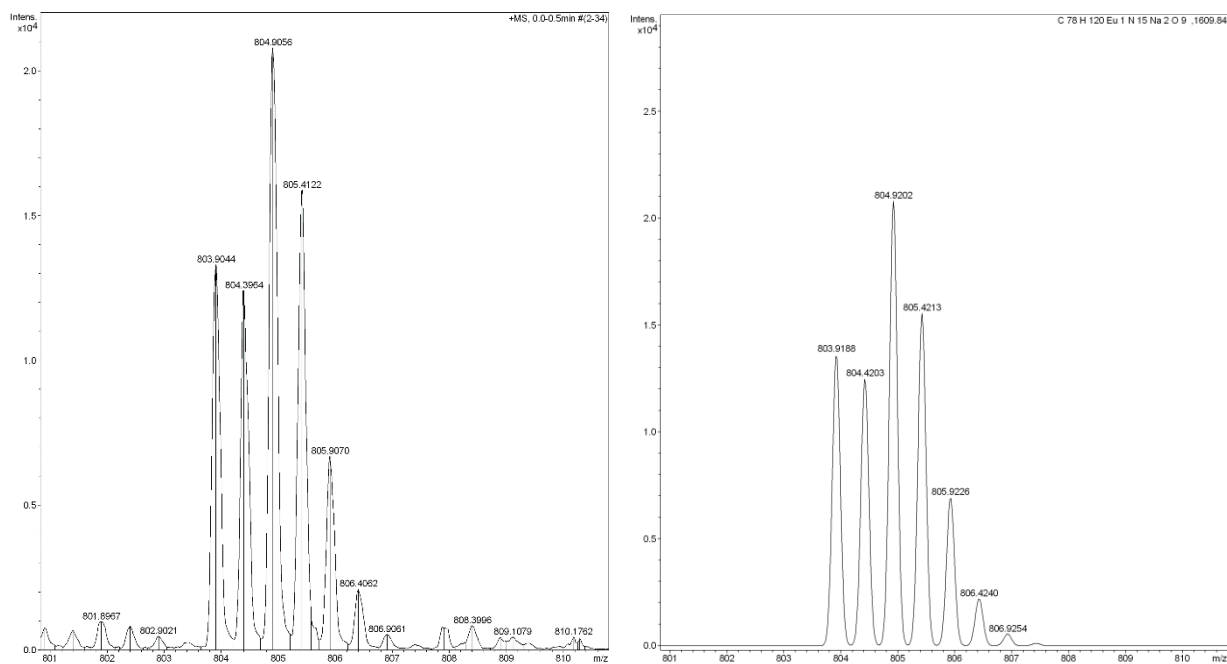


Figure S28. (Left) HRMS $m/z = 804.9050 [Eu(1)_3 + 2Na]^{2+}$. (Right) Calc. for $(C_{78}H_{120}N_{15}O_9EuNa_2)^{2+}$, 804.9202.

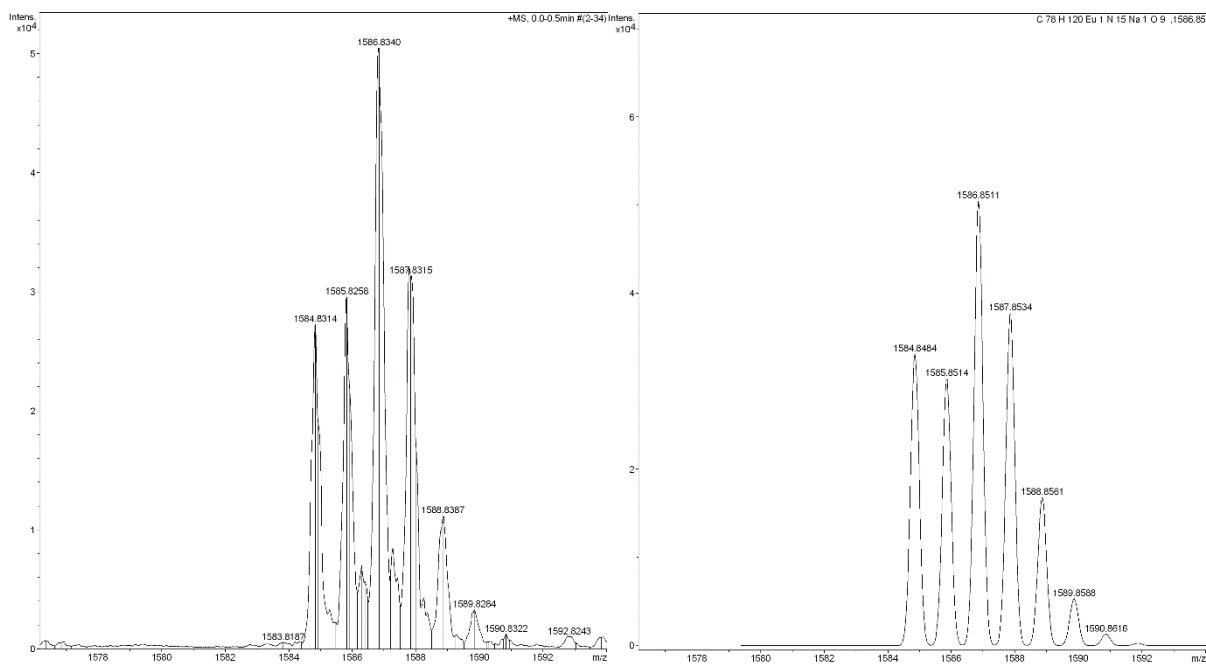


Figure S29. (Left) HRMS $m/z = 1586.8340$ $[Eu(1)_3 + Na]^+$. (Right) Calc. for $(C_{78}H_{120}N_{15}O_9EuNa)^+$, 1586.8511.

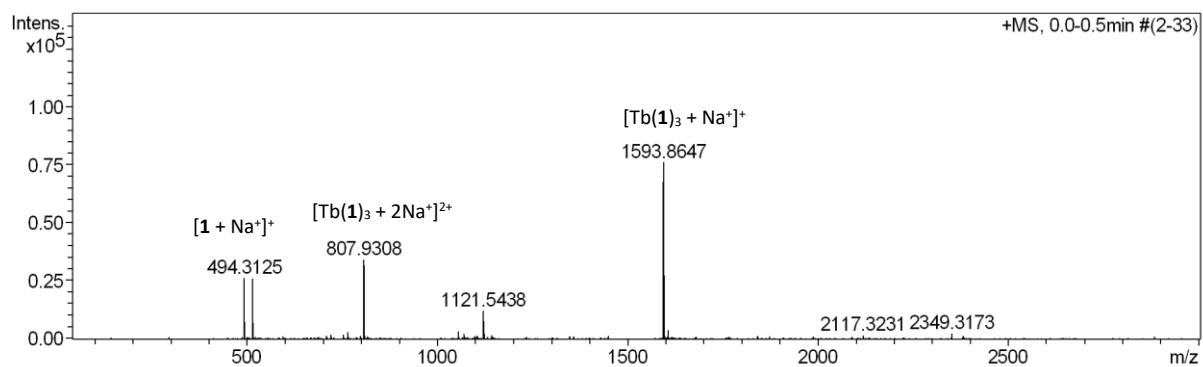


Figure S30. HRMS $Tb(1)_3$.

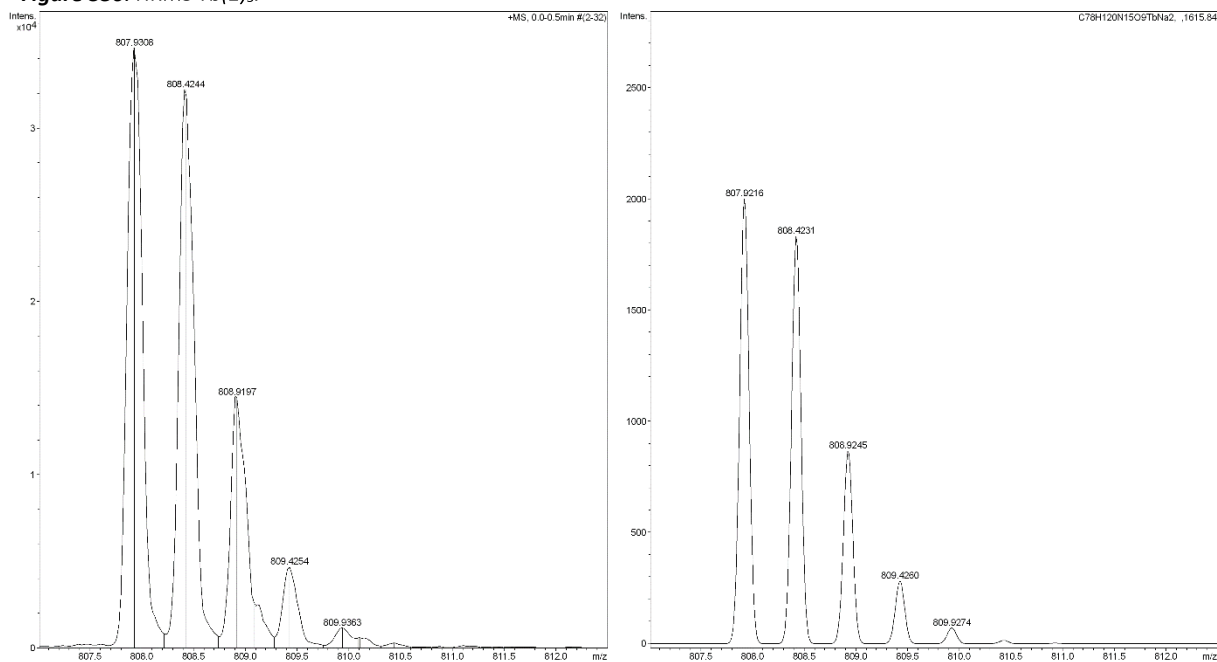


Figure S31. (Left) HRMS $m/z = 807.9306$ $[Tb(1)_3 + 2Na]^{2+}$. (Right) Calc. for $(C_{78}H_{120}N_{15}O_9TbNa_2)^{2+}$, 807.9216.

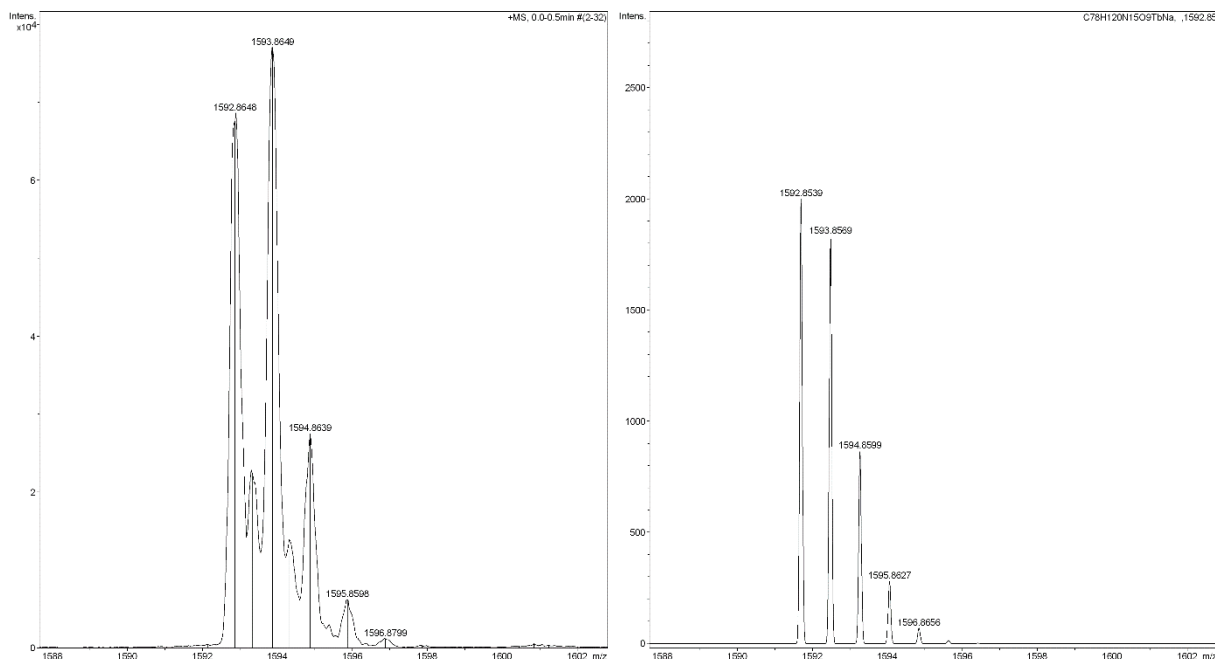


Figure S32. (Left) HRMS $m/z = 1592.8646$ $[\text{Tb}(\mathbf{1})_3 + \text{Na}]^+$. (Right) Calc. for $(\text{C}_{78}\text{H}_{120}\text{N}_{15}\text{O}_9\text{TbNa})^+$, 1592.8539.

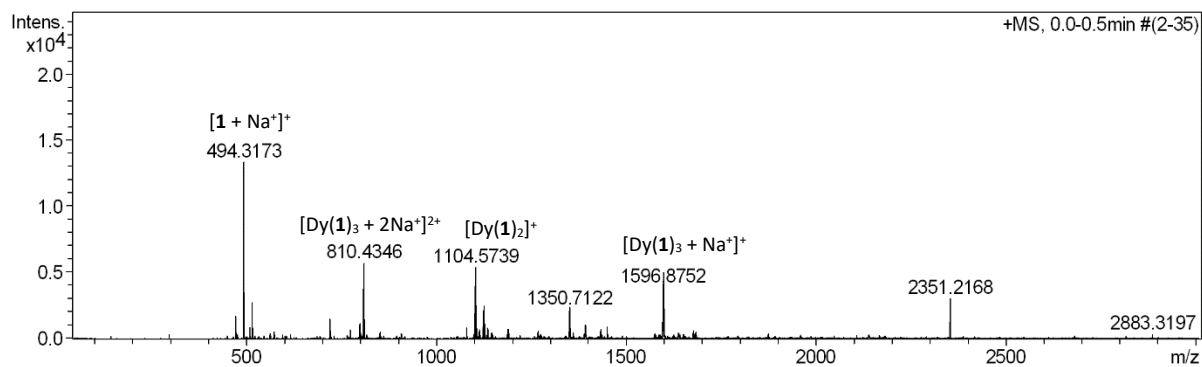


Figure S33. HRMS $\text{Dy}(\mathbf{1})_3$.

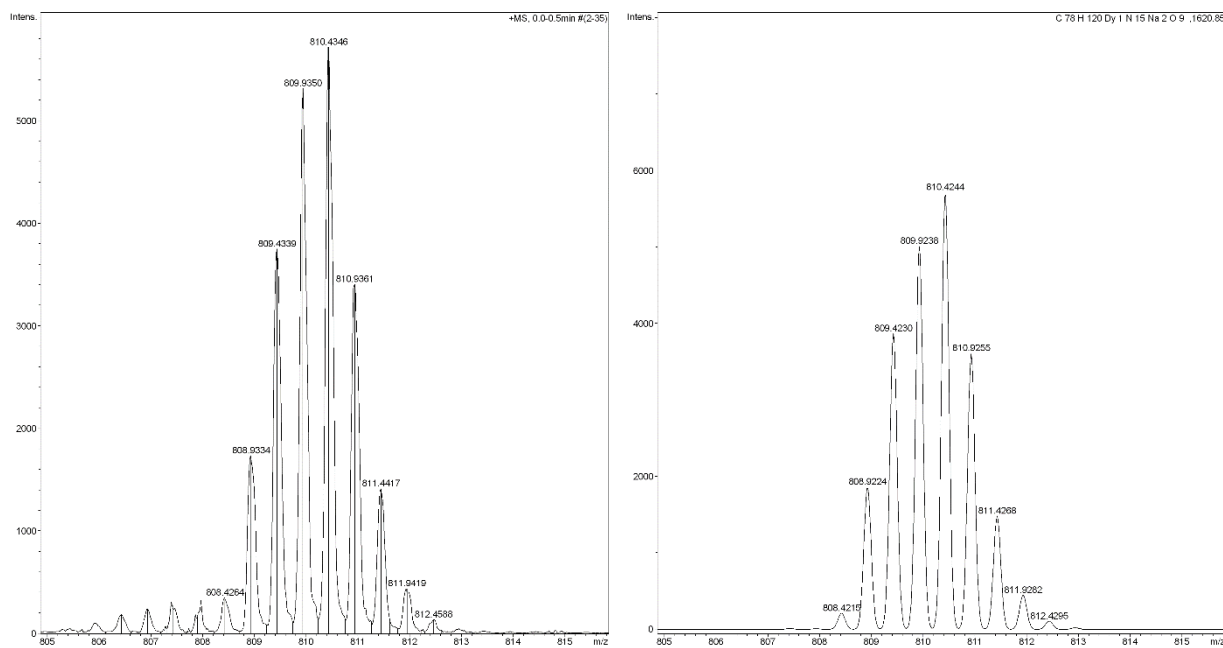


Figure S34. (Left) HRMS $m/z = 810.4346$ $[\text{Dy}(\mathbf{1})_3 + 2\text{Na}]^{2+}$. (Right) Calc. for $(\text{C}_{78}\text{H}_{120}\text{N}_{15}\text{O}_9\text{DyNa}_2)^{2+}$, 810.4244.

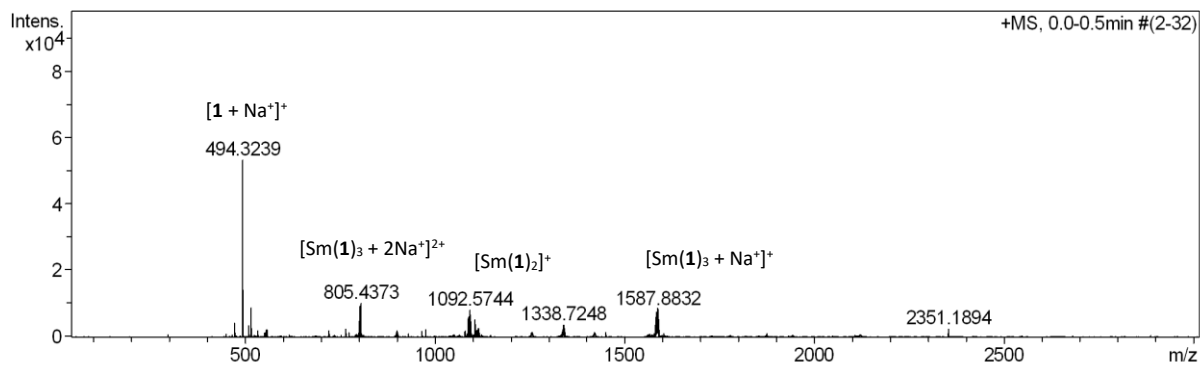


Figure S35. HRMS $\text{Sm}(\mathbf{1})_3$.

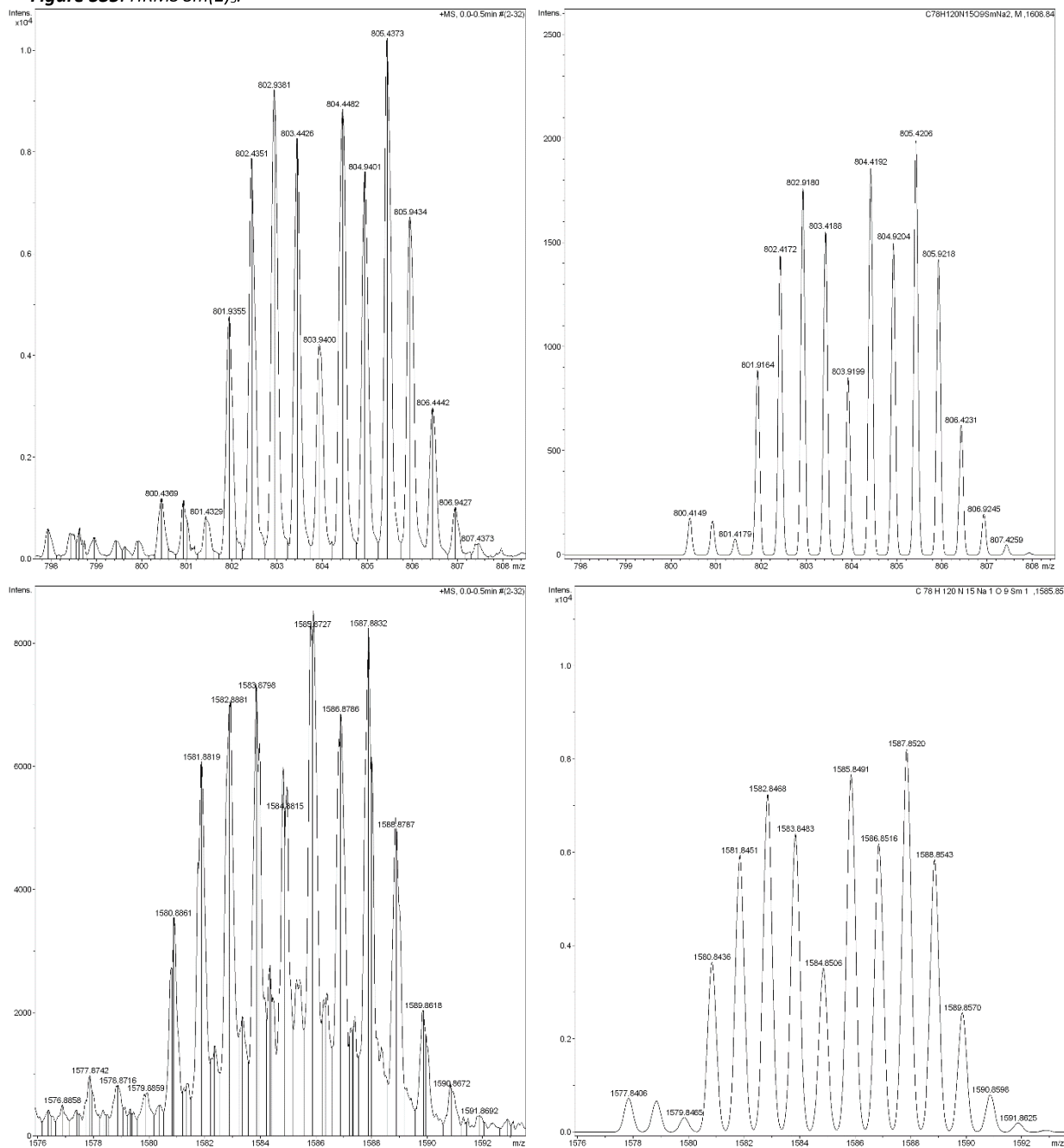


Figure S36. (Top left) HRMS $m/z = 804.4482$ $[\text{Sm}(\mathbf{1})_3 + 2\text{Na}^+]^{2+}$. (Top right) Calc. for $(\text{C}_{78}\text{H}_{120}\text{N}_{15}\text{O}_9\text{SmNa}_2)^{2+}$, 804.4192. (Bottom left) HRMS $m/z = 1585.8727$ $[\text{Sm}(\mathbf{1})_3 + \text{Na}^+]^+$. (Bottom right) Calc. for $(\text{C}_{78}\text{H}_{120}\text{N}_{15}\text{O}_9\text{EuNa})^+$, 1585.8491.

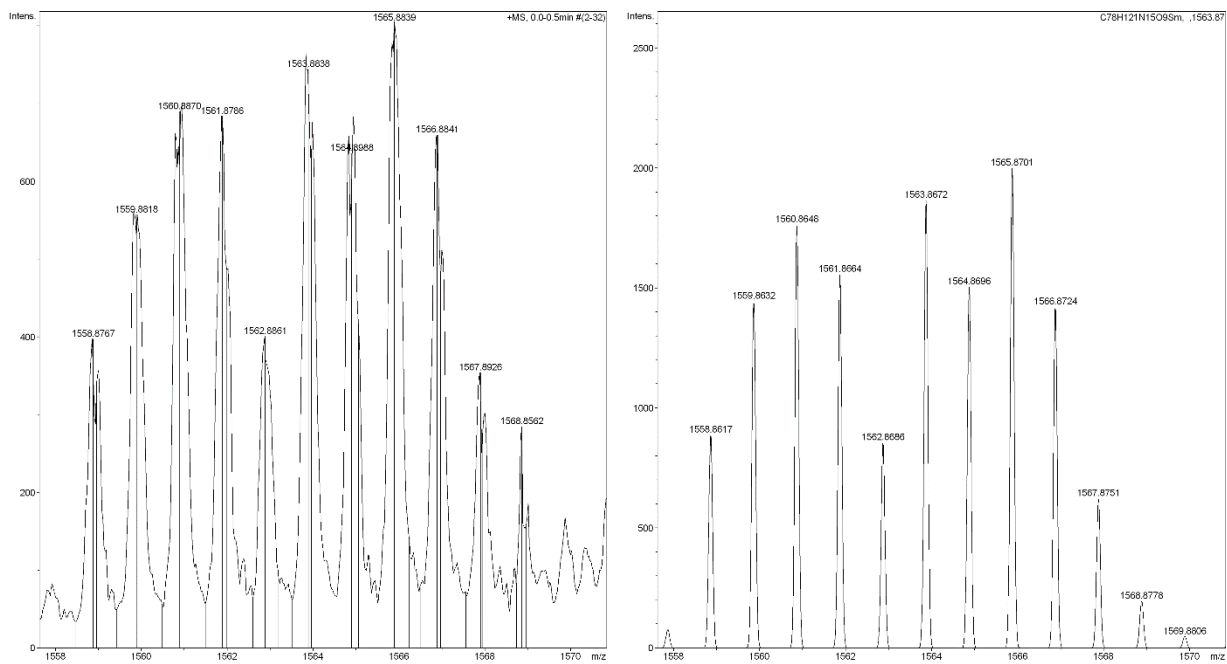


Figure S37. (Left) HRMS $m/z = 1563.8838$ [$Sm(1)_3 + H$] $^+$. (Right) Calc. for $(C_{78}H_{121}N_{15}O_9Sm)^+$, 1563.8672.

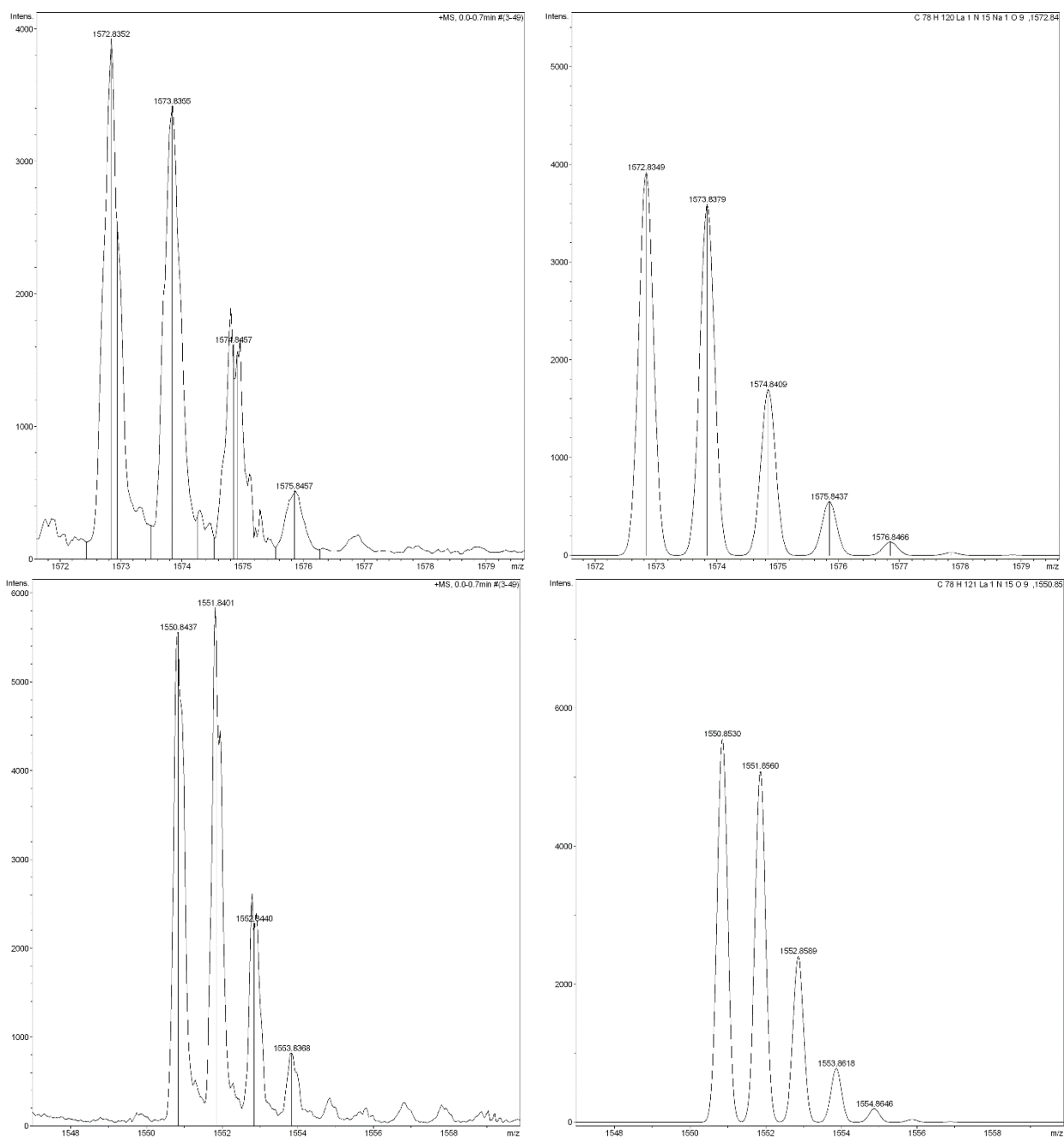


Figure S38. (Top left) HRMS $m/z = 1572.8352 [La(1)_3 + Na]^+$. (Top right) Calc. for $(C_{78}H_{120}N_{15}O_9LaNa)^+$, 1572.8349. (Bottom left) HRMS $m/z = 1550.8437 [La(1)_3 + H]^+$. (Bottom right) Calc. for $(C_{78}H_{121}N_{15}O_9La)^+$, 1550.8530.

Photophysical self-assembly titrations & non-linear regression analysis

Photophysical self-assembly titrations

The formation of 1:1, 1:2 and 1:3 (M:L) species was monitored by measuring changes in the UV-visible absorption and steady-state spectrum of a solution of ligand **1** (2×10^{-5} M MeOH:DCM:MeCN (0.005:0.005:9.99)) when titrated with $\text{Eu}(\text{CF}_3\text{SO}_3)_3 \cdot 6\text{H}_2\text{O}$ solution in MeCN (0 \rightarrow 4.5 equivalents) after being deprotonated by 1 equivalent of tetramethylammonium hydroxide. Titrations were carried out in triplicate and then fitted with ReactLab™ Equilibrium¹⁰ for non-linear regression analysis, however only steady-state data could be fit.

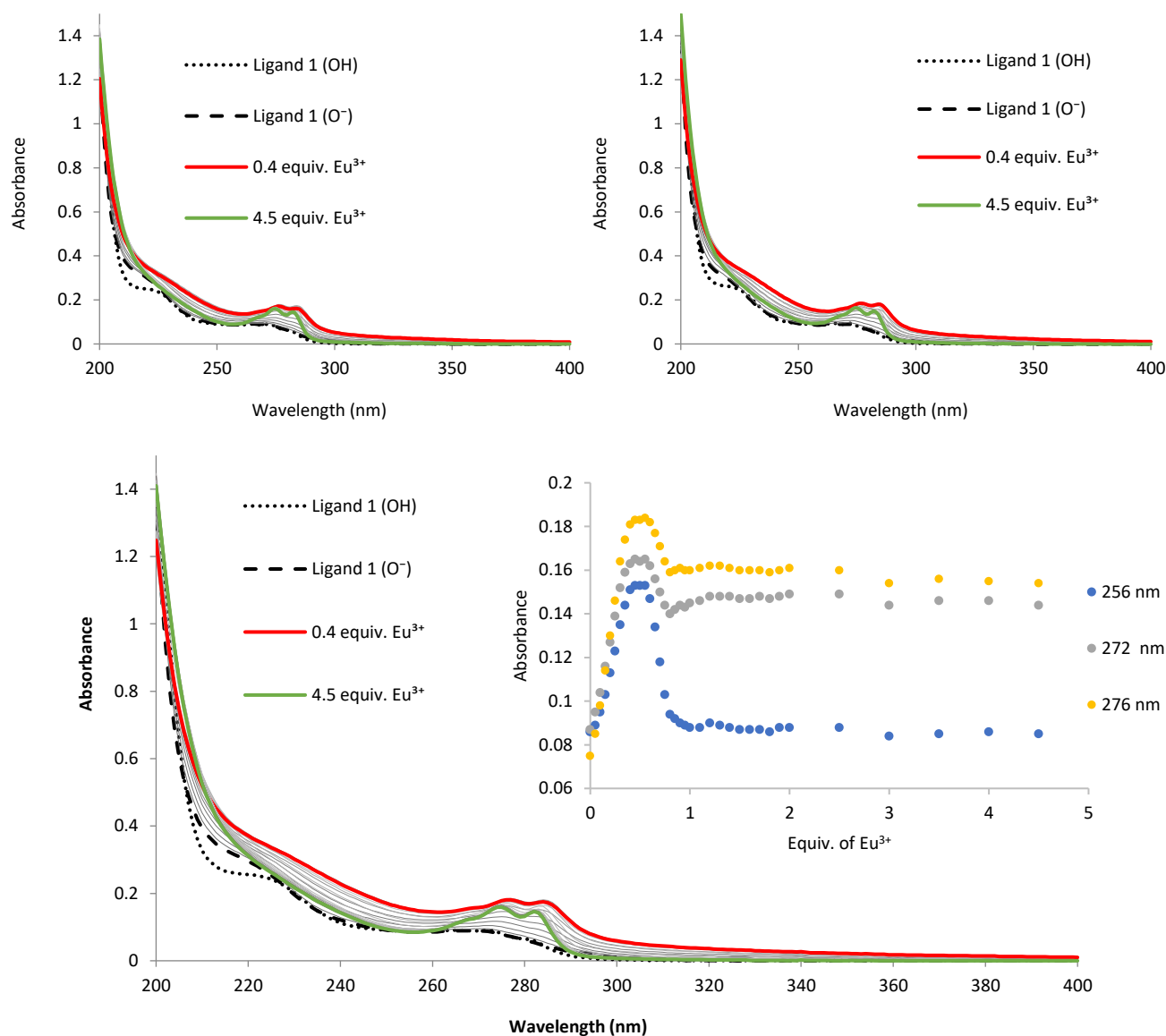


Figure S40. UV-visible absorption titration of **1** with $\text{Eu}(\text{CF}_3\text{SO}_3)_3$ 0 to 4.5 equivalents, done in triplicate. Insert: Monitoring changes in absorbance vs Ln equivalents at $\lambda = 256, 272$ and 276 nm. Upon the addition of 1 equivalent of TMAO base, the distinctive shoulder peaks associated with the central pyridine unit merge around 260–290 nm, while an absorbance increase is also observed from 210 to 220 nm. Upon the addition of Eu^{3+} salt significant increases are observed from 0 to 0.4 equivalents associated with the formation of the 1:3 M:L species. This increase stagnates until 0.6 equivalents, where significant absorbance decrease is observed from 0.6 to 0.8 or 1 equivalents where absorbance plateaus, indicative of the deformation into subspecies either 1:2 or 1:1 M:L species. Also a significant red shift is observed around 260–290 nm. From 0 to 0.4 equivalents indicative of lanthanide coordination pulling electron density out of the system. This red shift, similar to absorbance increase, stagnates from 0.4 to 0.6 equivalents, where upon 0.65 equivalents a reverse blue shift occurs until 0.8 or 1 equivalents.

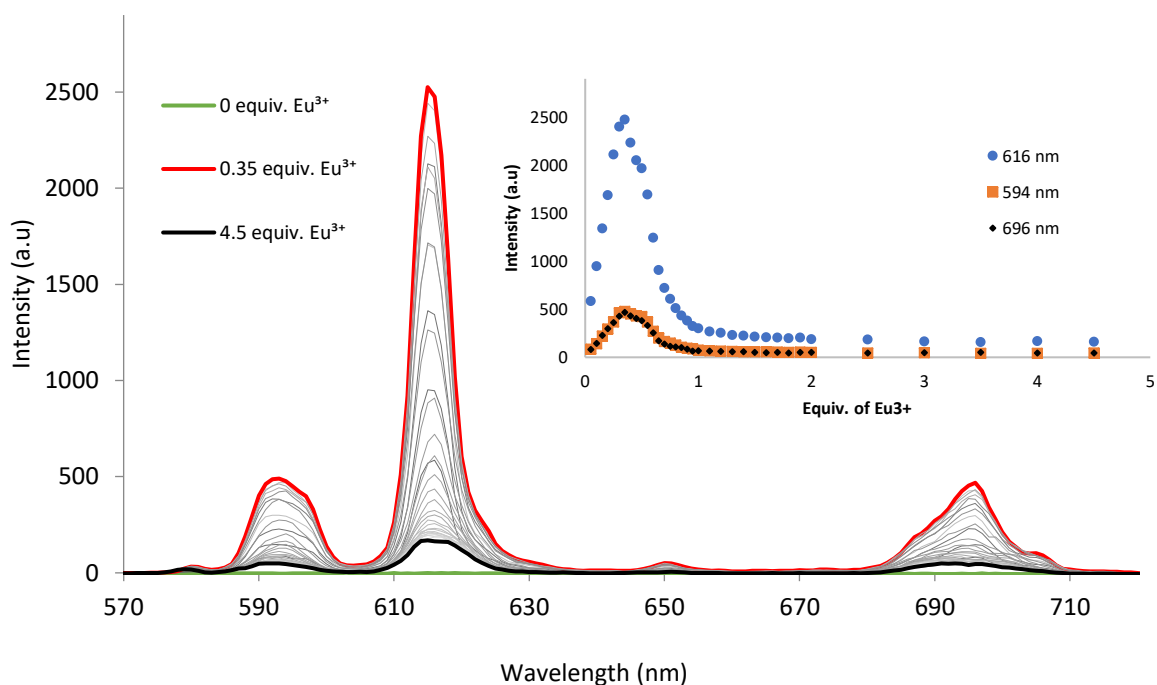
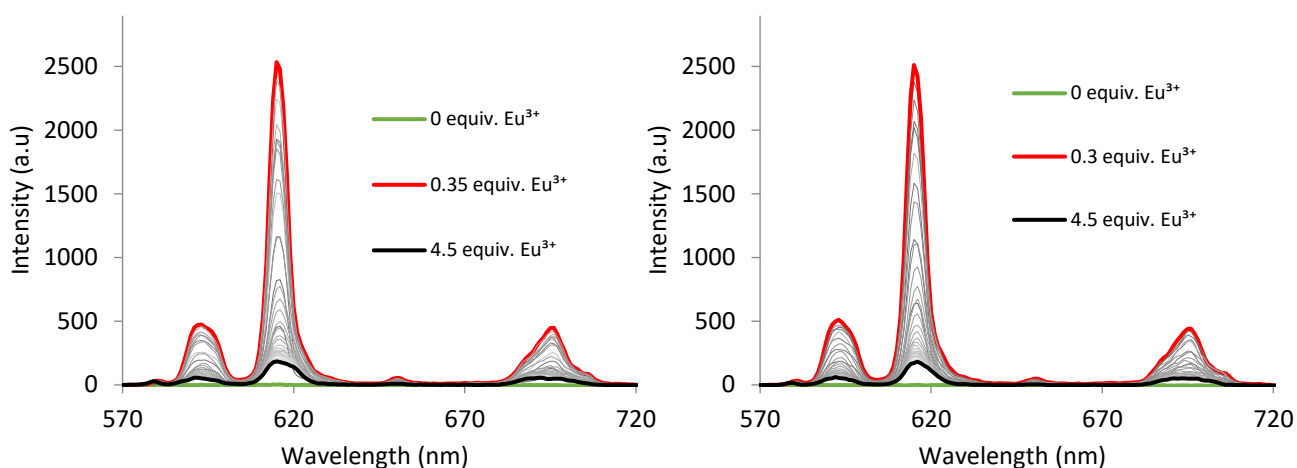
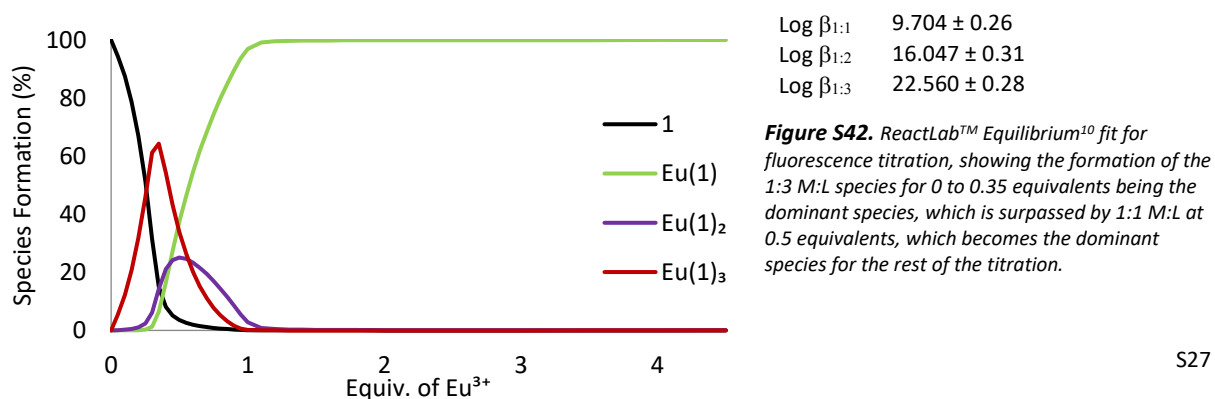


Figure S41. Fluorescence titration of **1** with $\text{Eu}(\text{CF}_3\text{SO}_3)_3$ 0 to 4.5 equivalents, done in triplicate. Insert: Monitoring changes in emission vs Ln equivalents at $\lambda = 594, 616$ and 696 nm. Upon the addition of Eu^{3+} salt significant increases are observed from 0 to 0.3 or 0.35 equivalents reaching a maximum intensity. This is associated with the formation of the 1:3 M:L species with the three-antenna surrounding the lanthanide ion. Upon further addition of Eu^{3+} salt significant decrease in emission is observed until a plateau is reached around 1 equivalent, indicative of the evolutionary formation of the 1:2 and 1:1 M:L species.



Langmuir Blodgett

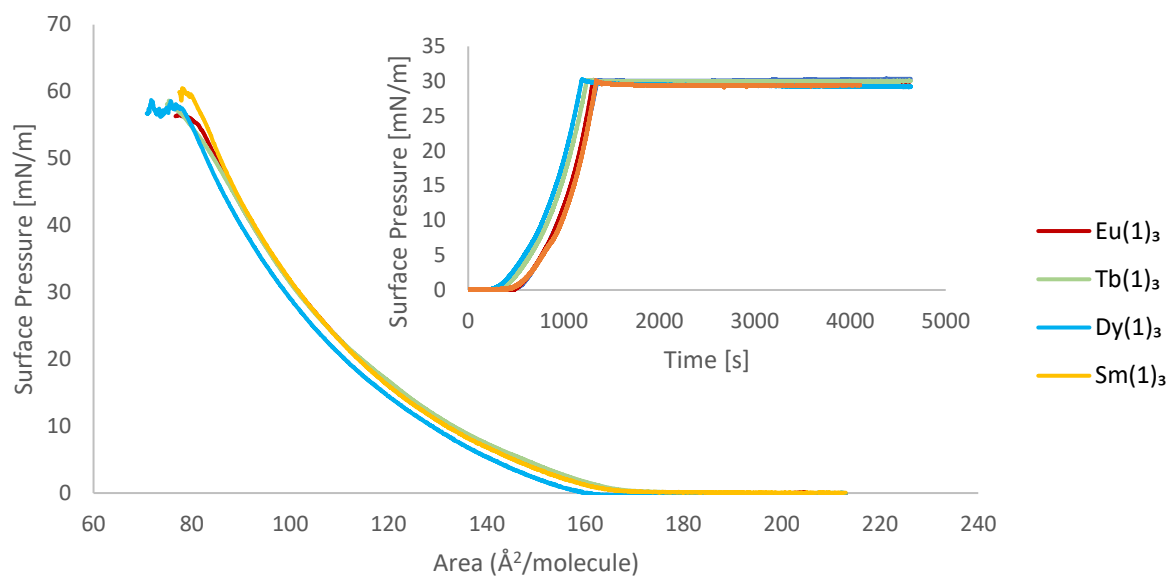


Figure S43. Surface area – pressure isotherms, of $\text{Ln}(\mathbf{1})_3$ complexes where $\text{Ln} = \text{Eu}^{3+}, \text{Tb}^{3+}, \text{Dy}^{3+}$ and Sm^{3+} . Insert: Surface pressure -stability of said complexes at 30 mN/m over the course of more than an hour.

Table S1. The transfer ratio (TR) is calculated by the decrease of area over the total substrate surface area which is $2(20 \text{ mm} \times 30 \text{ mm}) = 1200 \text{ mm}^2$ for two sides and $2(20 \text{ mm} \times 1 \text{ mm}) + (30 \text{ mm} \times 1 \text{ mm}) = 70 \text{ mm}^2$ edges, total = 1270 mm^2 . For example, $\text{Eu}(\mathbf{1})_3$ monolayer $\text{Tr} = 1335/1270 \text{ mm}^2 = 1.05$.

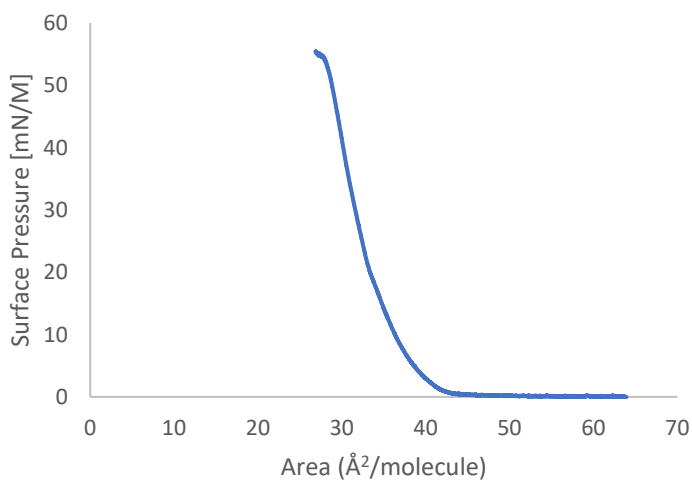


Figure S44. Surface area – pressure isotherms of **1**.

Langmuir Blodgett Films of	TR
$\text{Eu}(\mathbf{1})_3$	1.05
$\text{Eu}(\mathbf{1})_3$ Triple layered	1.09, 0.51, 1.06
$\text{Eu}(\mathbf{1})_3$ Five layered	1.15, 0.43 1.20, 0.74, 1.01
$\text{Eu}(\mathbf{1})_3$ Seven layered	1.03, 0.33 1.15, 0.63, 1.07, 0.68, 1.1
$\text{Tb}(\mathbf{1})_3$	1.04
$\text{Sm}(\mathbf{1})_3$	1.01
$\text{Dy}(\mathbf{1})_3$	1.01
$\text{Eu}(\mathbf{1})_3\text{Tb}(\mathbf{1})_3$ 1:1 mixture	1.13
$\text{Eu}(\mathbf{1})_3\text{Dy}(\mathbf{1})_3$ 1:10 mixture	1
$\text{Eu}(\mathbf{1})_3\text{Tb}(\mathbf{1})_3\text{Dy}(\mathbf{1})_3$ 1:1:1 mixture	0.98
$\text{Eu}(\mathbf{1})_3\text{Tb}(\mathbf{1})_3\text{Dy}(\mathbf{1})_3$ 1:1:10 mixture	0.98
$\text{Eu}(\mathbf{1})_3\text{Tb}(\mathbf{1})_3\text{Dy}(\mathbf{1})_3\text{Sm}(\mathbf{1})_3$ 1:1:1:1 mixture	0.97
$\text{Eu}(\mathbf{1})_3\text{Tb}(\mathbf{1})_3\text{Dy}(\mathbf{1})_3\text{Sm}(\mathbf{1})_3$ 1:1:10:10 mixture	1.06
$\text{Eu}(\mathbf{1})_3\text{Tb}(\mathbf{1})_3\text{Dy}(\mathbf{1})_3\text{Sm}(\mathbf{1})_3$ 1:1:10:50 mixture	1.02

Table S2. Langmuir film collapse position.

Complex or Ligand	Surface-pressure at collapse (mN/m)	Area =(Å²/molecule)
1	53	28
$\text{Eu}(\mathbf{1})_3$	55	81
$\text{Tb}(\mathbf{1})_3$	56	78
$\text{Sm}(\mathbf{1})_3$	59	80
$\text{Dy}(\mathbf{1})_3$	57	78

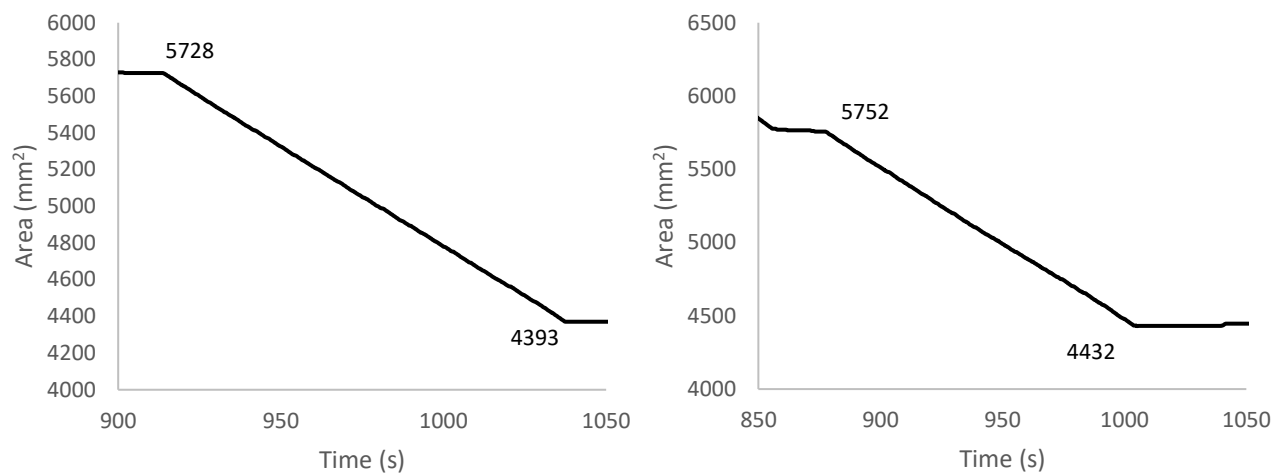


Figure S45. Zoomed in deposition plots of monolayer $\text{Eu}(1)_3$ (right) and (left) $\text{Tb}(1)_3$ LB films.

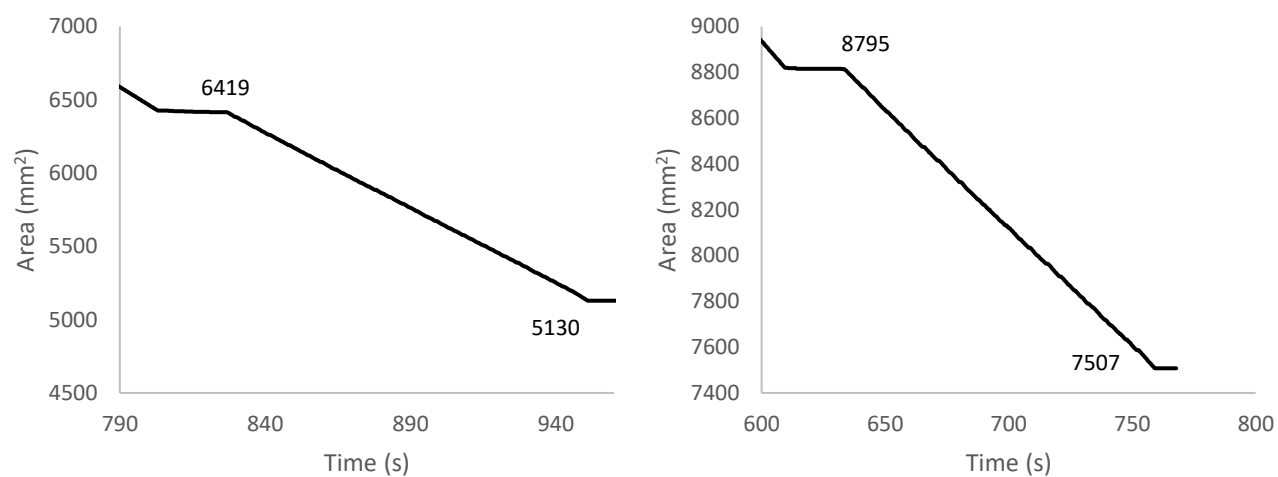


Figure S46. Zoomed in deposition plots of monolayer $\text{Dy}(1)_3$ (right) and (left) $\text{Sm}(1)_3$ LB films.

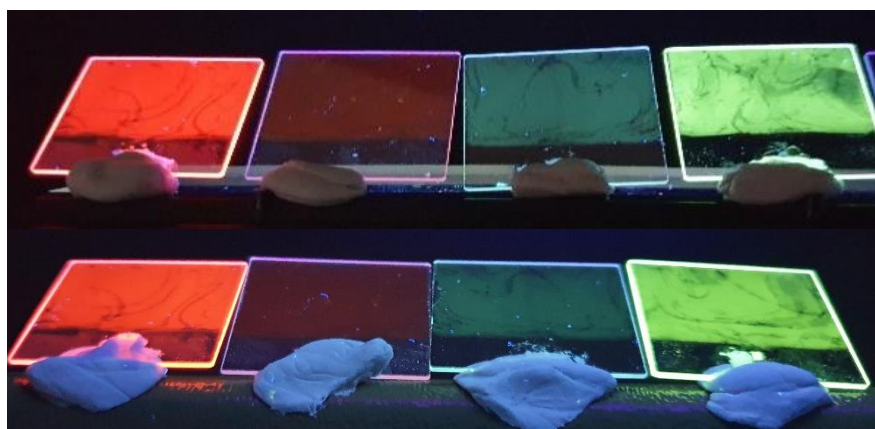


Figure S47. (Top) LB films fresh after deposition and (bottom) LB films 6 months after initial deposition.

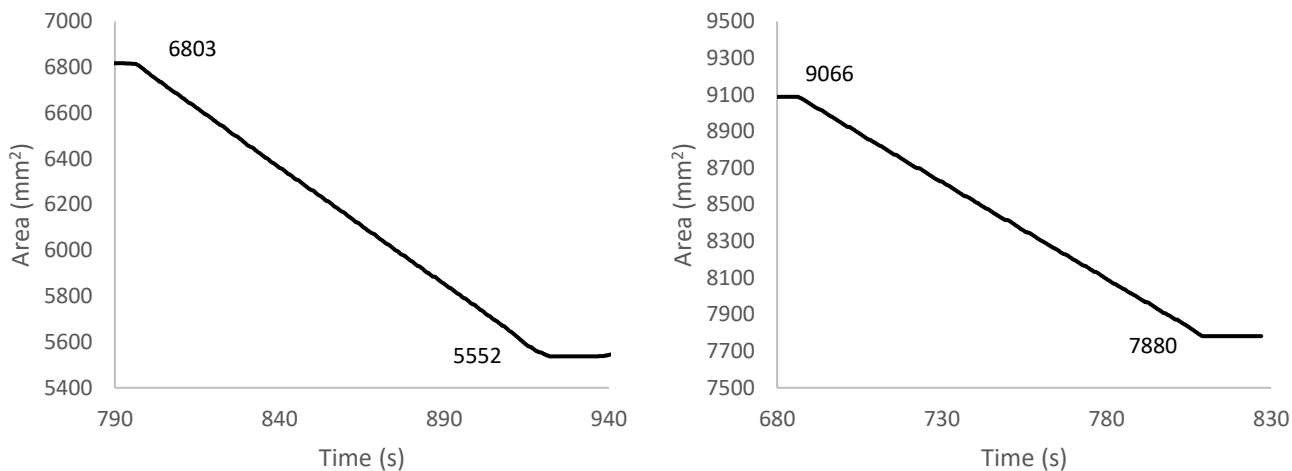


Figure S48. Zoomed in deposition plots of monolayer Eu(1)₃:Dy(1)₃ (1:1) (right) and (left) Eu(1)₃:Dy(1)₃ (1:10) LB films.

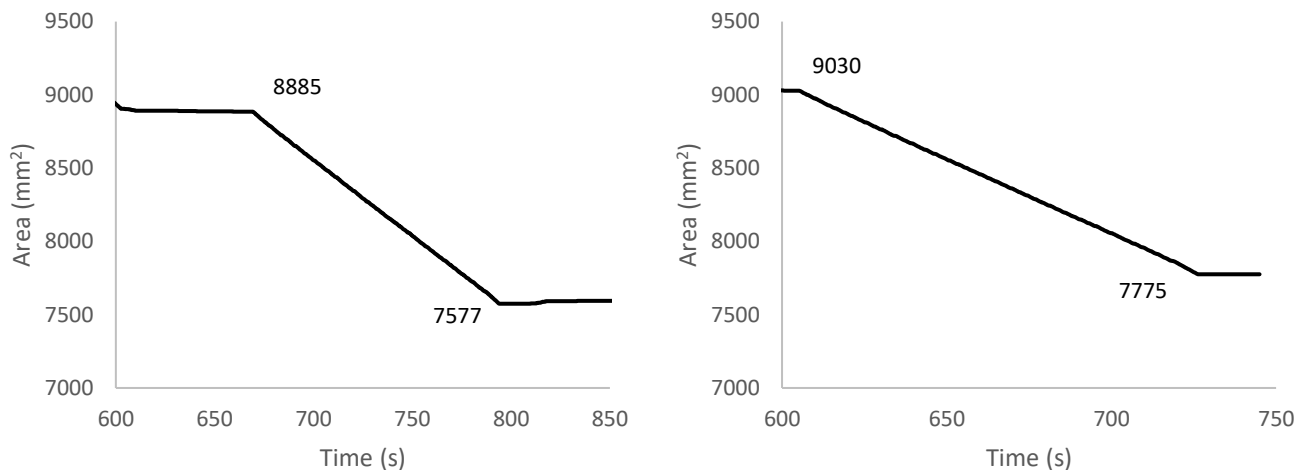


Figure S49. Zoomed in deposition plots of monolayer Eu(1)₃:Tb(1)₃:Dy(1)₃ (1:1:1) (right) and (left) Eu(1)₃:Tb(1)₃:Dy(1)₃ (1:1:10) LB films.

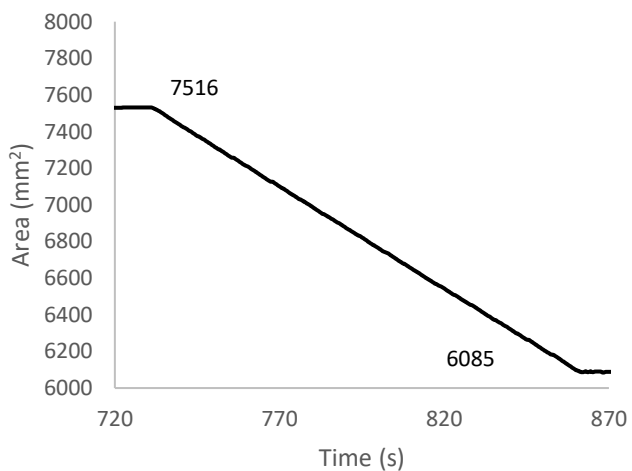


Figure S50. Zoomed in deposition plot of monolayer Eu(1)₃:Tb(1)₃ (1:1) LB film.

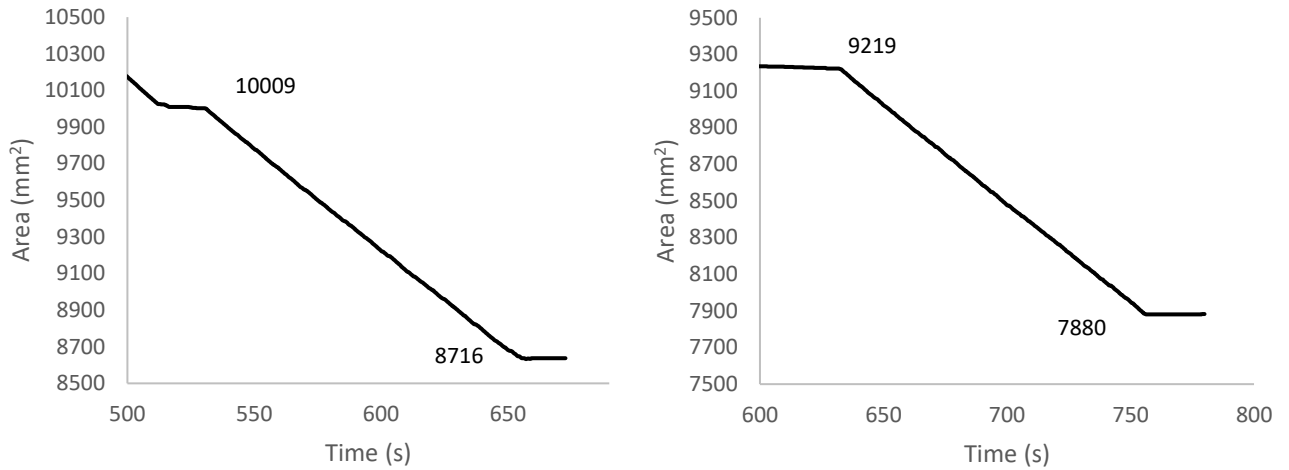


Figure S51. Zoomed in deposition plots of monolayer $\text{Eu}(1)_3\text{Tb}(1)_3\text{Dy}(1)_3\text{Sm}(1)_3$ (Left) 1:1:10:10 and (right) 1:1:10:50 LB films.

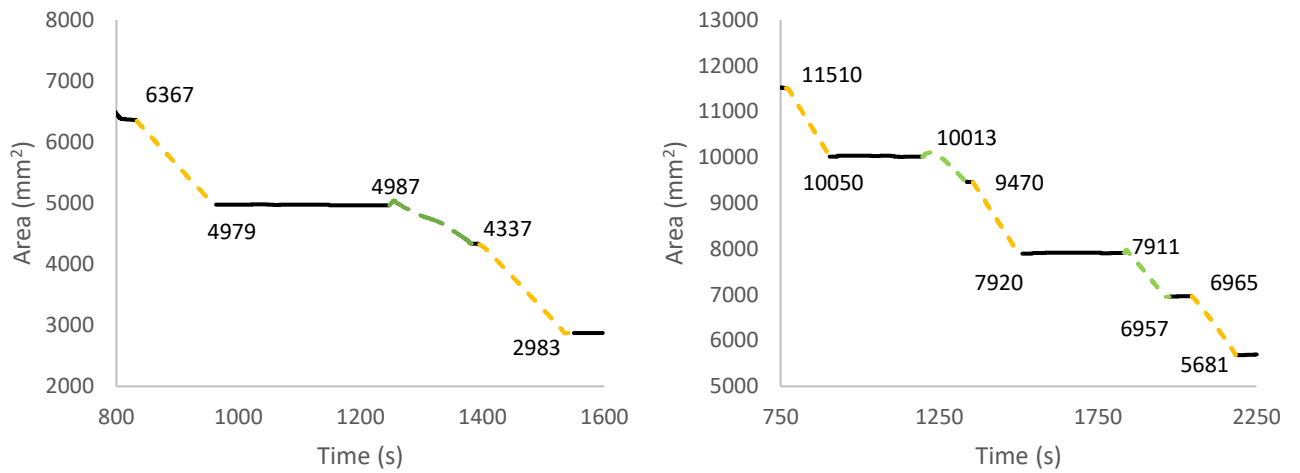


Figure S52. Zoomed in deposition plots of triple layer $\text{Eu}(1)_3$ LB film (right) and five layer $\text{Eu}(1)_3$ LB films. Yellow – immersion, green – emersion.

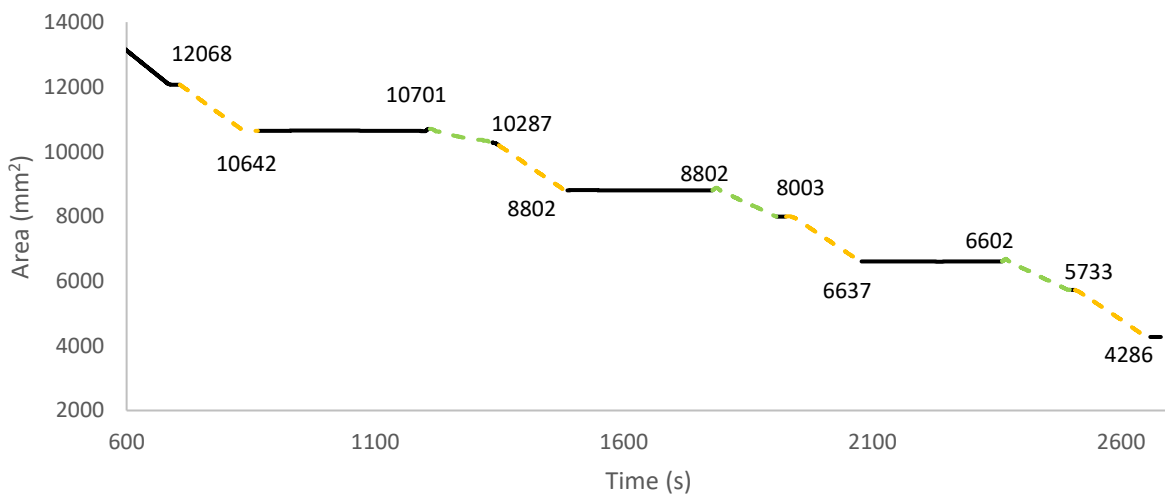


Figure S53. Zoomed in deposition plots of seven-layer $\text{Eu}(1)_3$ LB film. Yellow – immersion, green – emersion

Lanthanide complex bulk and film characterisation

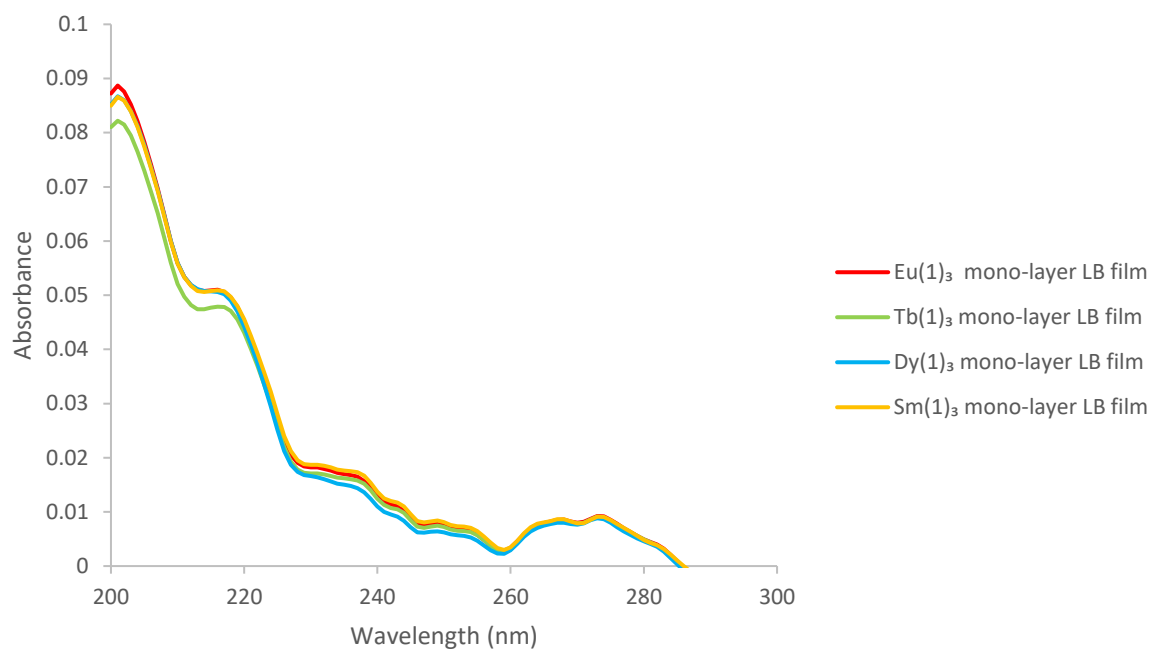


Figure S54. UV-visible absorption Ln(1)₃ where Ln = Eu³⁺, Tb³⁺, Dy³⁺ and Sm³⁺ on monolayer LB films.

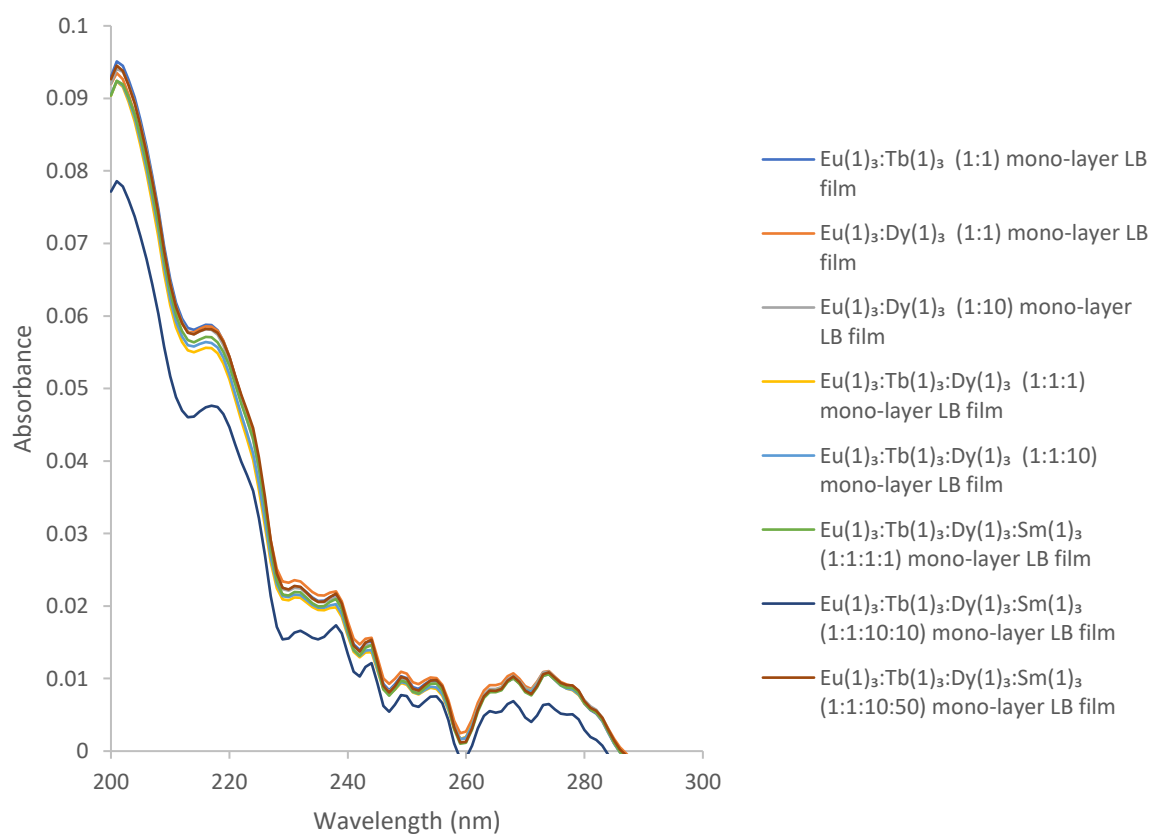


Figure S55. UV-visible absorption of mixed mono-layer LB films.

FT-IR

FT-IR measurements were taken on a multi-layered LB film (specifically an 8 layered film) of $\text{Eu}(\mathbf{1})_3$ deposited on a CaF_2 slide which was pre-washed by sonicating in $(\text{CH}_3)_2\text{CO}$, MeOH and finally with type 1 water.



Figure S56. 8 layered $\text{Eu}(\mathbf{1})_3$ film on CaF_2 slide.

Table S3. IR stretch difference of solid ligand and $\text{Eu}(\mathbf{1})_3$ complex compared to on the CaF_2 slide.

IR stretch	Solid 1	Solid $\text{Eu}(\mathbf{1})_3$	Film $\text{Eu}(\mathbf{1})_3$
CH_2	2919 and 2849 cm^{-1}	2919 and 2849 cm^{-1}	2945, 2918 and 2850 cm^{-1}
$\text{C}=\text{O}$	1744 and 1668 cm^{-1}	1640-1625 cm^{-1}	1638 cm^{-1}

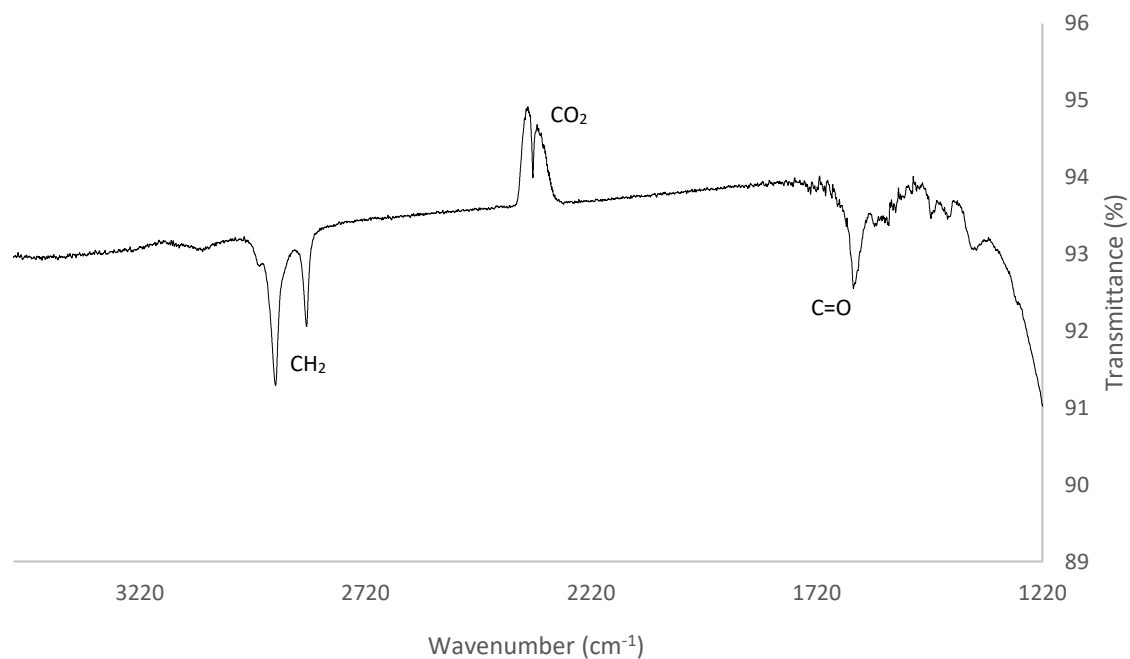


Figure S57. Infra-red spectra of $\text{Eu}(\mathbf{1})_3$ on a CaF_2 slide with 8 layers.

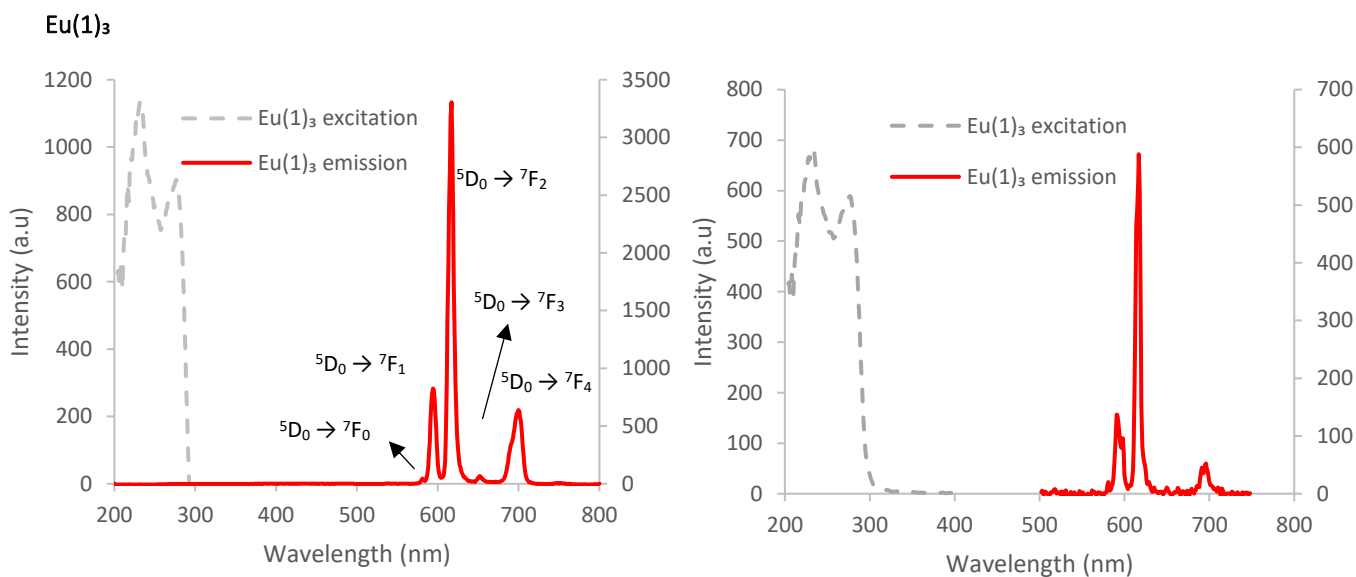


Figure S58. (Left) Steady-state emission and excitation spectra (monitoring 616 nm) of $\text{Eu}(\mathbf{1})_3$ in MeCN (0.01 mM). (Right) Time-resolved emission and excitation spectra (monitoring 616 nm) of $\text{Eu}(\mathbf{1})_3$ in MeCN (0.01 mM). Notably the emission at 580 nm assigned to the ${}^5\text{D}_0 \rightarrow {}^7\text{F}_0$, although commonly weak, allows for the point symmetry to be narrowed down to a selected few (C_{nv} , C_n or C_s), further reduced down to a likely C_3 or possible but unlikely C_{3v} . This indicates that the ligands retain a similar orientation with respect to one another.

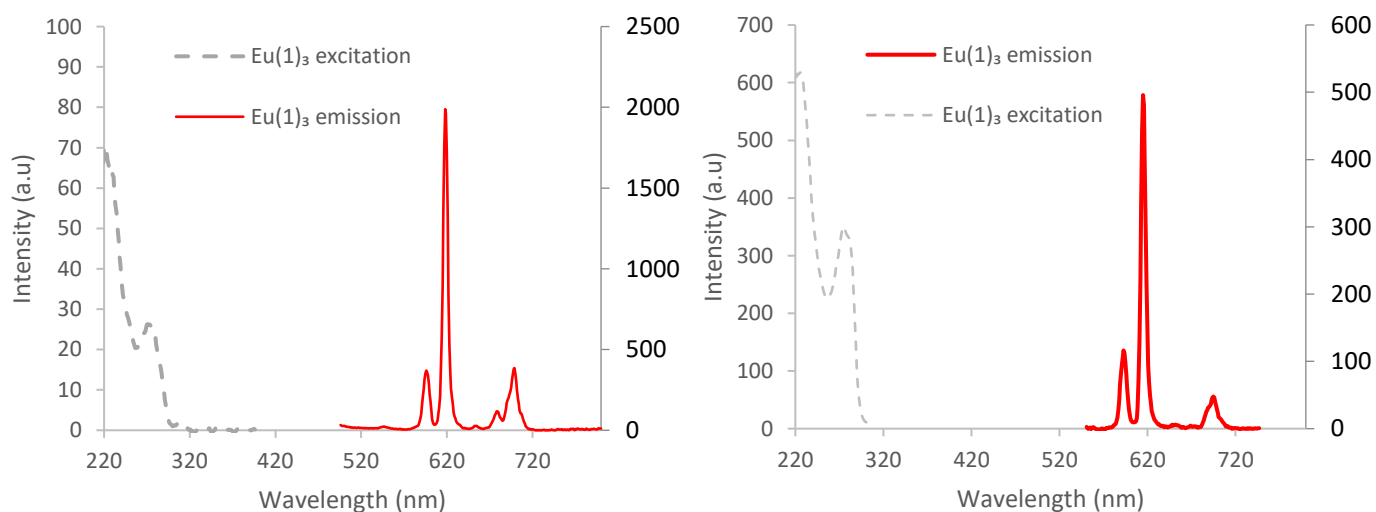


Figure S59. (Left) Steady-state emission and excitation spectra (monitoring 616 nm) of monolayer LB film of $\text{Eu}(\mathbf{1})_3$. (Right) Time-resolved emission and excitation spectra (monitoring 616 nm) of monolayer LB film of $\text{Eu}(\mathbf{1})_3$.

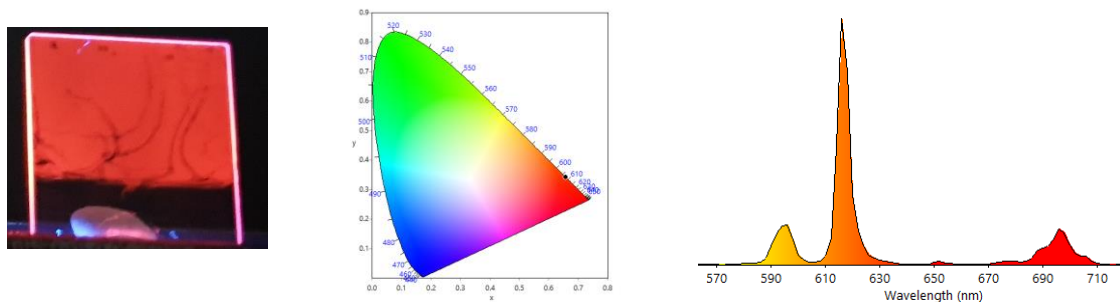


Figure S60. (Left) Image of monolayer film of $\text{Eu}(\mathbf{1})_3$. (Middle) 1931 CIE chromaticity diagram with calculated CIE coordinates of $x = 0.6593$ and $y = 0.3403$. (Right) Fluorescent emission plot of monolayer LB film used to generate CIE plot, also showing corresponding colour gradient to emission wavelength. Both plots were generated by ColourCalculator ver. 7.77 software, licenced by OSRAM.⁶

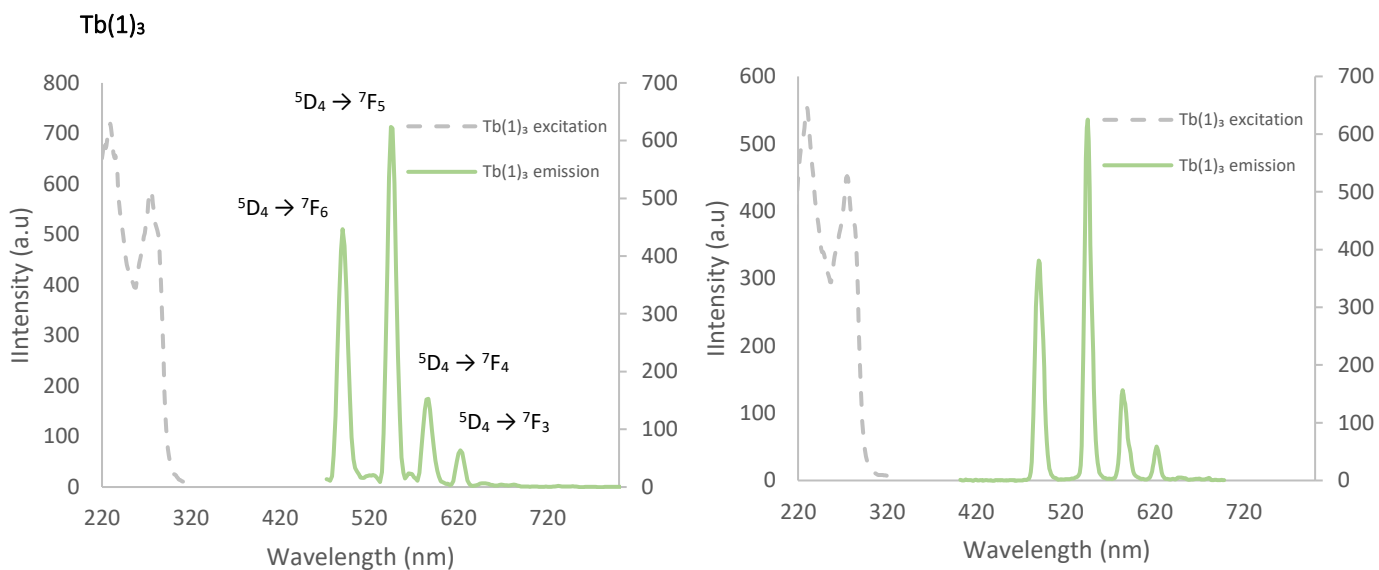


Figure S61. (Left) Steady-state emission and excitation spectra (monitoring 545 nm) of $Tb(1)_3$ in MeCN (0.01 mM). (Right) Time-resolved emission and excitation spectra (monitoring 545 nm) of $Tb(1)_3$ in MeCN 0.01 mM.

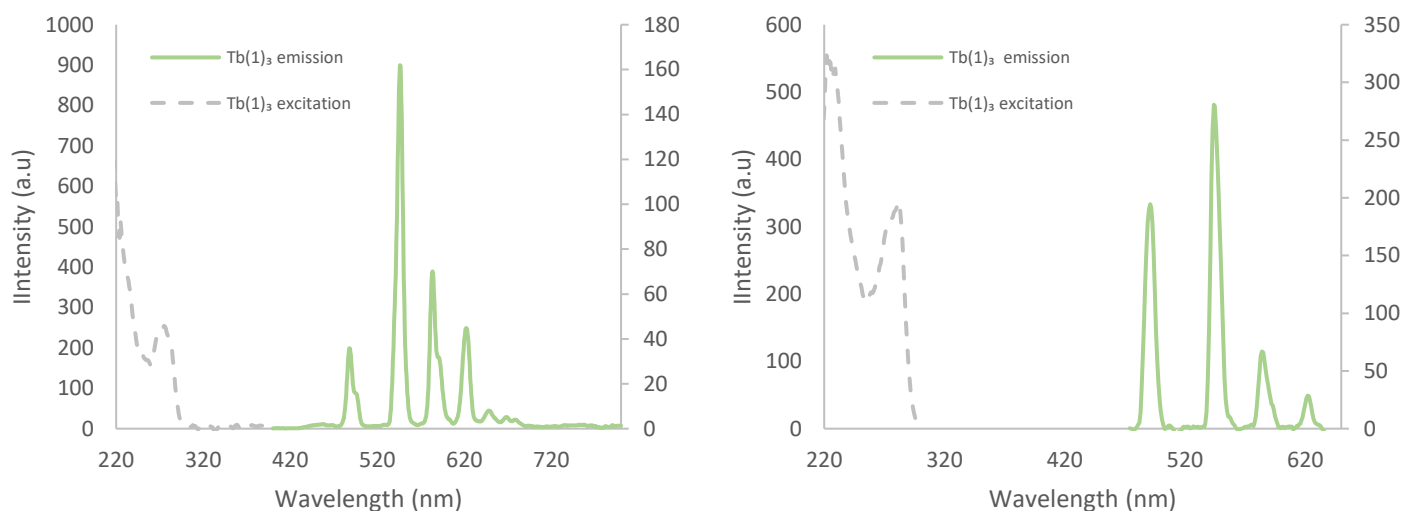


Figure S62. (Left) Steady-state emission and excitation spectra (monitoring 545 nm) of $Tb(1)_3$ in MeCN films. (Right) Time-resolved emission and excitation spectra (monitoring 545 nm) of $Tb(1)_3$ in MeCN (0.01 mM).

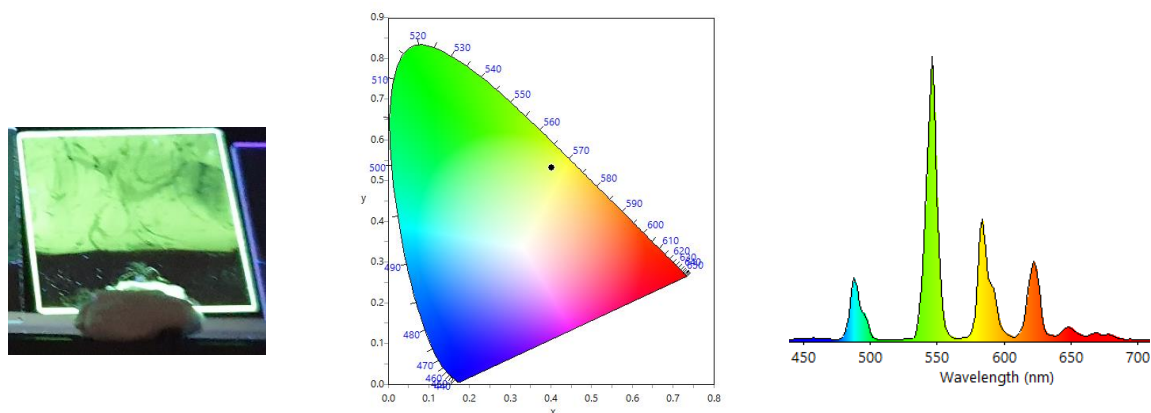


Figure S63. (Left) Image of monolayer film of $Tb(1)_3$. (Middle) 1931 CIE chromaticity diagram with calculated CIE coordinates of $x = 0.4011$ and $y = 0.5322$. (Right) Fluorescent emission plot of monolayer LB film used to generate CIE plot, also showing corresponding colour gradient to emission wavelength. Both plots were generated by ColourCalculator ver. 7.77 software, licenced by OSRAM.⁶

Dy(1)₃

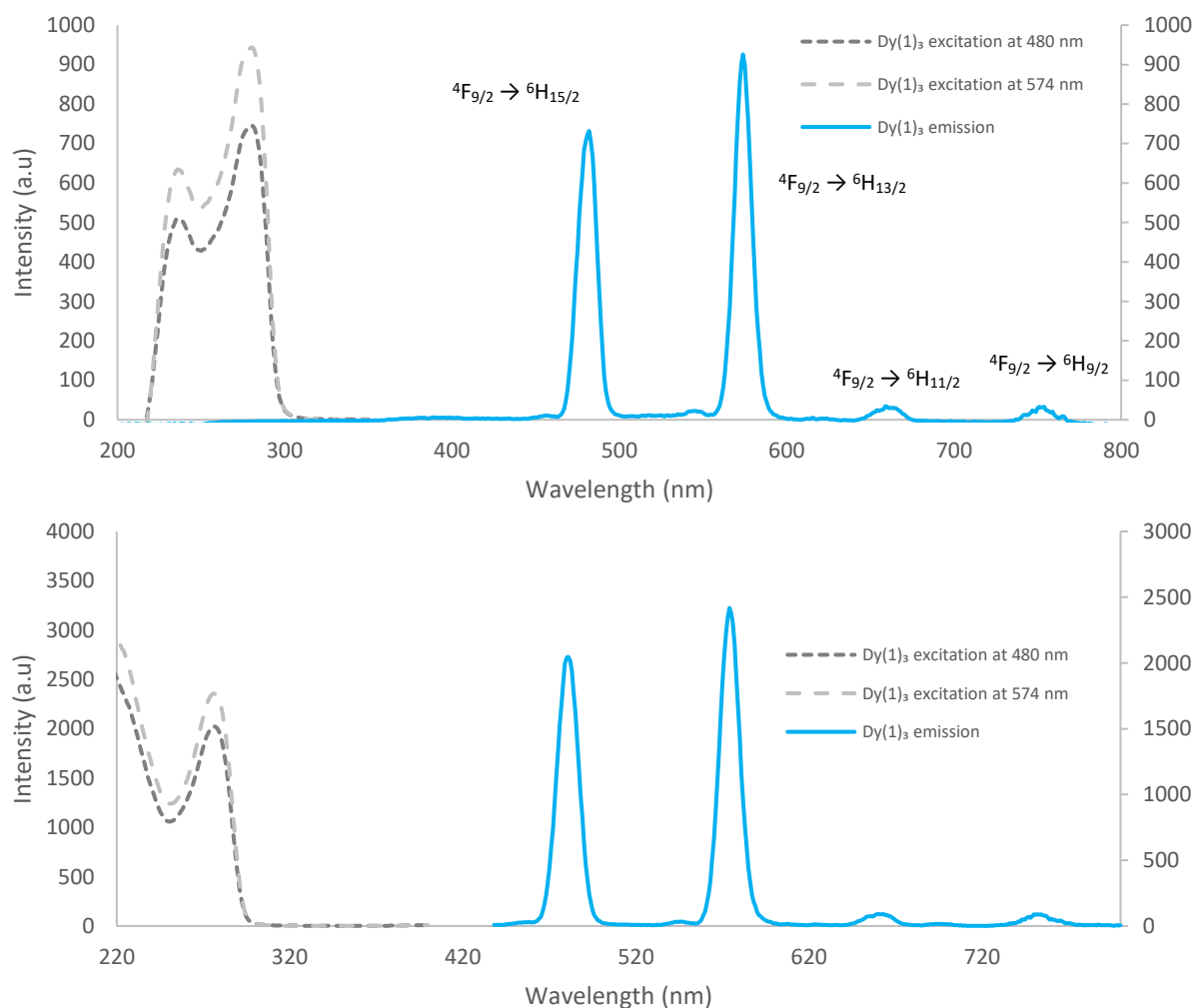


Figure S64. (Top) Steady-state emission and excitation plots of Dy(1)₃ in MeCN (0.01 mM). (Bottom) Steady-state emission and excitation plots of Dy(1)₃ monolayer film.

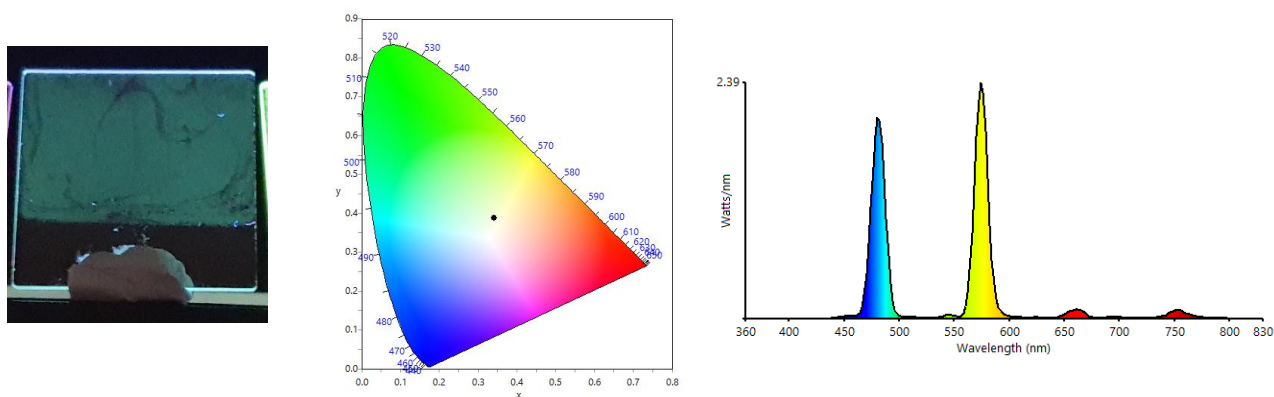


Figure S65. (Left) Image of monolayer film of Dy(1)₃. (Middle) 1931 CIE chromaticity diagram with calculated CIE coordinates of $x = 0.3416$ and $y = 0.3876$. (Right) Fluorescent emission plot of monolayer LB film used to generate CIE plot, also showing corresponding colour gradient to emission wavelength. Both plots were generated by ColourCalculator ver. 7.77 software, licenced by OSRAM.⁶

Sm(1)₃

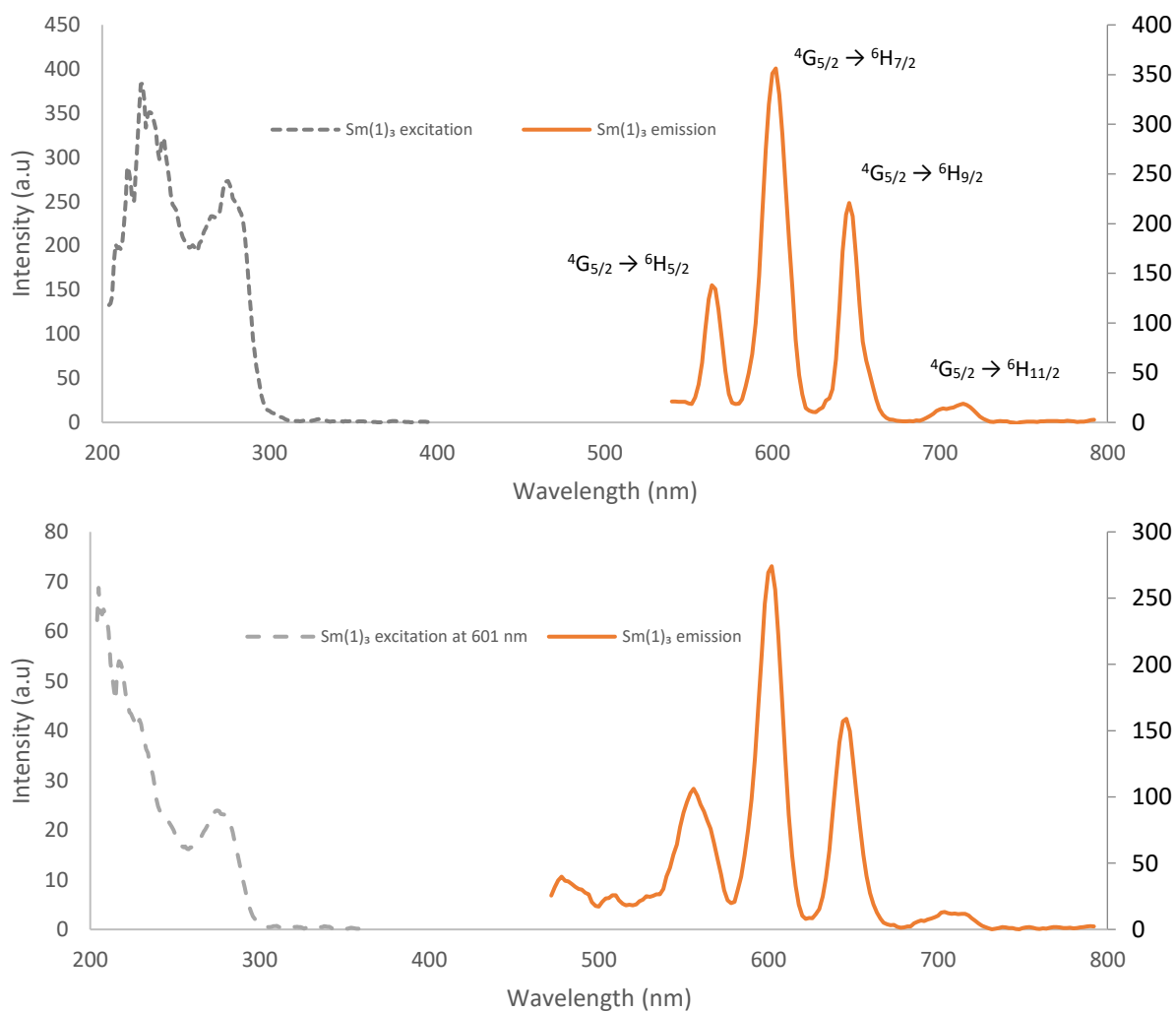


Figure S66. (Top) Steady-state emission and excitation spectra (monitoring 600 nm) of Sm(1)₃ in MeCN (0.01 mM). (Bottom) Steady-state emission and excitation spectra (monitoring 600 nm) of Sm(1)₃ monolayer film.

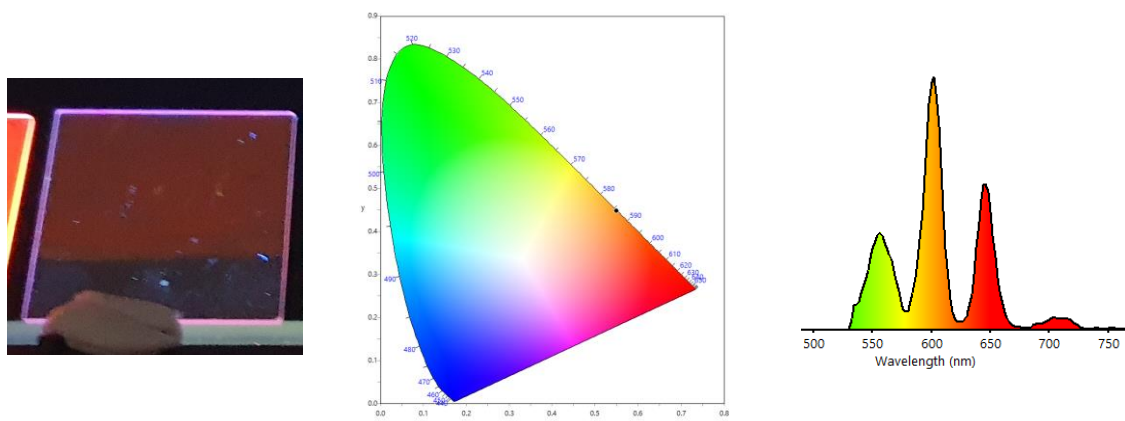


Figure S67. (Left) Image of monolayer film of Dy(1)₃. (Middle) 1931 CIE chromaticity diagram with calculated CIE coordinates of $x = 0.5504$ and $y = 0.4478$. (Right) Fluorescent emission plot of monolayer LB film used to generate CIE plot, also showing corresponding colour gradient to emission wavelength. Both plots were generated by ColourCalculator ver. 7.77 software, licenced by OSRAM.⁶

Tb:Eu mixed monolayer 1:1 ratio

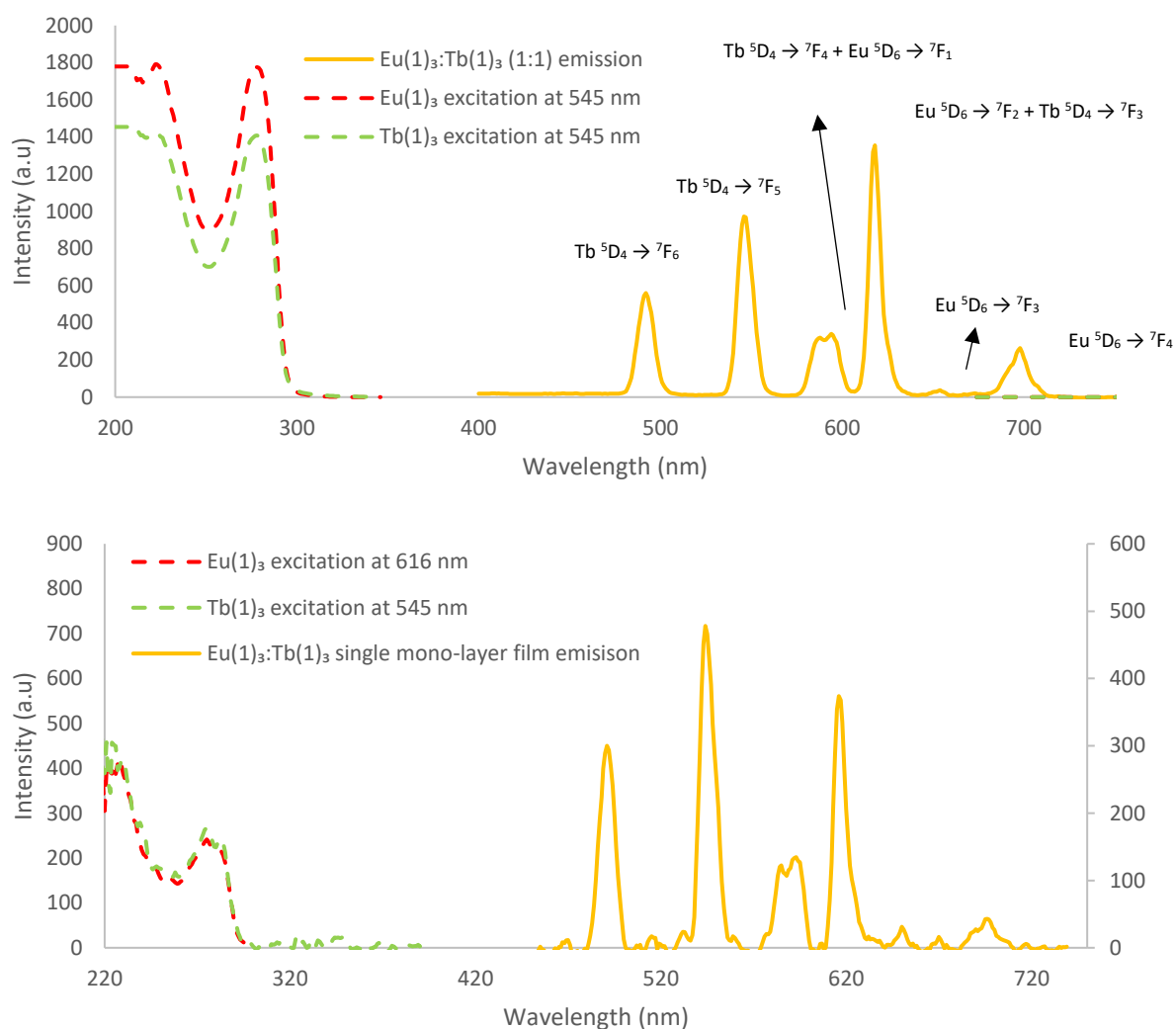


Figure S68. (Top) Steady-state emission and excitation plots of $\text{Eu}(\mathbf{1})_3:\text{Tb}(\mathbf{1})_3$ (1:1) in monolayer film. (Bottom) Time-resolved emission and excitation plots of $\text{Eu}(\mathbf{1})_3:\text{Tb}(\mathbf{1})_3$ (1:1) in monolayer film.

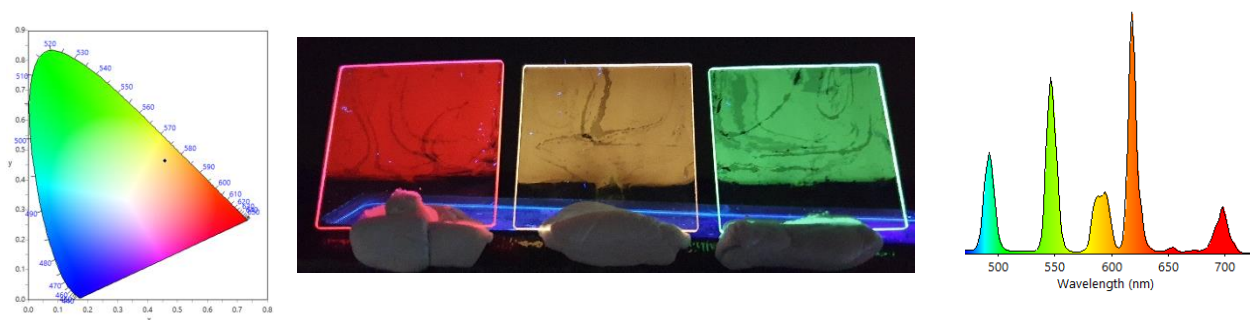


Figure S69. (Left) 1931 CIE chromaticity diagram with calculated CIE coordinates of $x = 0.4580$ and $y = 0.4630$. (Middle) Image of monolayer LB films of $\text{Eu}(\mathbf{1})_3$ (red), $\text{Eu}(\mathbf{1})_3:\text{Tb}(\mathbf{1})_3$ (1:1) mixed monolayer (yellow) and $\text{Tb}(\mathbf{1})_3$ (green). (Right) Fluorescent emission plot of monolayer LB film used to generate CIE plot, also showing corresponding colour gradient to emission wavelength. Both plots were generated by ColourCalculator ver. 7.77 software, licenced by OSRAM.⁶

Dy:Eu mixed monolayer 10:1 ratio

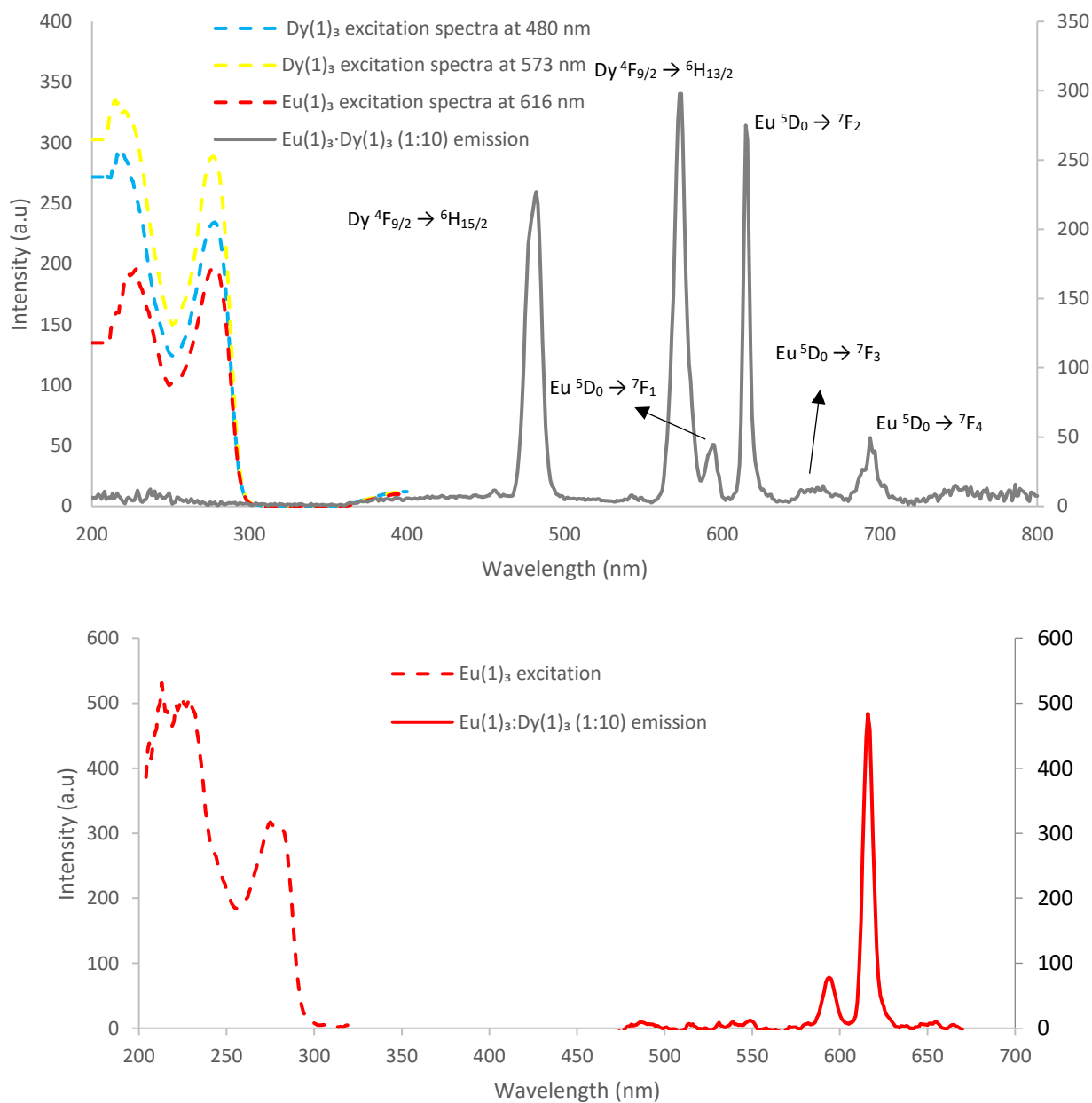


Figure S70. (Top) Steady-state emission and excitation plots of Eu(1)₃:Dy(1)₃ (1:10) in a monolayer film. (Bottom) Time-resolved emission and excitation spectra (monitoring 616 nm) Eu(1)₃:Dy(1)₃ (1:10) in monolayer film.

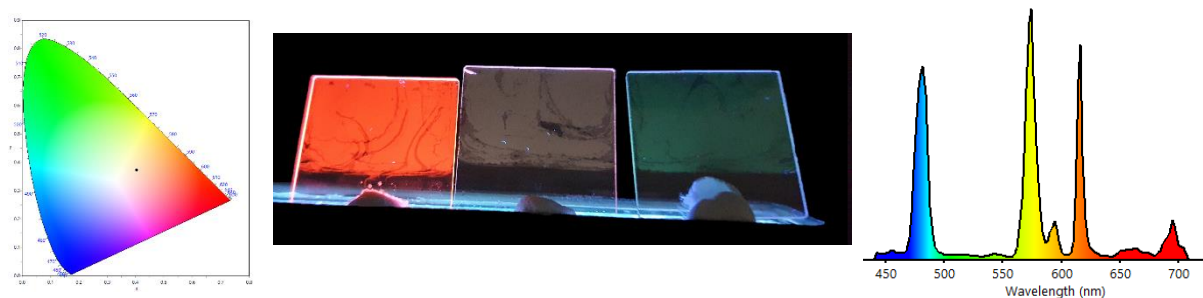


Figure S71. (Left) 1931 CIE chromaticity diagram with calculated CIE coordinates of $x = 0.4050$ $y = 0.3723$. (Middle) Image of monolayer LB films of Eu(1)₃ (red), Eu(1)₃:Dy(1)₃ (1:10) mixed monolayer (grey) and Dy(1)₃ (blue). (Right) Fluorescent emission plot of monolayer LB film used to generate CIE plot, also showing corresponding colour gradient to emission wavelength. Both plots were generated by ColourCalculator ver. 7.77 software, licenced by OSRAM.⁶

Eu(1)₃: Tb(1)₃: Dy(1)₃ mixed monolayer 1:1:10 ratio

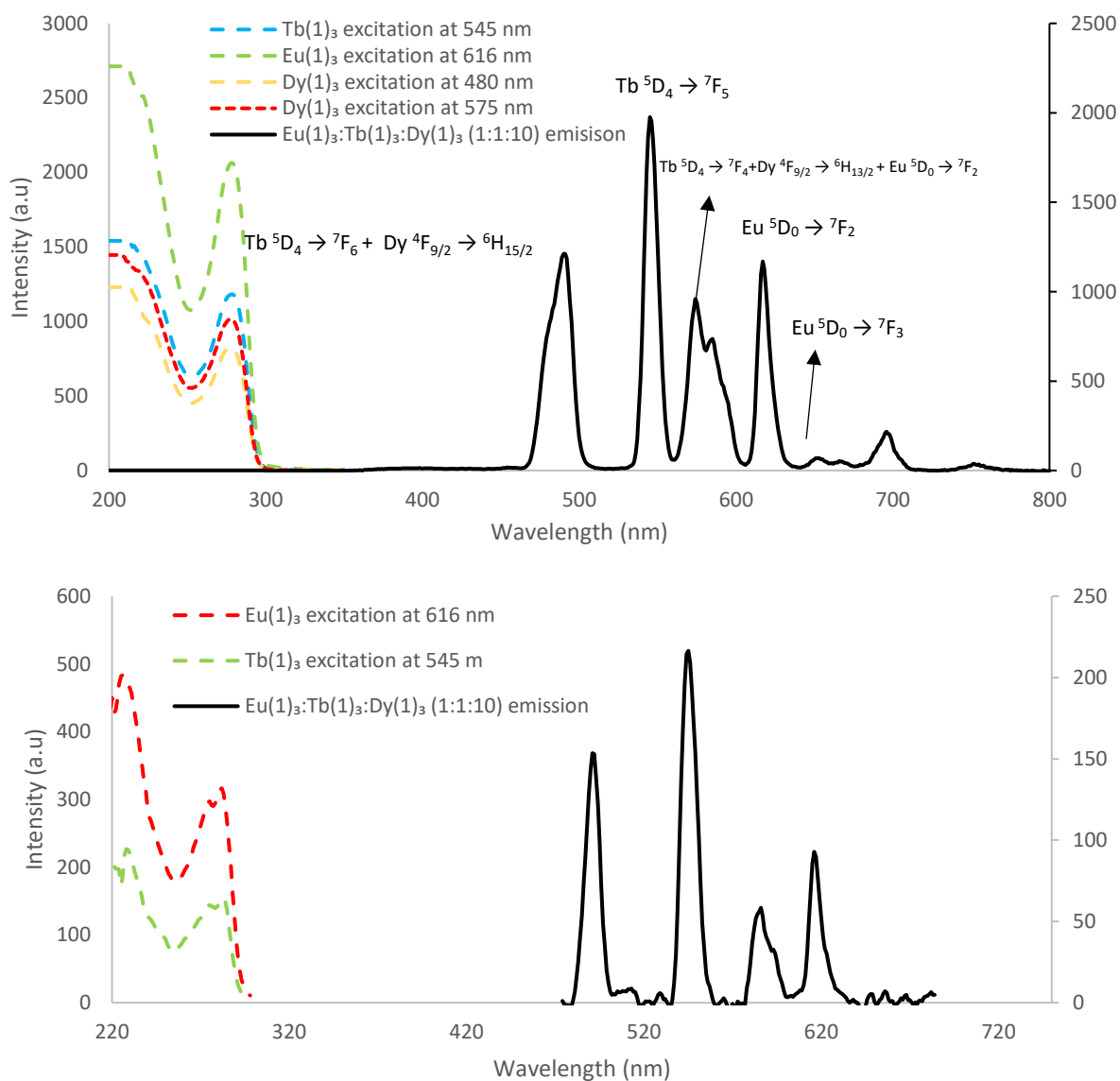


Figure S72. (Top) Steady-state emission and excitation plots of Eu(1)₃:Tb(1)₃:Dy(1)₃ (1:1:10) in monolayer film. (Bottom) Time-resolved emission and excitation plots Eu(1)₃:Tb(1)₃:Dy(1)₃ (1:1:10) in monolayer film.

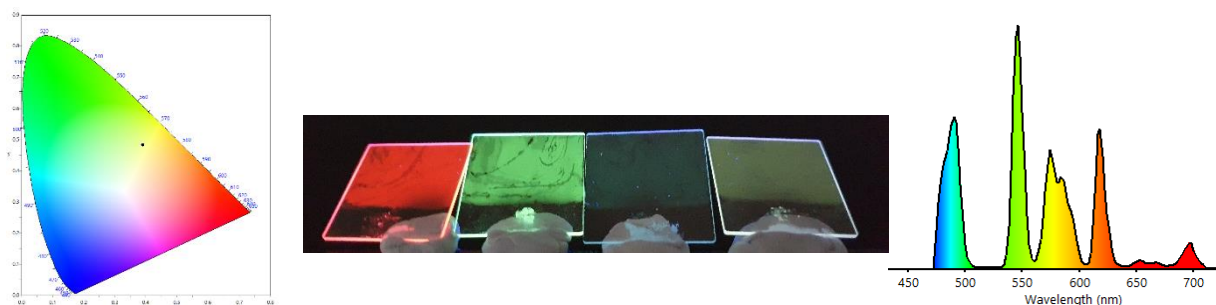


Figure S73. (Left) 1931 CIE chromaticity diagram with calculated CIE coordinates of $x = 0.3904$ $y = 0.4821$. (Middle) Image of monolayer LB films of Eu(1)₃ (red), Tb(1)₃ (green), Dy(1)₃ (blue) and mixed monolayer Eu(1)₃:Tb(1)₃:Dy(1)₃ (light yellow). (Right) Fluorescent emission plot of monolayer LB film used to generate CIE plot, also showing corresponding colour gradient to emission wavelength. Both plots were generated by ColourCalculator ver. 7.77 software, licenced by OSRAM.⁶

Eu(1)₃: Tb(1)₃: Dy(1)₃: Sm(1)₃ mixed monolayer 1:1:10:50 ratio

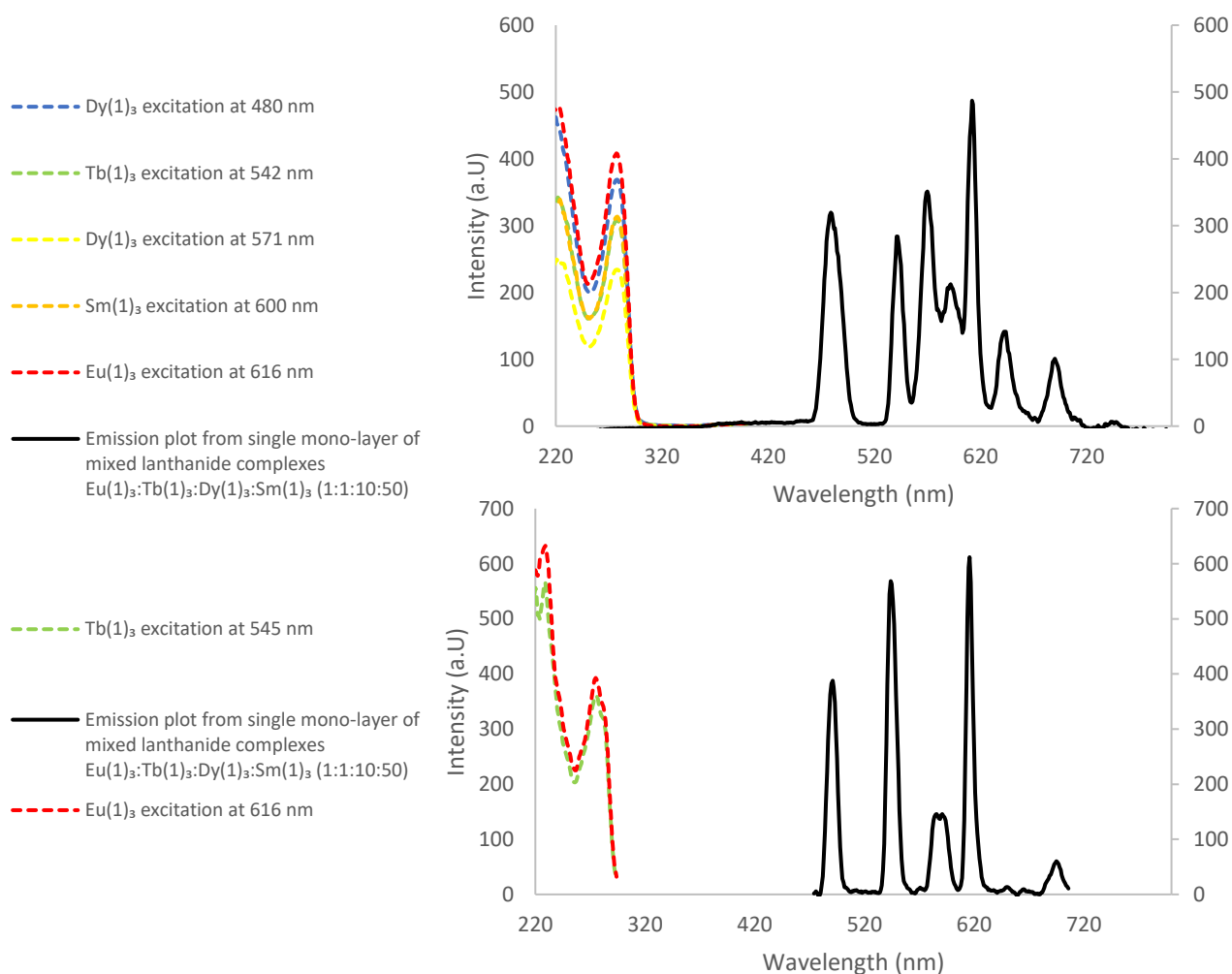


Figure S74. (Top) Fluorescence emission and excitation plots of Eu(1)₃:Tb(1)₃:Dy(1)₃:Sm(1)₃ (1:1:10:50) in a monolayer film. (Bottom) Time-resolved emission and excitation plots of Eu(1)₃:Tb(1)₃:Dy(1)₃:Sm(1)₃ (1:1:10:50) in a monolayer film.

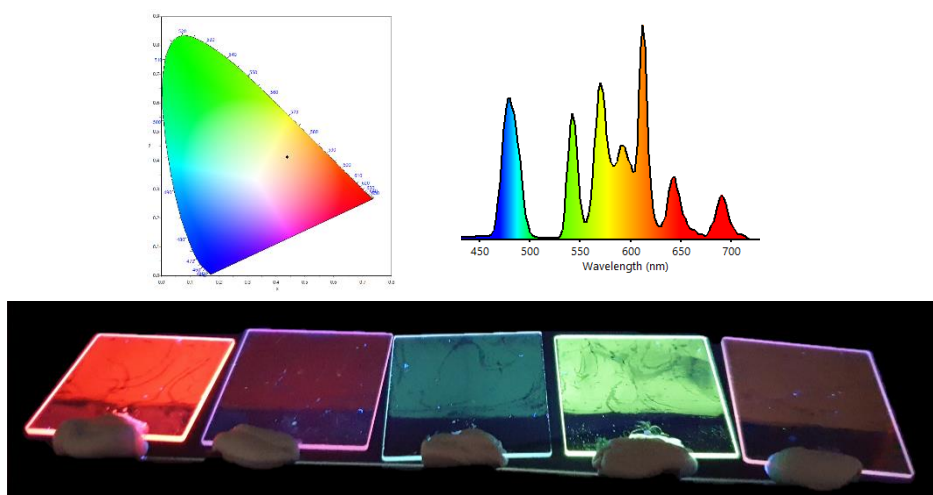


Figure S75. (Top left) 1931 CIE chromaticity diagram with calculated CIE coordinates of $x = 0.4385$ $y = 0.4115$. (Top Right) Fluorescent emission plot of monolayer LB film used to generate CIE plot, also showing corresponding colour gradient to emission wavelength. Both plots were generated by ColourCalculator ver. 7.77 software, licenced by OSRAM.⁶ (Bottom) Image of monolayer LB films of Eu(1)₃ (red), Sm(1)₃ (orange), Dy(1)₃ (blue), Tb(1)₃ (green), Eu(1)₃:Tb(1)₃:Dy(1)₃:Sm(1)₃ (1:1:10:50) (left to right).

Eu(1)₃: Tb(1)₃: Dy(1)₃: Sm(1)₃ mixed monolayer 1:1:1:1 and 1:1:10:10 ratio

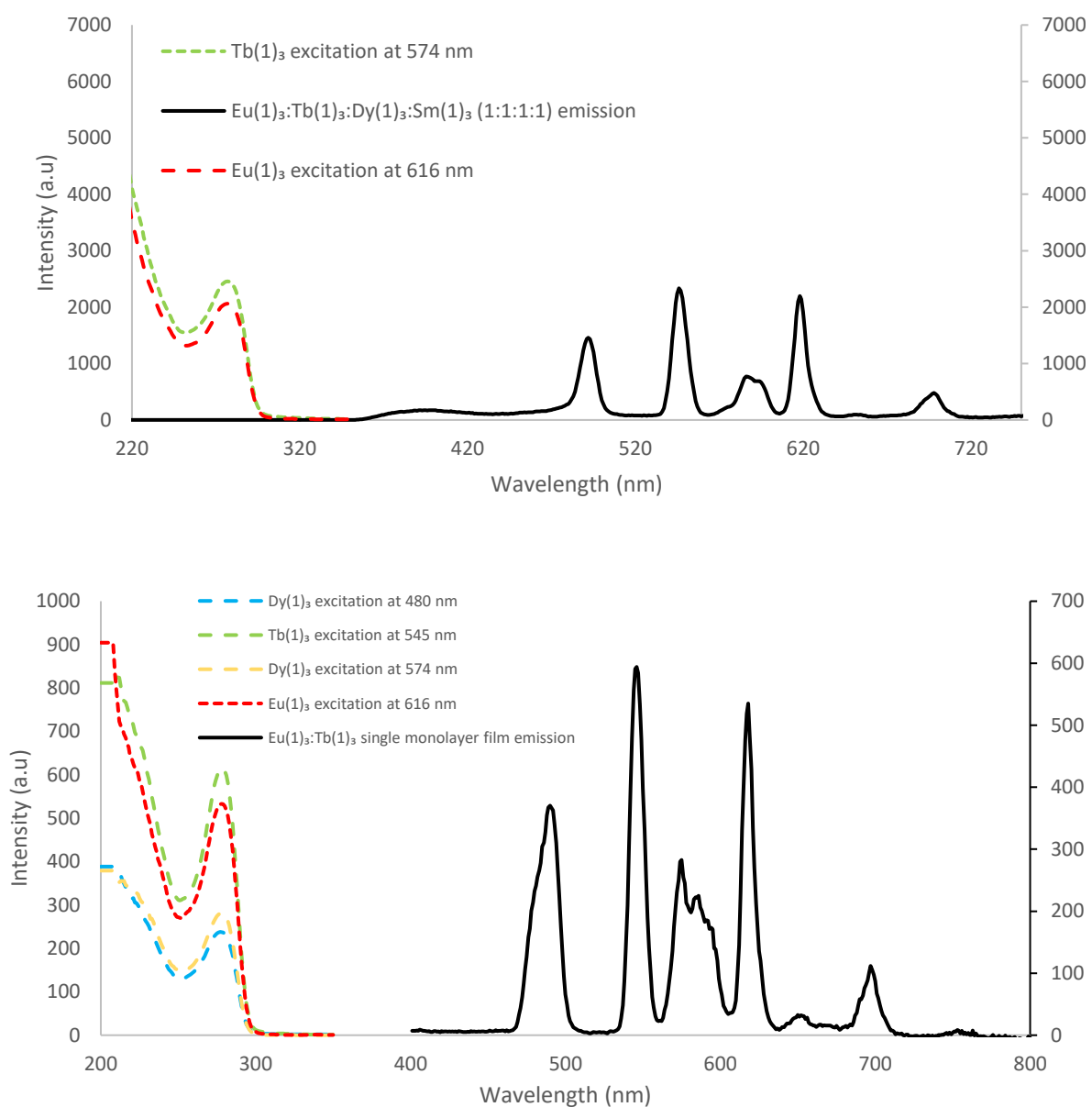


Figure S76. (Top) Fluorescence emission and excitation plots of Eu(1)₃:Tb(1)₃:Dy(1)₃:Sm(1)₃ (1:1:1:1) in a monolayer film. (Bottom) Fluorescence emission and excitation plots Eu(1)₃:Tb(1)₃:Dy(1)₃:Sm(1)₃ (1:1:10:10) in a monolayer film.

Eu(1)₃:Dy(1)₃ mixed monolayer 1:1 and Eu(1)₃:Tb(1)₃:Dy(1)₃ mixed monolayer 1:1:1

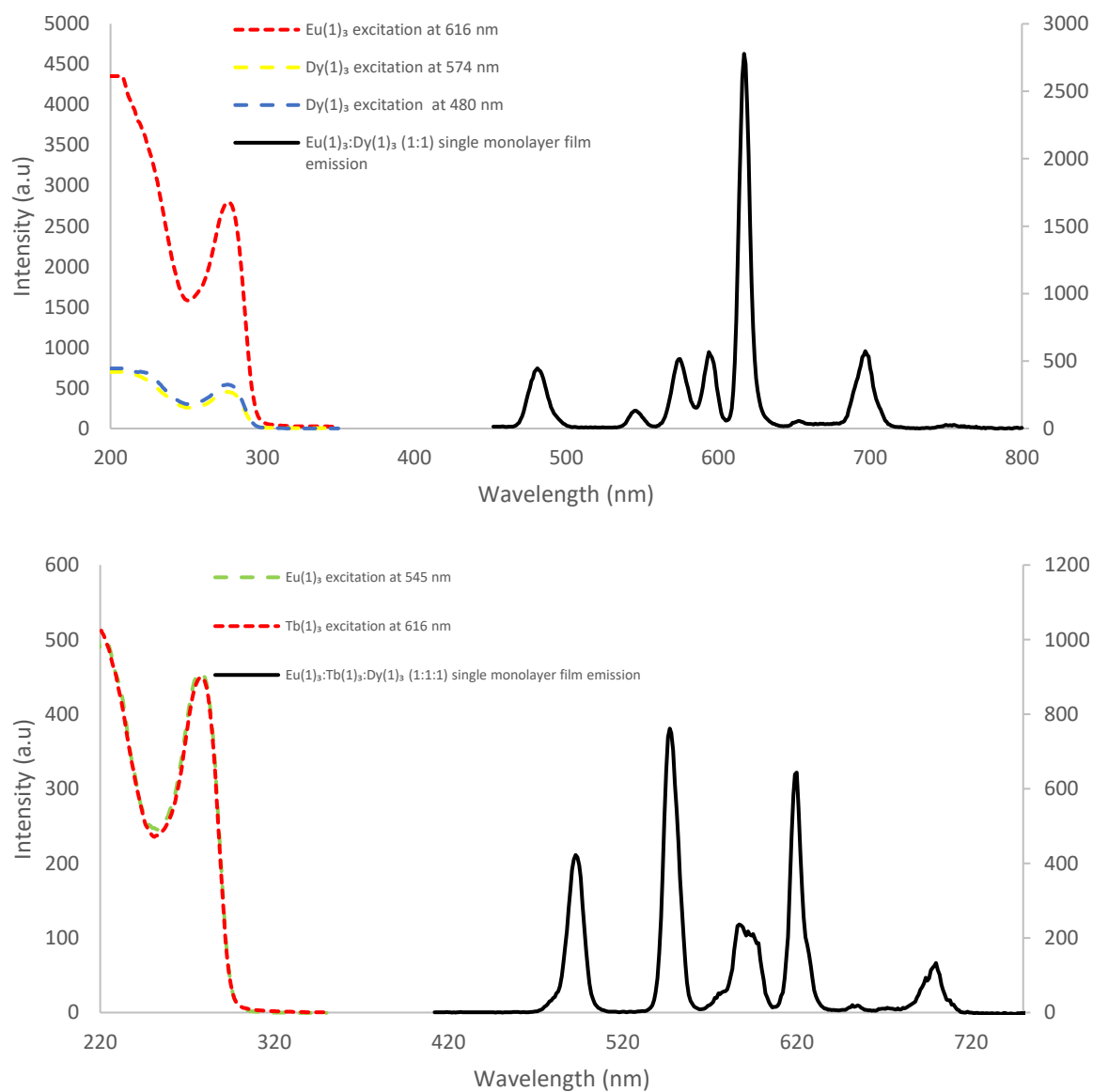


Figure S77. (Top) Fluorescence emission and excitation plots of Eu(1)₃:Dy(1)₃ (1:1) in a monolayer film (Bottom). Fluorescence emission and excitation plots of Eu(1)₃:Tb(1)₃:Dy(1)₃ (1:1:1) in a monolayer film.

It is worth noting that for all mixed films there was no noticeable energy transfer between different Ln³⁺ with emission remain similar across all film combinations.

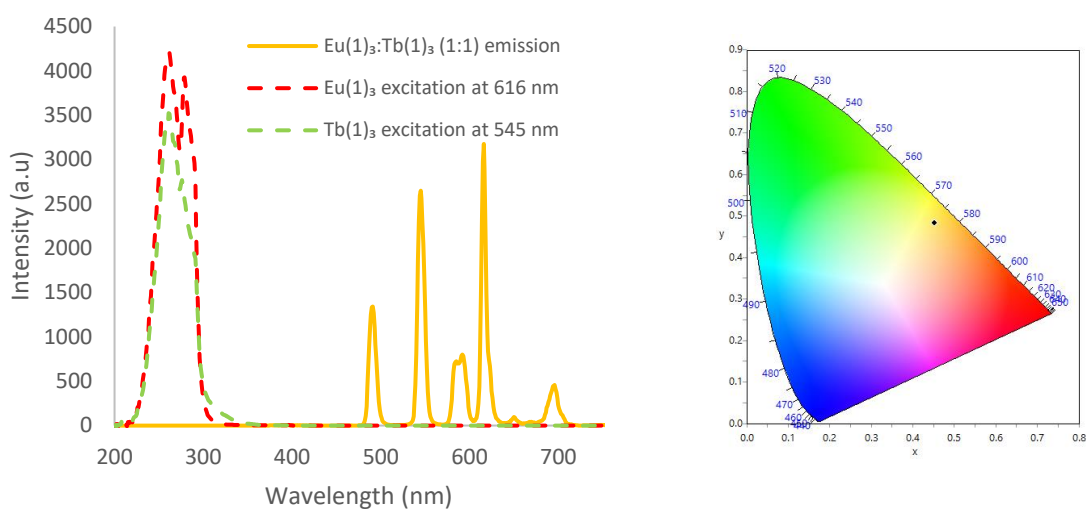


Figure S78. (Top) Image of 1mM MeOH solutions of $\text{Eu}(\mathbf{1})_3$ (left), $\text{Eu}(\mathbf{1})_3$: $\text{Tb}(\mathbf{1})_3$ (1:1) 0.1mM (middle) and $\text{Tb}(\mathbf{1})_3$ (left). (Bottom Left) Fluorescent emission and excitation plot of $\text{Eu}(\mathbf{1})_3$: $\text{Tb}(\mathbf{1})_3$ (1:1) 0.1mM used to generate CIE plot. (Bottom Left) 1931 CIE chromaticity diagram with calculated CIE coordinates of $x = 0.4530$ $y = 0.4828$, plot was generated by ColourCalculator ver. 7.77 software, licenced by OSRAM.⁶

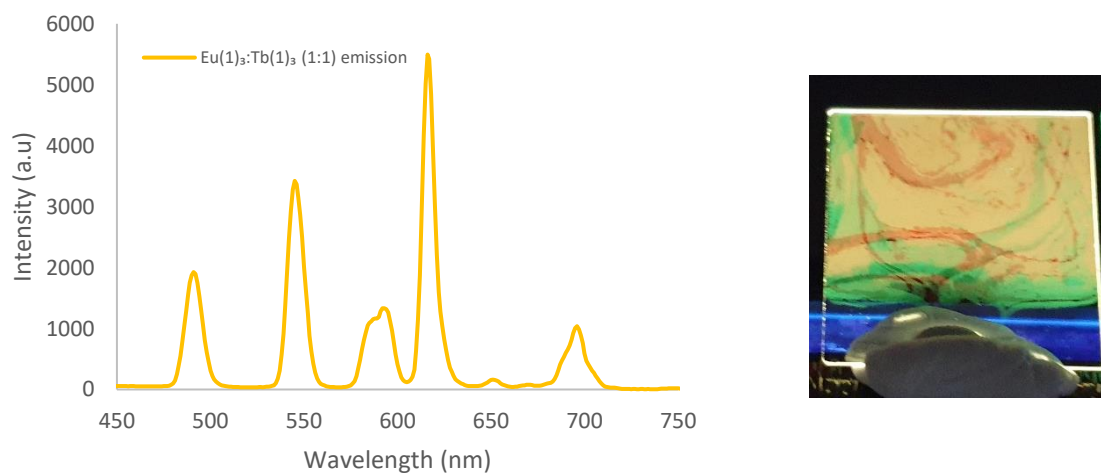


Figure S79. (Left) Fluorescent emission plot of a $\text{Eu}(\mathbf{1})_3$: $\text{Tb}(\mathbf{1})_3$ (1:1) multilayer film with initial layer being $\text{Eu}(\mathbf{1})_3$. (Right) Image of $\text{Eu}(\mathbf{1})_3$: $\text{Tb}(\mathbf{1})_3$ (1:1) film.

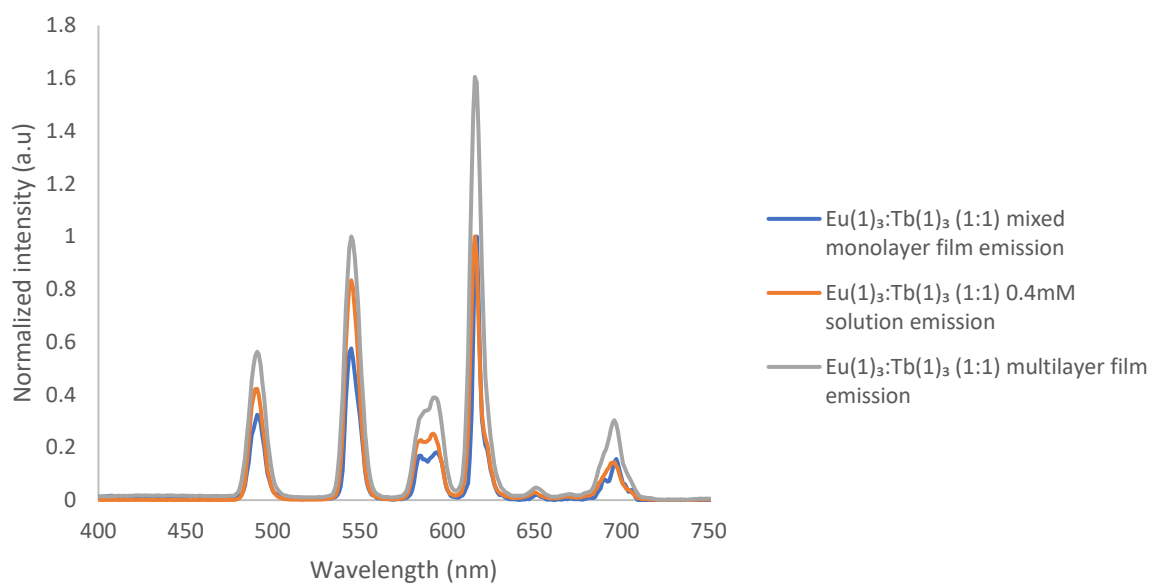


Figure S80. Fluorescent emission plot of $\text{Eu}(1)_3:\text{Tb}(1)_3$ (1:1) mixed monolayer film, multilayer film and mixed solution 0.1 mM in MeOH with normalized intensity.

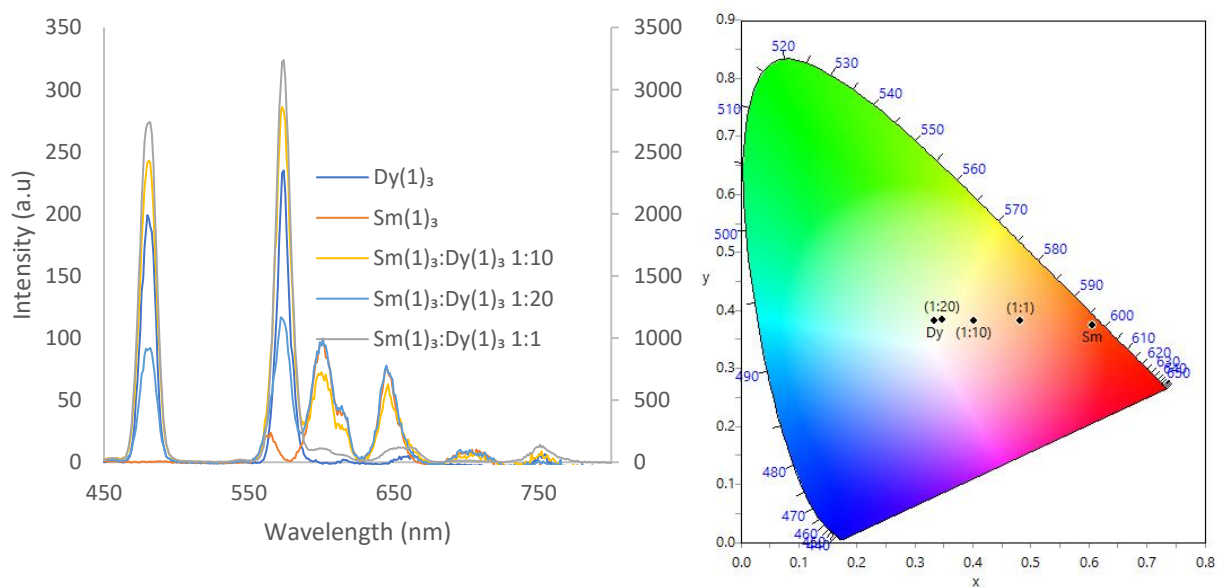


Figure S81. (Left) Fluorescence spectra of different ratios of $\text{Sm}(1)_3:\text{Dy}(1)_3$. (Right) 1931 CIE chromaticity diagram with calculated CIE coordinates of $\text{Sm}(1)_3:\text{Dy}(1)_3$ ratios: (0:1) $x = 0.3346$ $y = 0.3829$, (1:0) $x = 0.6071$ $y = 0.3743$, (1:1), $x = 0.4815$ $y = 0.4815$, (1:10) $x = 0.4023$ $y = 0.3829$, and (1:20) $x = 0.3474$ $y = 0.3840$.

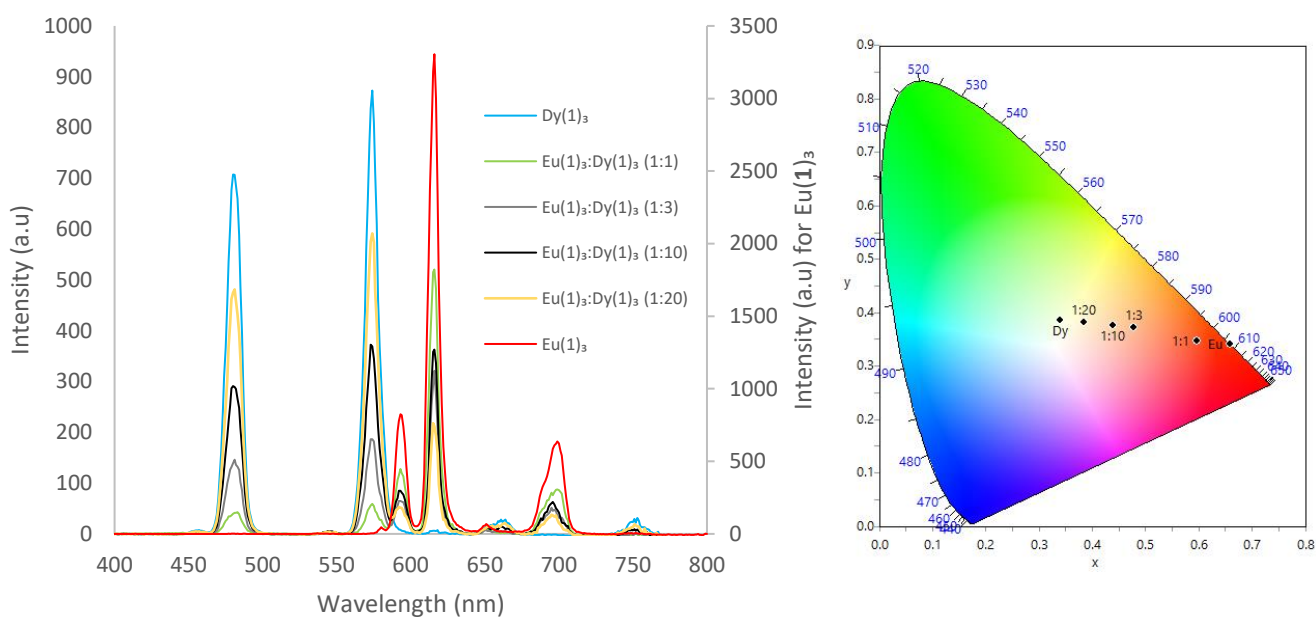


Figure S82. (Left) Fluorescence spectra of different ratios of $\text{Eu}(\mathbf{1})_3:\text{Dy}(\mathbf{1})_3$. (Right) 1931 CIE chromaticity diagram with calculated CIE coordinates of $\text{Eu}(\mathbf{1})_3:\text{Dy}(\mathbf{1})_3$ ratios: (0:1) $x = 0.3392$ $y = 0.3867$, (1:0) $x = 0.6580$ $y = 0.3414$, (1:1), $x = 0.5962$ $y = 0.3461$, (1:3) $x = 0.4772$ $y = 0.3713$, (1:10) $x = 0.43980$ $y = 0.3766$, and (1:20) $x = 0.3846$ $y = 0.3825$.

Multi-layering

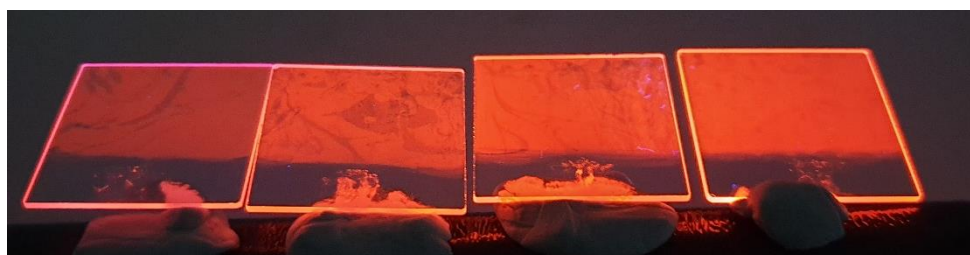


Figure S83. Image of monolayer and multi-layered LB films of $\text{Eu}(1)_3$ with 1, 3, 5 and 7 layers running from left to right.

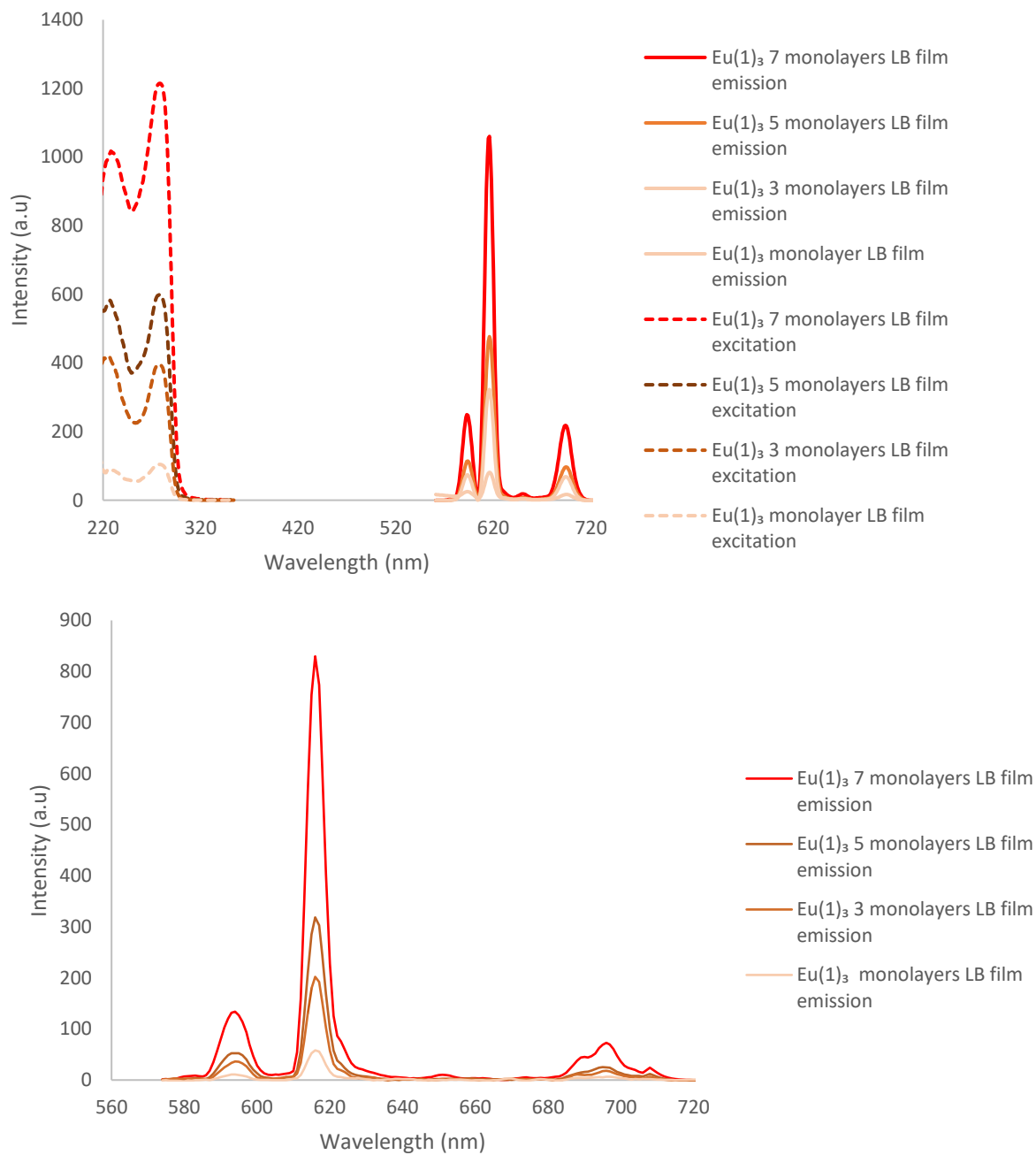


Figure S84. (Top) Fluorescence emission and excitation spectra (monitoring 616 nm) of $\text{Eu}(1)_3$ LB films with 1, 3, 5 and 7 layers. (Bottom) Phosphorescence emission plots of $\text{Eu}(1)_3$ LB films with 1, 3, 5 and 7 layers.

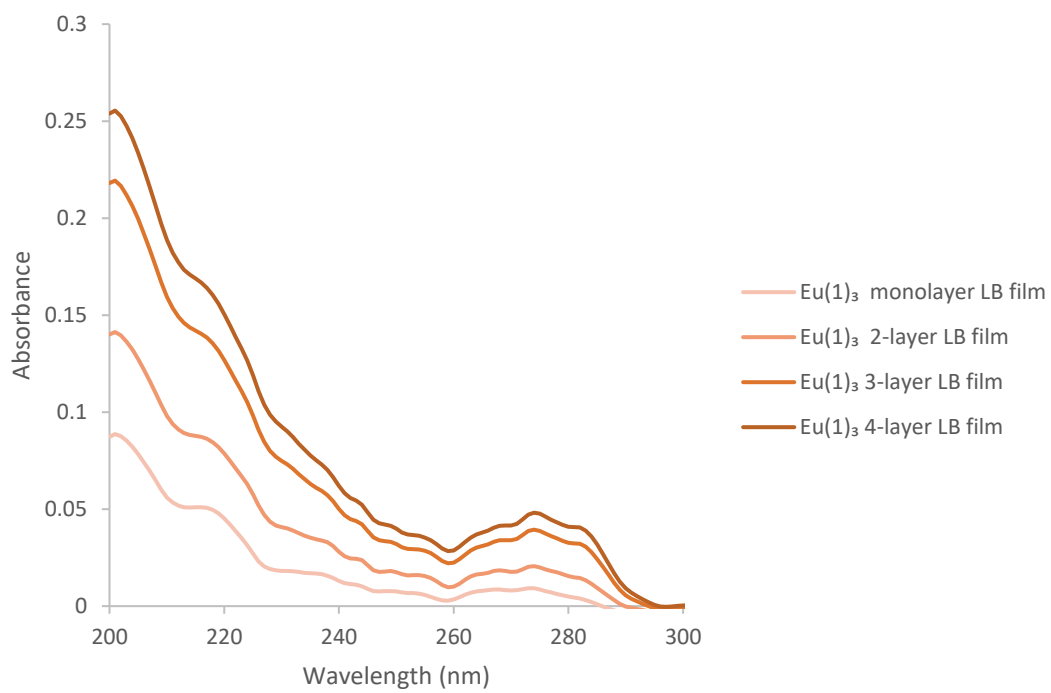


Figure S85. UV-visible absorption $\text{Eu}(1)_3$ of LB films with escalating layers.

Lifetimes

Table S4. Single and double exponential lifetimes of Eu(**1**)₃ and Tb(**1**)₃ complexes in solutions (0.01 mmol).

Complex	Single Exponential	Average (ms)
Eu(1) ₃ solution MeOH (⁵ D ₀ → ⁷ F ₂)	1.522	1.505
	1.512	
	1.481	
Eu(1) ₃ solution MeOH (⁵ D ₀ → ⁷ F ₁)	1.426	1.442
	1.427	
	1.473	
Eu(1) ₃ solution MeCN (⁵ D ₀ → ⁷ F ₂)	1.996	1.960
	1.936	
	1.947	
Eu(1) ₃ solution MeCN (⁵ D ₀ → ⁷ F ₁)	1.899	1.888
	1.880	
	1.885	
Tb(1) ₃ solution MeCN (⁵ D ₄ → ⁷ F ₅)	0.980	0.984
	0.988	
	0.983	

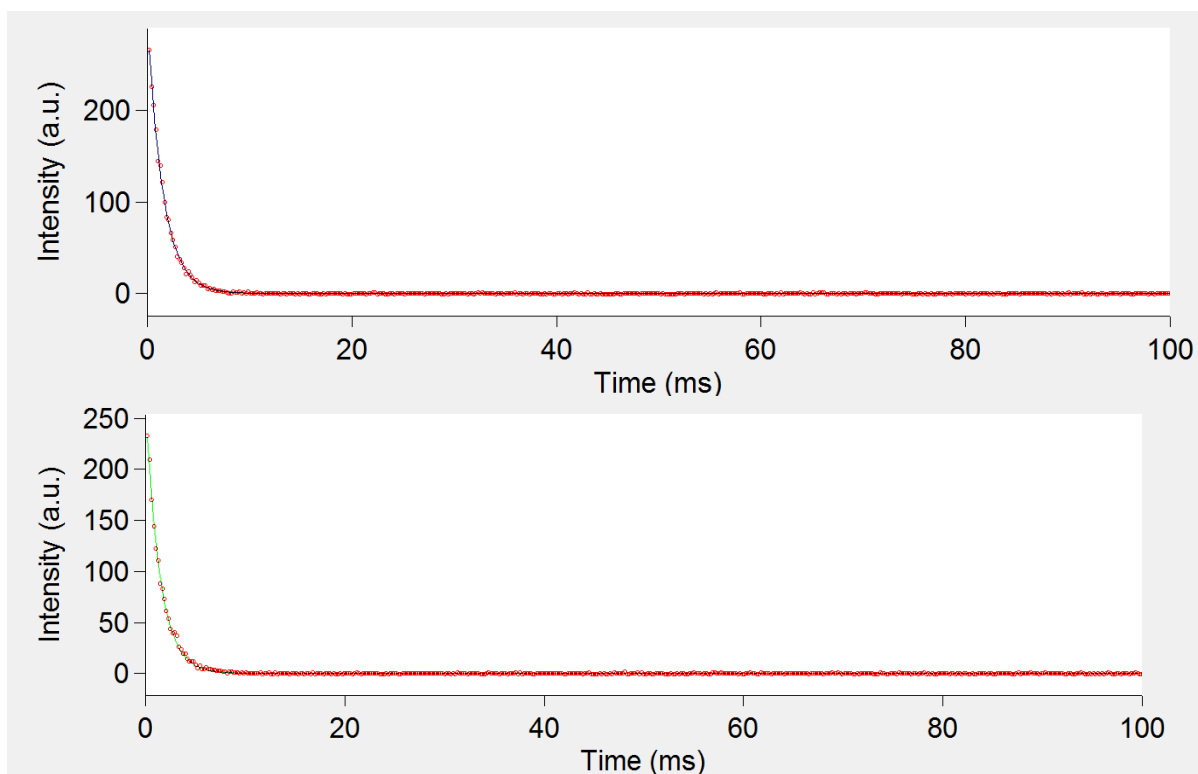


Figure S86. Lifetime of Eu(**1**)₃ complex in a solution of 0.01 mmol MeOH fit with a single exponential (top 616 nm and bottom 594 nm).

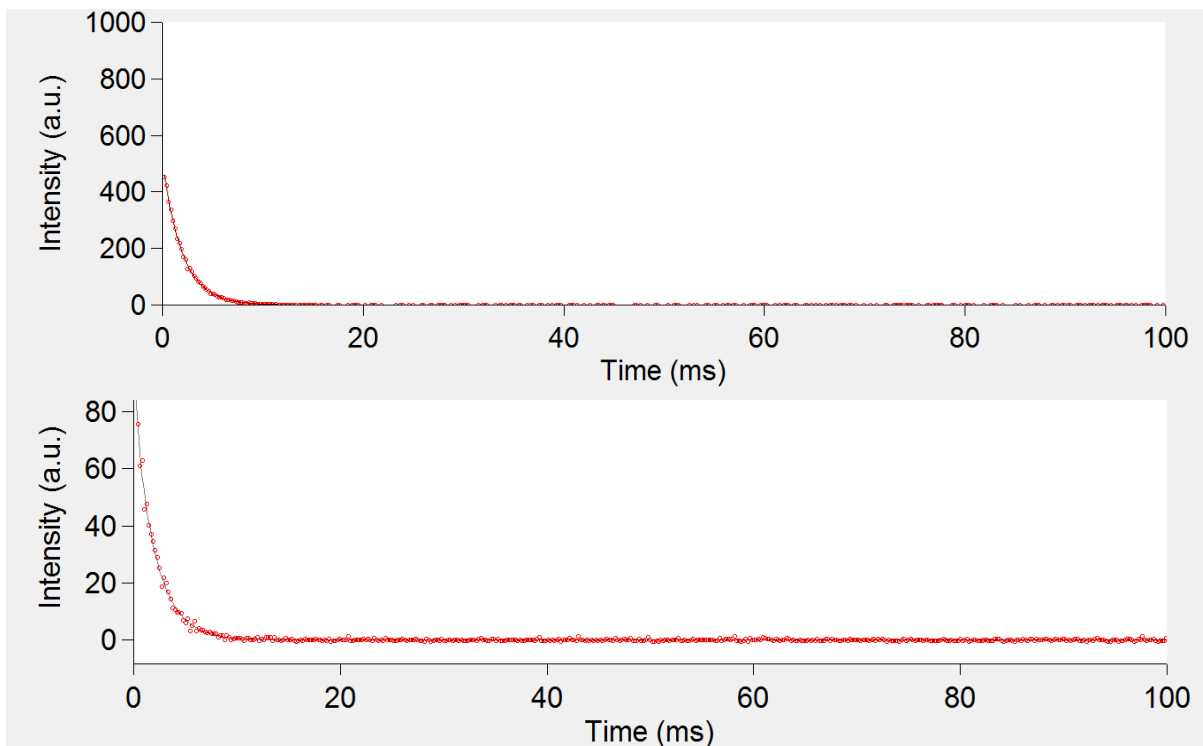


Figure S87. Lifetime of Eu(1)₃ complex in a solution of 0.01 mmol MeCN fit with single exponential (top 616 nm and bottom 594 nm).

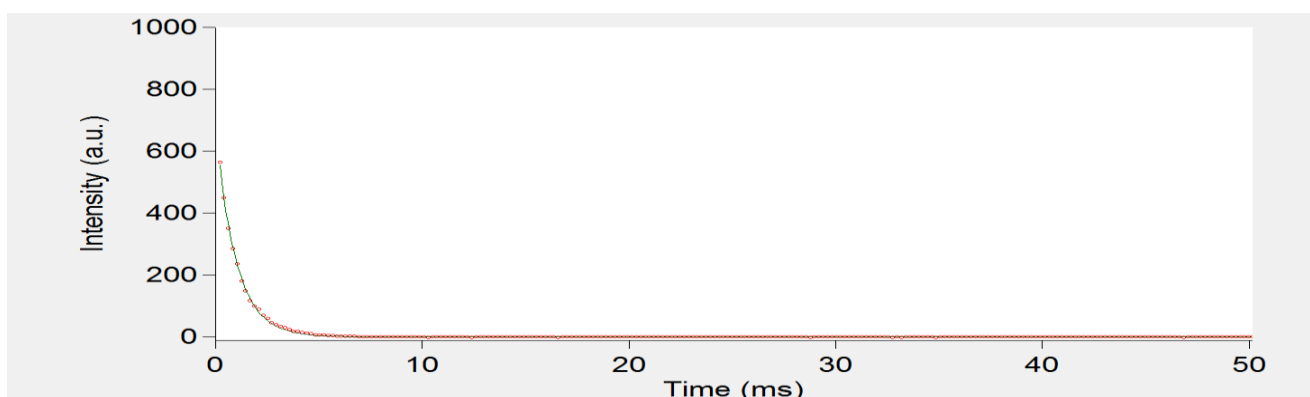


Figure S88. Lifetime of Tb(1)₃ complex in a solution of 0.01 mmol MeCN fit with single exponential (545 nm).

Table S5. Single and double exponential lifetimes of $\text{Eu}(\mathbf{1})_3$ and $\text{Tb}(\mathbf{1})_3$ complexes on LB films. Complex in bold is the lifetime measured.

Films	Single Exponential	Average (ms)
$\text{Eu}(\mathbf{1})_3$ monolayer film	1.412	1.396
	1.400	
	1.376	
$\text{Eu}(\mathbf{1})_3$ 3 layer film	1.457	1.439
	1.463	
	1.397	
$\text{Eu}(\mathbf{1})_3$ 5 layer film	1.359	1.374
	1.359	
	1.403	
$\text{Eu}(\mathbf{1})_3$ 7 layer film	1.535	1.569
	1.596	
	1.576	
$\text{Tb}(\mathbf{1})_3$ monolayer film	1.527	1.552
	1.568	
	1.562	
$\text{Eu}(\mathbf{1})_3$: $\text{Tb}(\mathbf{1})_3$ (1:1) monolayer film	1.516	1.551
	1.549	
	1.587	
$\text{Eu}(\mathbf{1})_3$: $\text{Tb}(\mathbf{1})_3$ (1:1) monolayer film	1.366	1.387
	1.473	
	1.321	
$\text{Eu}(\mathbf{1})_3$: $\text{Dy}(\mathbf{1})_3$ (1:10) monolayer film	0.899	0.882
	0.899	
	0.849	
$\text{Eu}(\mathbf{1})_3$: $\text{Tb}(\mathbf{1})_3$: $\text{Dy}(\mathbf{1})_3$ (1:1:10) monolayer film	1.077	1.059
	1.033	
	1.068	
$\text{Eu}(\mathbf{1})_3$: $\text{Tb}(\mathbf{1})_3$: $\text{Dy}(\mathbf{1})_3$ (1:1:10) monolayer film	1.712	1.748
	1.817	
	1.714	
$\text{Eu}(\mathbf{1})_3$: $\text{Tb}(\mathbf{1})_3$: $\text{Dy}(\mathbf{1})_3$: $\text{Sm}(\mathbf{1})_3$ (1:1:10:50) monolayer film	1.397	1.358
	1.361	
	1.317	
$\text{Eu}(\mathbf{1})_3$: $\text{Tb}(\mathbf{1})_3$: $\text{Dy}(\mathbf{1})_3$: $\text{Sm}(\mathbf{1})_3$ (1:1:10:50) monolayer film	1.136	1.135
	1.105	
	1.163	

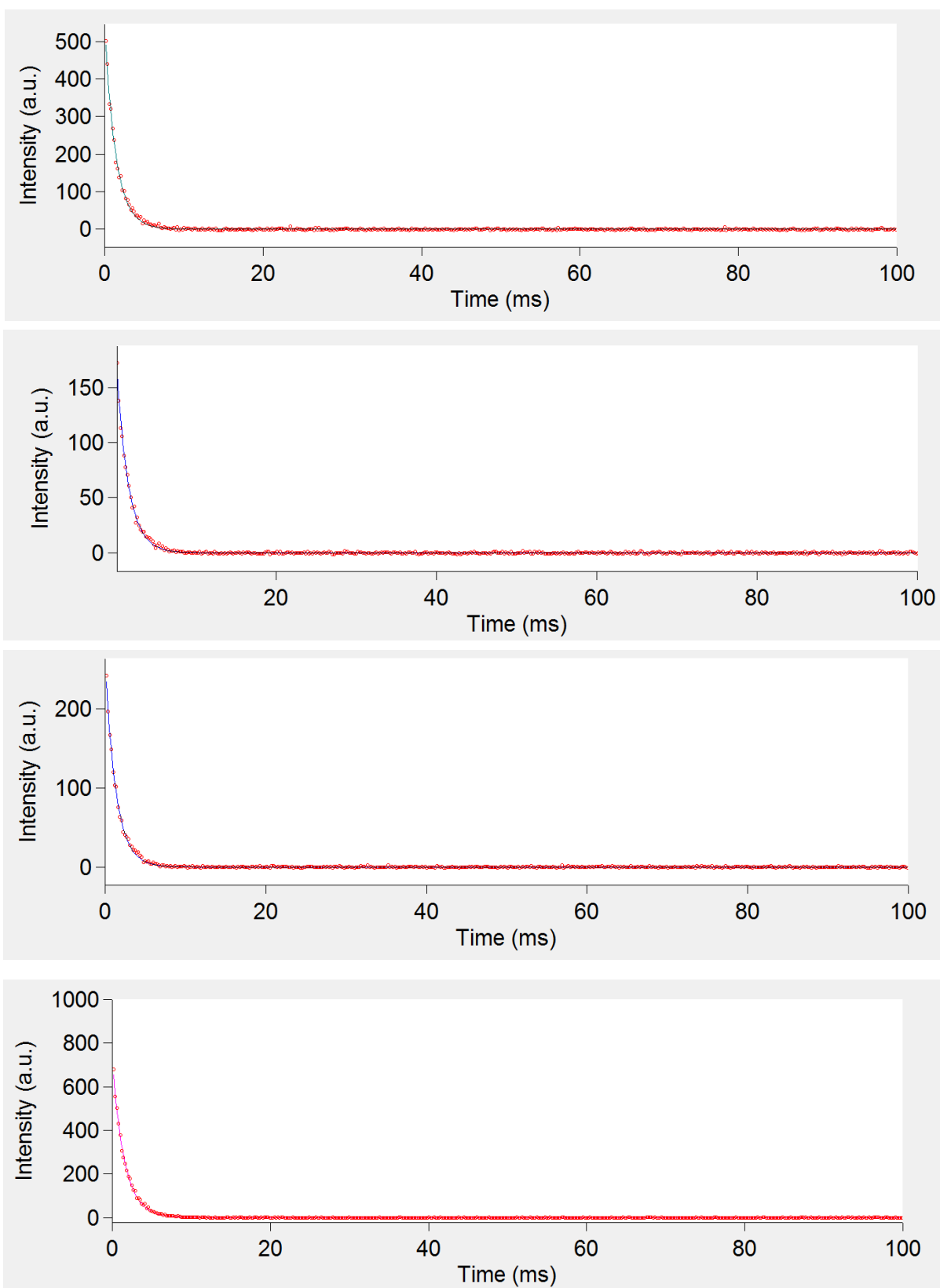


Figure S89. Lifetime of LB films of Eu(1)₃ complex. From top to bottom: 1, 3, 5 and 7 layers. All fit to a single exponential and monitoring 616 nm band.

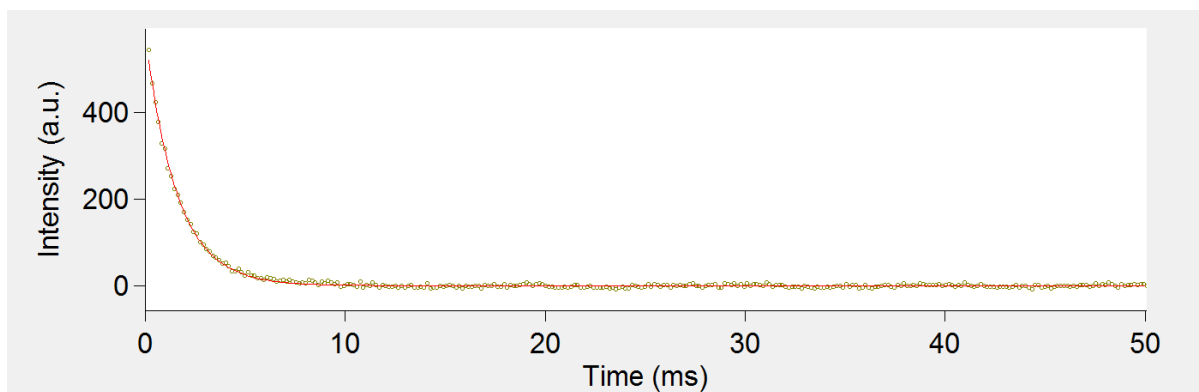


Figure S90. Lifetimes of a monolayer LB film of Tb(1)₃ complex, fit to a single exponential and monitoring 545 nm band.

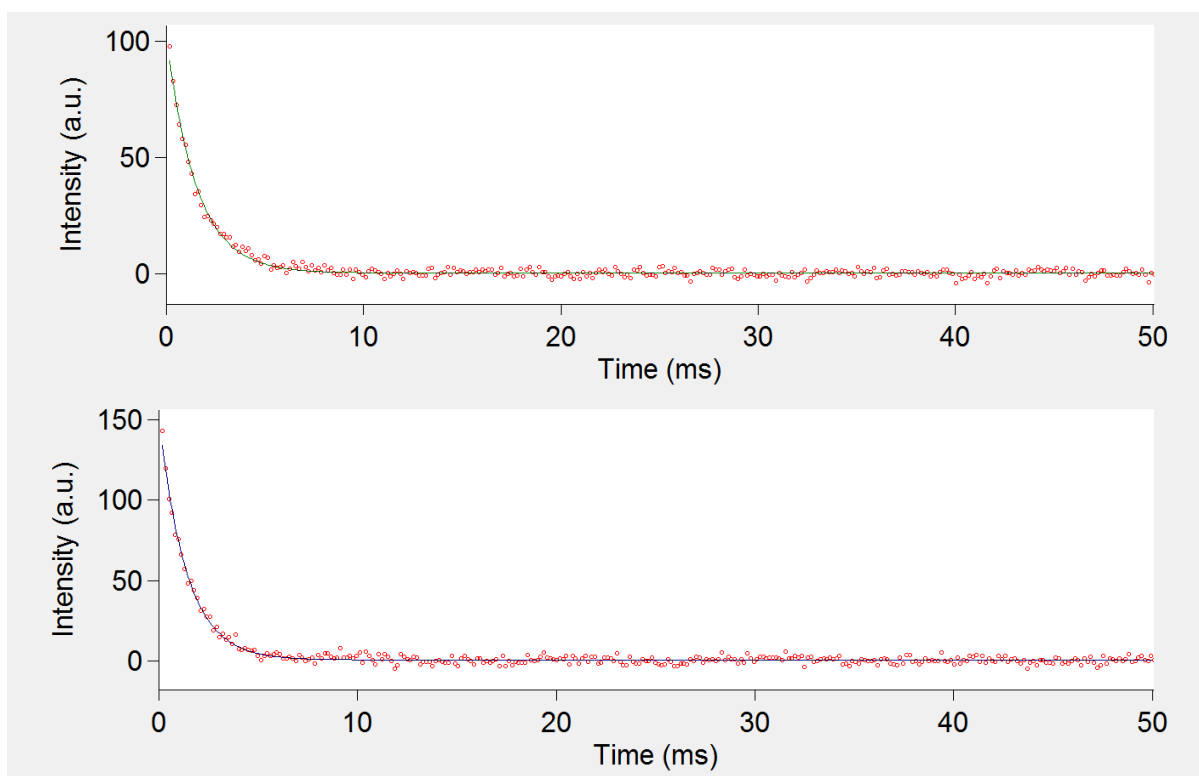


Figure S91. Lifetime of a monolayer LB film of Eu(1)₃:Tb(1)₃ complex, fit to a single exponential and monitoring (top) 616 nm and (bottom) 545 nm band.

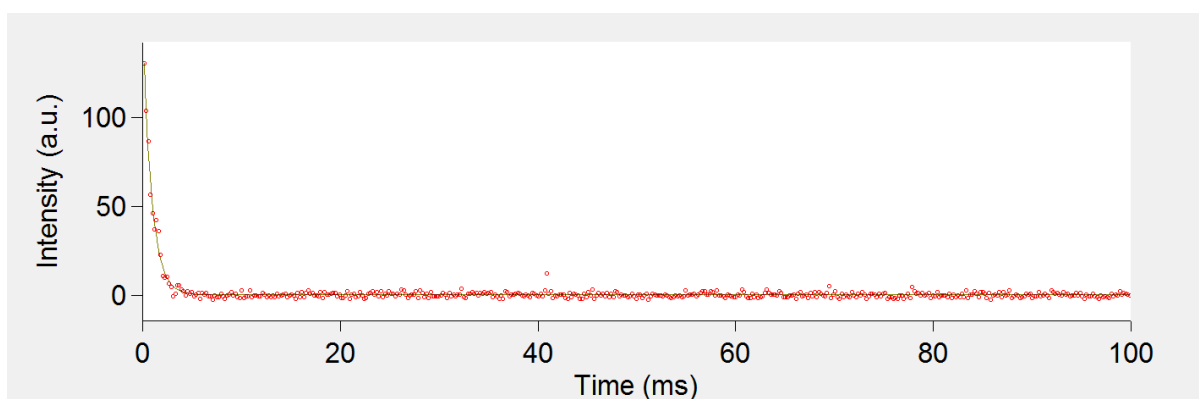


Figure S92. Lifetime of a monolayer LB film of Eu(1)₃Dy(1)₃ complex, fit to a single exponential and monitoring 616 nm.

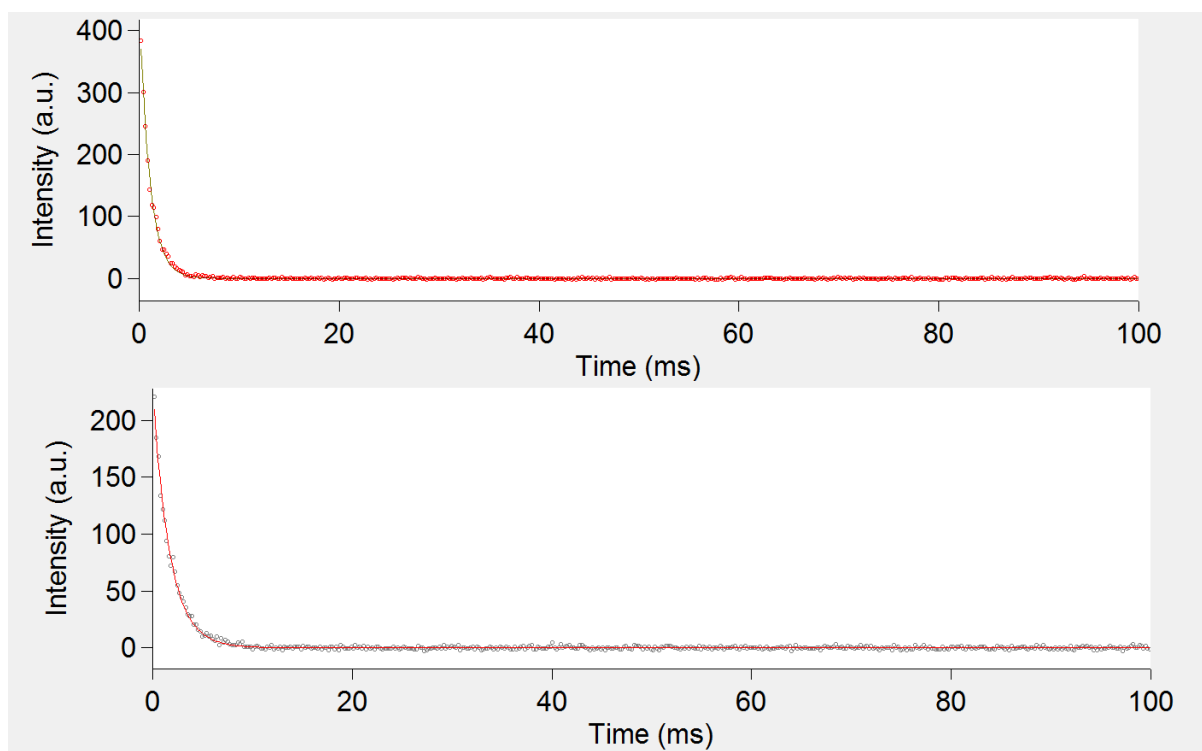


Figure S93. Lifetime of a monolayer LB film of $\text{Eu}(\mathbf{1})_3:\text{Tb}(\mathbf{1})_3:\text{Dy}(\mathbf{1})_3$ complex, fit to a single exponential and monitoring (top) 616 nm and (bottom) 545 nm band.

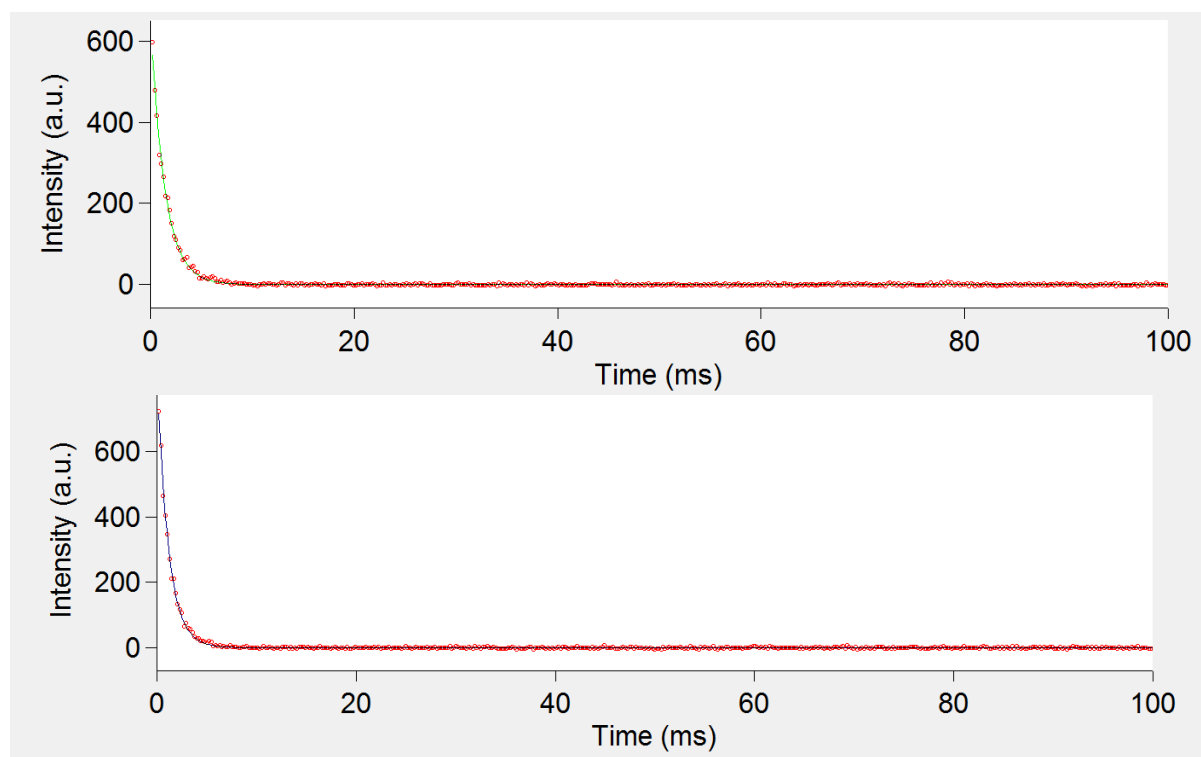


Figure S94. Lifetime of monolayer LB film of $\text{Eu}(\mathbf{1})_3:\text{Tb}(\mathbf{1})_3:\text{Dy}(\mathbf{1})_3:\text{Sm}(\mathbf{1})_3$ complex, fit to a single exponential and monitoring (top) 616 nm and (bottom) 545 nm band.

Quantum Yield

Quantum yield measurements were determined by the dilute comparison method⁷ using relative standards $\text{Cs}_3[\text{Eu}(\text{dpa})_3] \cdot 8\text{H}_2\text{O}$ and $\text{Cs}_3[\text{Tb}(\text{dpa})_3] \cdot 8\text{H}_2\text{O}$ complex in a 0.1 M Tri-HCl buffer solution (pH \approx 7.45), with known quantum yields of $\Phi_{\text{ref}} = 24 \pm 2.5\%$ and $\Phi_{\text{ref}} = 22 \pm 2.5\%$ respectively.^{8,9} $\text{Cs}_3[\text{Eu}(\text{dpa})_3] \cdot 9\text{H}_2\text{O}$ was used for $\text{Eu}(\mathbf{1})_3$ and $\text{Cs}_3[\text{Tb}(\text{dpa})_3] \cdot 9\text{H}_2\text{O}$ for $\text{Tb}(\mathbf{1})_3$, where $\text{Sm}(\mathbf{1})_3$ and $\text{Dy}(\mathbf{1})_3$ were averaged from comparisons to both standards. Barrier slit widths remained the same between measurements for different compounds with either 1.5, 3 nm excitation and emission widths (except for Sm which required 3,3 nm slit widths to have observable emission, which in turn the standard was also measured with). Excitation wavelength was the same for all measurements with the standard 279 nm excitation wavelength. Standards were initially cross calibrated with one another to be within the range of error before being compared to lanthanide complexes. Complexes were dissolved in a 1:1 MeOH: CH_2Cl_2 stock solution and then diluted into MeOH to the appropriate concentration for quantum yield studies MeCN was also used for $\text{Eu}(\mathbf{1})_3$ but showed lower quantum yield which was put down to the complex notably slowly precipitating out over time.

Estimated overall quantum yields $\Phi_{Ln}^L = \Phi_x$ were calculated according to the following equation 1. Here grad refer to the slope of plotted emission area vs absorbance (emission area was taken from specific emission peaks, $\text{Eu}(\mathbf{1})_3$ (${}^5\text{D}_0 \rightarrow {}^7\text{F}_2$), $\text{Tb}(\mathbf{1})_3$ (${}^5\text{D}_4 \rightarrow {}^7\text{F}_5$), $\text{Dy}(\mathbf{1})_3$ (${}^4\text{F}_{9/2} \rightarrow {}^6\text{H}_{13/2}$) and $\text{Sm}(\mathbf{1})_3$ (${}^4\text{G}_{5/2} \rightarrow {}^6\text{H}_{7/2}$)), n refers to refractive index of the solution (a refractive index of $n = 1.3295$ was found for MeOH: CH_2Cl_2 solution and $n = 1.3355$ for MeCN solution), and subscript are ref for reference and x for sample.⁸

$$\Phi_x = \Phi_{std} \left(\frac{\text{grad}_x}{\text{grad}_{ref}} \times \left(\frac{n_x^2}{n_{ref}^2} \right) \right) \quad (1)$$

Radiative lifetime (τ_{rad}) of $\text{Eu}(\mathbf{1})_3$ was estimated by equation 2 which assumes that the magnetic dipole of Eu^{3+} (${}^5\text{D}_0 \rightarrow {}^7\text{F}_1$) is independent of its coordination environment. Abbreviations refer to; n for refractive index, $\frac{I_{MD}}{I_{tot}}$ is the ratio of area under the Eu^{3+} (${}^5\text{D}_0 \rightarrow {}^7\text{F}_1$) to the integrated total emission ($J=0-6$), and $A_{MD,0}$ is the spontaneous emission probability of the Eu^{3+} (${}^5\text{D}_0 \rightarrow {}^7\text{F}_1$) transition (14.65 s^{-1}).⁸

$$\tau_{rad} = \frac{1}{A_{MD,0} n^3} \left(\frac{I_{MD}}{I_{tot}} \right) \quad (2)$$

From this intrinsic quantum yields (Φ_{Ln}^L) can be estimated with equation 3 using observed lifetime (τ_{osb}) and in turn used to find the sensitization efficiency (n_{sens}) with equation 4.⁸

$$\Phi_{Ln}^L = \frac{\tau_{osb}}{\tau_{rad}} \quad (3) \quad n_{sens} = \frac{\Phi_{Ln}^L}{\Phi_{Ln}^L} \quad (4)$$

Table S6. Quantum yield results.

Complex	Φ_{Ln}^L	τ_{osb} (ms)	τ_{rad} (ms)	Φ_{Ln}^L	n_{sens}
$\text{Eu}(\mathbf{1})_3$ MeOH	22.43 %	1.442 ± 0.0	4.570	31.55 %	71 %
$\text{Eu}(\mathbf{1})_3$ MeCN	11.85 %	1.888 ± 0.0	4.402	42.89 %	28 %
$\text{Tb}(\mathbf{1})_3$ (${}^5\text{D}_4 \rightarrow {}^7\text{F}_5$)	14.21 %	0.984 ± 0.0			
$\text{Dy}(\mathbf{1})_3$ (${}^4\text{F}_{9/2} \rightarrow {}^6\text{H}_{13/2}$)	2.93 %				
$\text{Sm}(\mathbf{1})_3$ (${}^4\text{G}_{5/2} \rightarrow {}^6\text{H}_{7/2}$)	0.32 %				

Elemental analysis for $\text{C}_{21}\text{H}_9\text{N}_3\text{O}_{12}\text{EuCs}_3 \cdot 8\text{H}_2\text{O}$ ($1190.1162 \text{ g mol}^{-1}$) Calculated: C 21.19, H 2.12, N 3.53 %. Found C 21.19, H 2.13, N 3.72 %.

Elemental analysis for $\text{C}_{21}\text{H}_9\text{N}_3\text{O}_{12}\text{TbCs}_3 \cdot 8\text{H}_2\text{O}$ ($1197.0792 \text{ g mol}^{-1}$) Calculated: C 21.07, H 2.10, N 3.51 %. Found C 21.00, H 2.00, N 3.65 %.

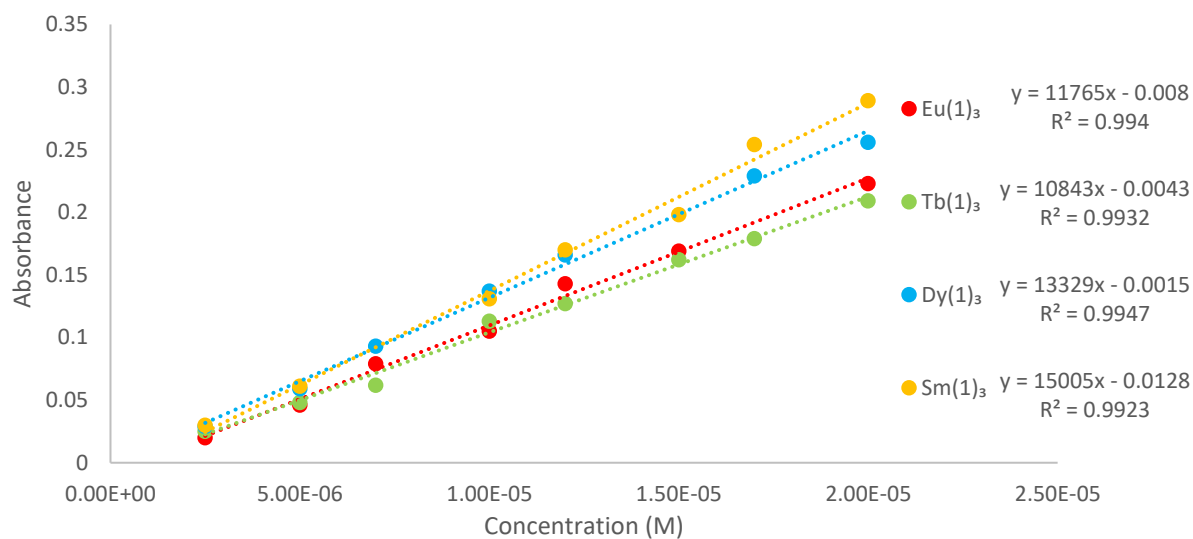


Figure S95. Concentration vs absorbance of lanthanide complexes.

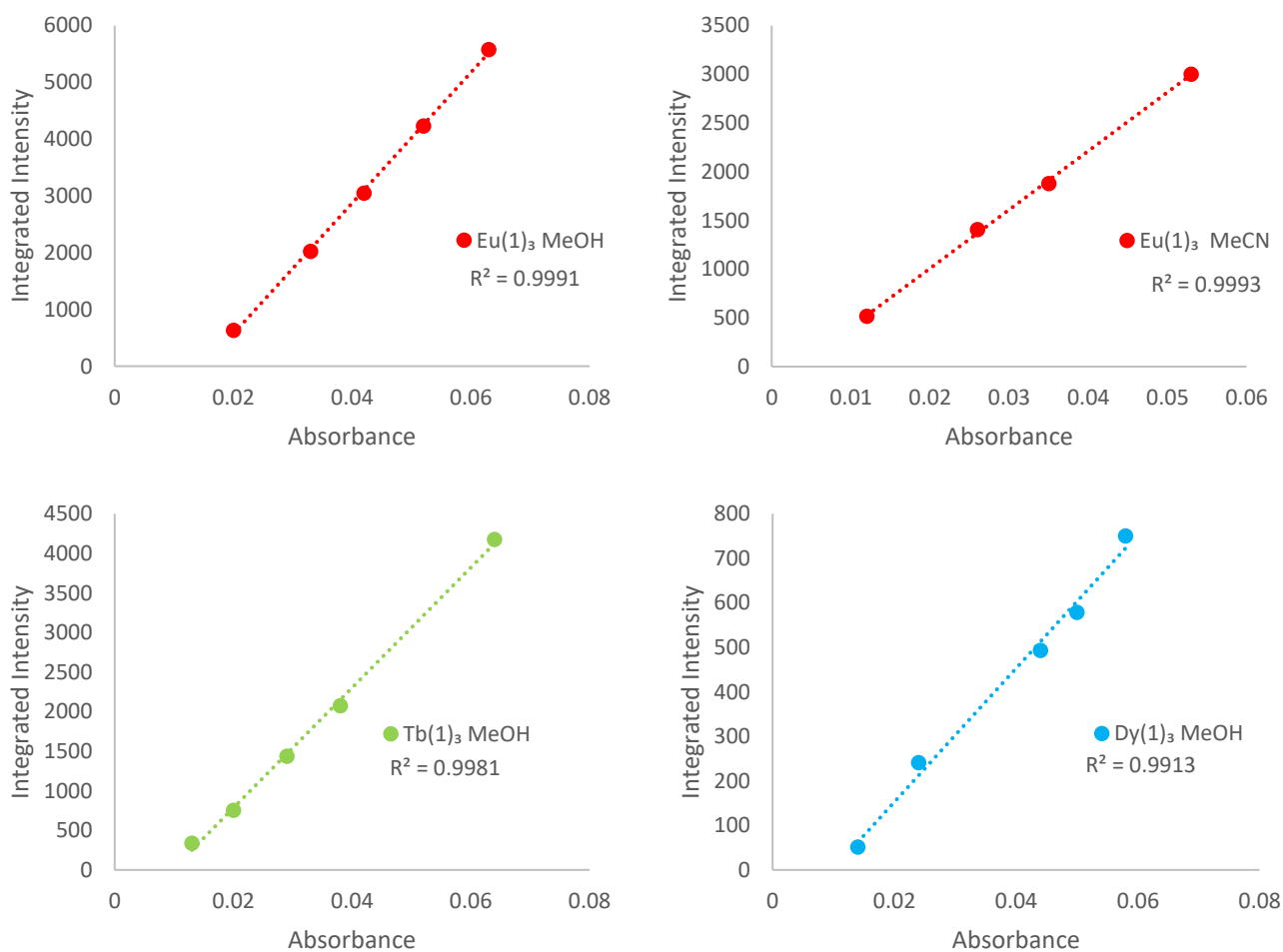


Figure S96. Absorbance vs integrated intensity of lanthanide complexes in MeOH (and MeCN for Eu(1)₃), 1.5 and 3 nm excitation and emission widths.

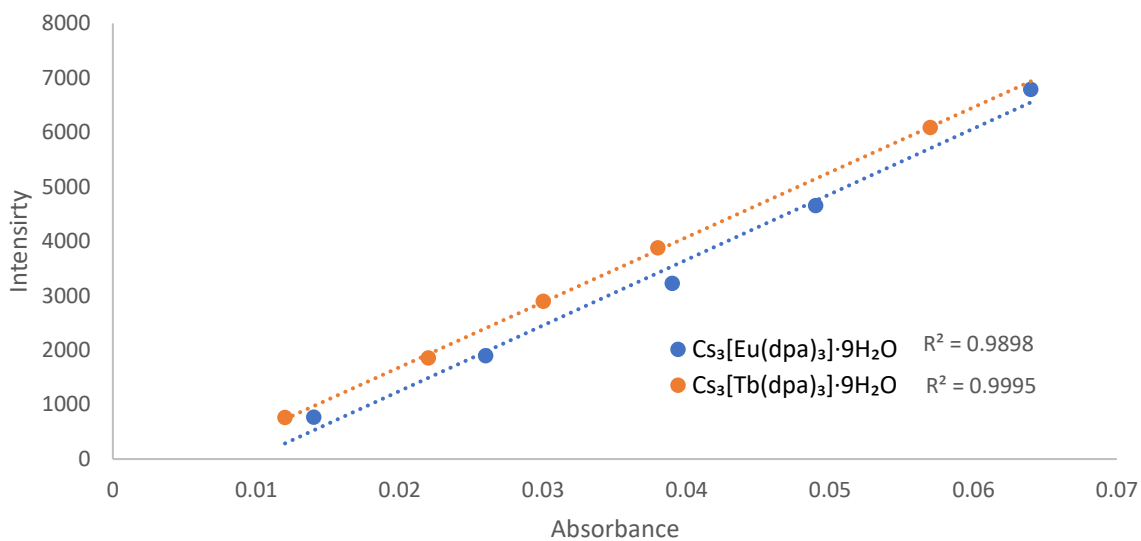


Figure S97. Absorbance vs integrated intensity of $\text{Cs}_3[\text{Eu}(\text{dpa})_3] \cdot 8\text{H}_2\text{O}$ and $\text{Cs}_3[\text{Tb}(\text{dpa})_3] \cdot 8\text{H}_2\text{O}$, 1.5 and 3 nm excitation and emission widths.

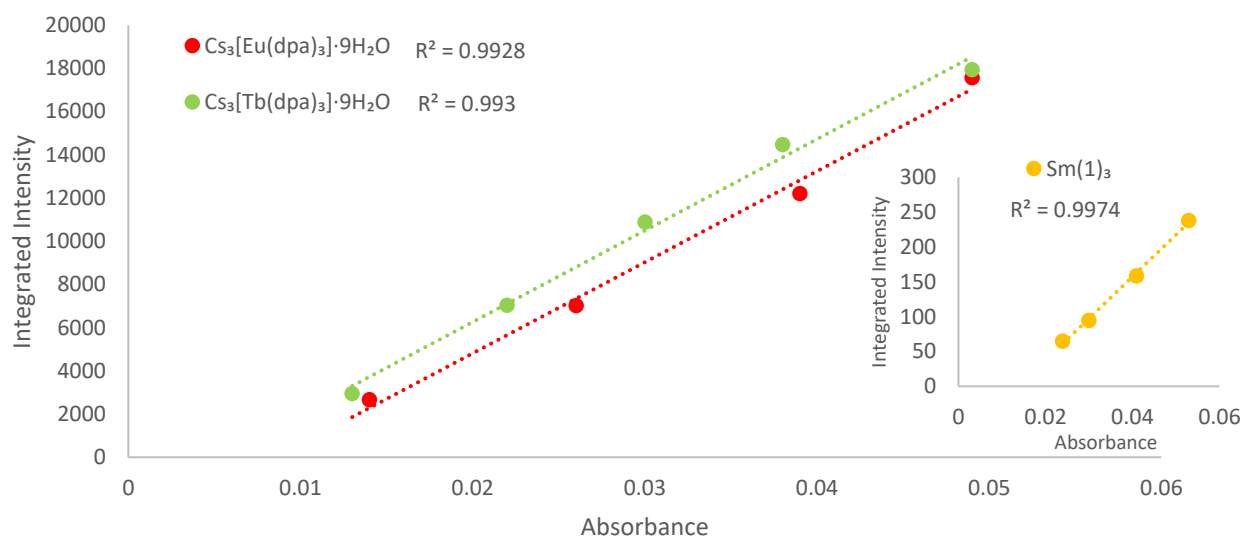


Figure S98. Absorbance vs integrated intensity of $\text{Cs}_3[\text{Eu}(\text{dpa})_3] \cdot 8\text{H}_2\text{O}$ and $\text{Cs}_3[\text{Tb}(\text{dpa})_3] \cdot 8\text{H}_2\text{O}$, 3 and 3 nm excitation and emission widths. Insert : Absorbance vs integrated intensity of $\text{Sm}(\mathbf{1})_3$.

X-ray Photoelectron Spectroscopy (XPS)

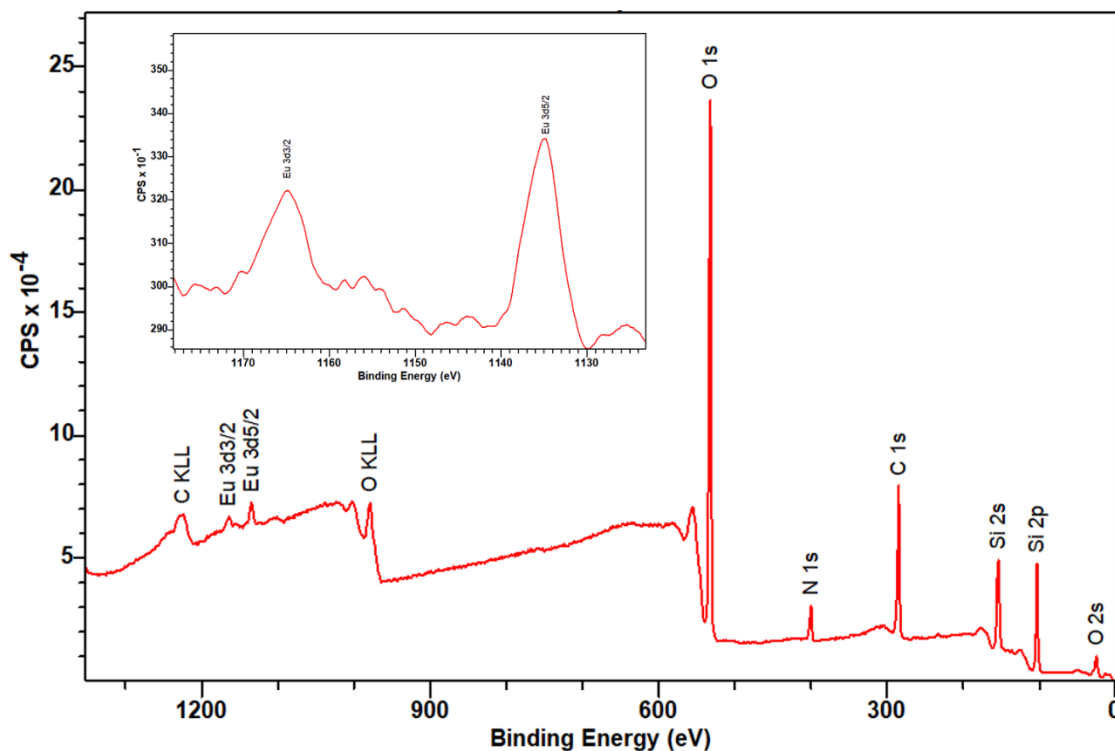


Figure S99. Survey scan XPS spectrum of $\text{Eu}(\text{1})_3$ monolayer LB film. Insert: Enclosed window scan of $\text{Eu}(\text{III})$ 3d peaks (a total of 20 scans) with $\text{Eu}(\text{III})$ $3d_{3/2} = 1135$ and $3d_{5/2} = 1165$ eV, expected being 1166 and 1135 eV for $\text{Eu}(\text{III})$ respectively.¹¹

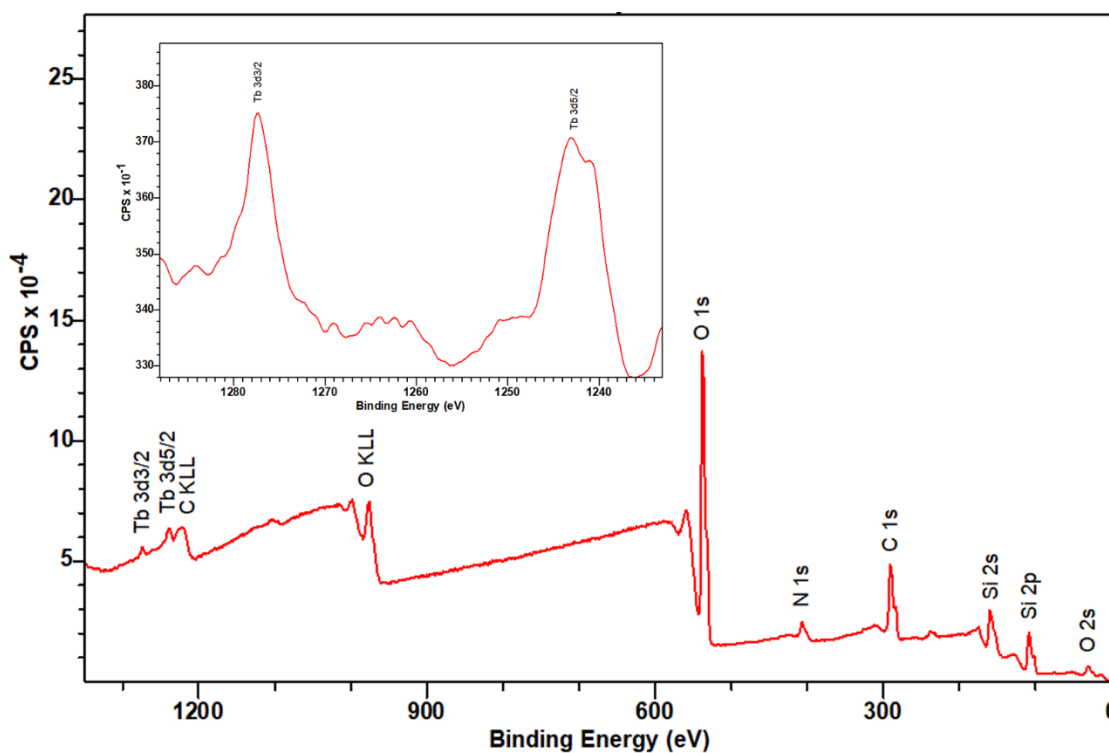


Figure S100. Survey scan XPS spectrum of $\text{Tb}(\text{1})_3$ monolayer LB film. Insert: Enclosed window scan of $\text{Tb}(\text{III})$ 3d peaks (a total of 20 scans) with $\text{Tb}(\text{III})$ $3d_{3/2} = 1177$ and $3d_{5/2} = 1142$ eV, expected being 1176 and 1141 eV for $\text{Tb}(\text{III})$ respectively.¹²

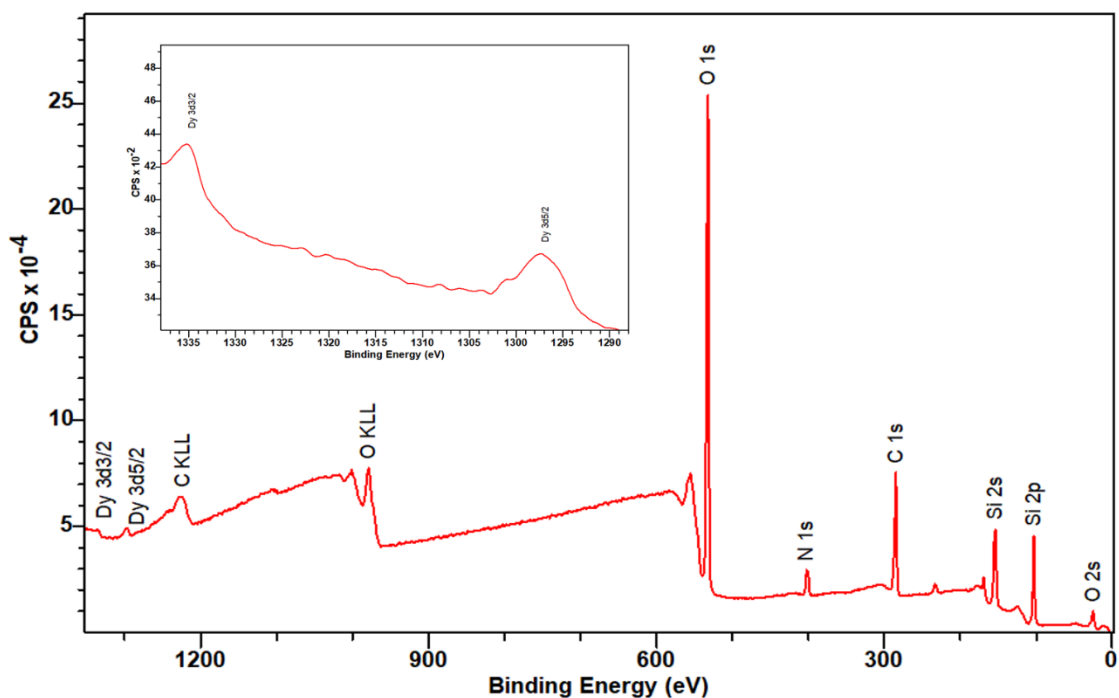


Figure S101. Survey scan XPS spectrum of Dy(1)₃ monolayer LB film. Insert: Enclosed window scan of Dy(III) 3d peaks (a total of 20 scans) with Dy(III) 3d_{3/2} = 1334 and 3d_{5/2} = 1297 eV, expected being 1333 and 1296 eV for Dy(III) respectively.^{12,13}

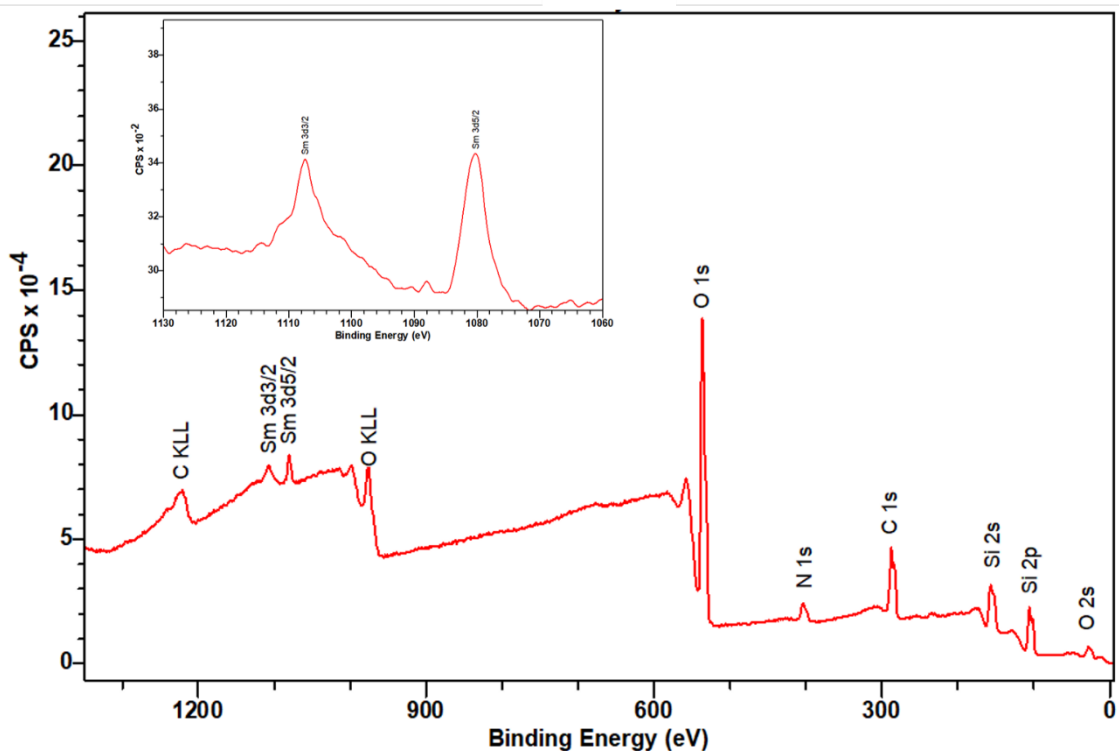


Figure S102. Survey scan XPS spectrum of Sm(1)₃ monolayer LB film. Insert: Enclosed window scan of Sm(III) 3d peaks (a total of 20 scans) with Sm(III) 3d_{3/2} = 1107 and 3d_{5/2} = 1080 eV, expected being 1108 and 1081 eV for Sm(III) respectively.¹²

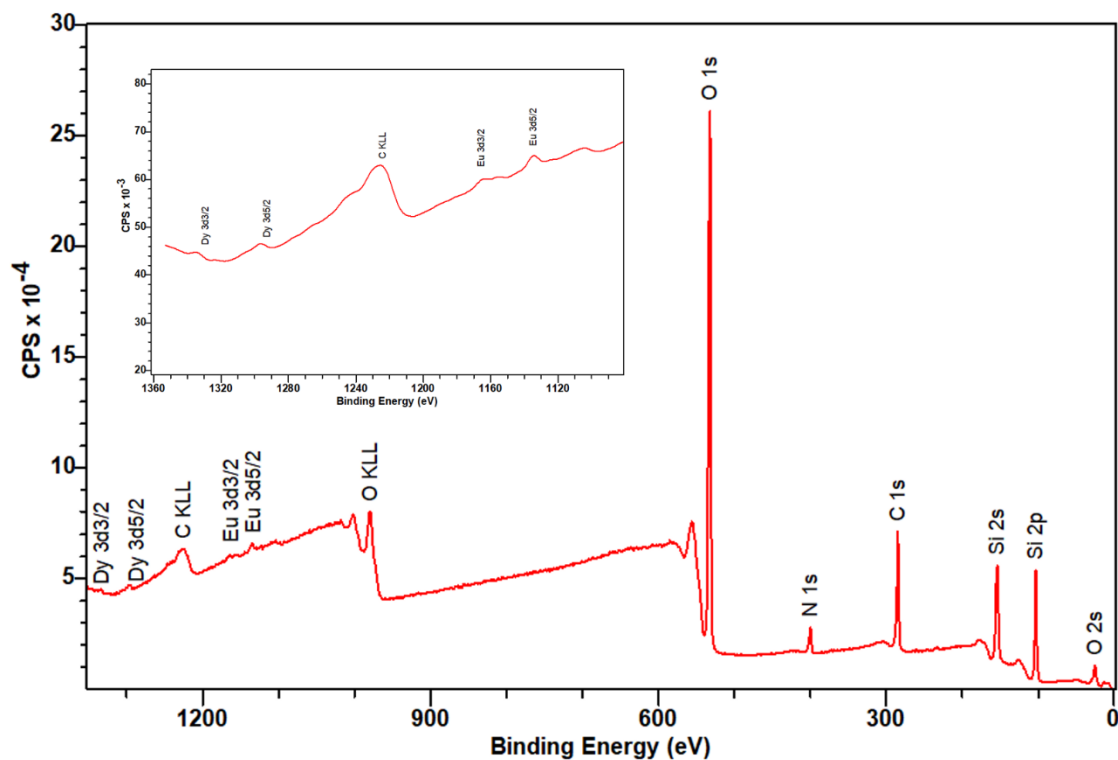


Figure S103. Survey scan XPS spectrum of $\text{Eu}(\mathbf{1})_3:\text{Dy}(\mathbf{1})_3$ (1:1) monolayer LB film. Insert: Smoothed zoomed in of survey scan of $\text{Eu}(\text{III})$ and $\text{Dy}(\text{III})$ 3d peaks, with $\text{Eu}(\text{III})$ $3d_{3/2} = 1165$ and $3d_{5/2} = 1134$ eV, expected being 1136 and 1166 eV for $\text{Eu}(\text{III})$ respectively¹¹ and $\text{Dy}(\text{III})$ $3d_{3/2} = 1334$ and $3d_{5/2} = 1296$ eV, expected being 1333 and 1296 eV for $\text{Dy}(\text{III})$ respectively.^{12,13}

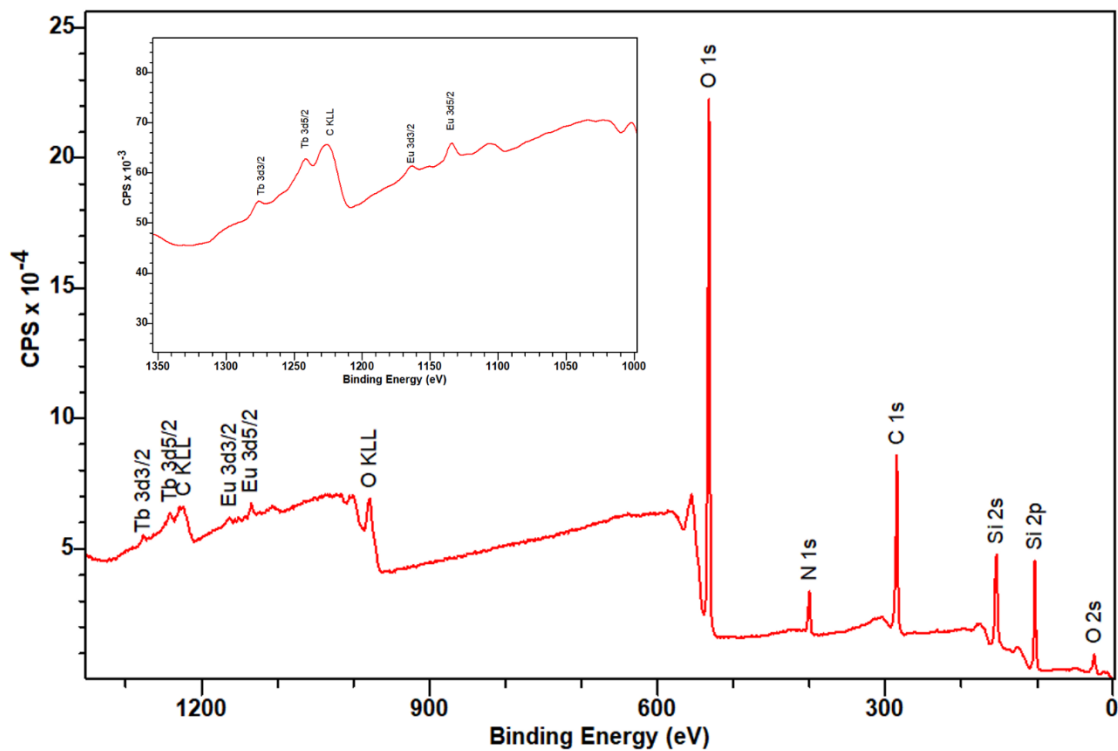


Figure S104. Survey scan XPS spectrum of $\text{Eu}(\mathbf{1})_3:\text{Tb}(\mathbf{1})_3$ (1:1) monolayer LB film. Insert: Smoothed zoomed in of survey scan of $\text{Eu}(\text{III})$ and $\text{Tb}(\text{III})$ 3d peaks, with Eu $3d_{3/2} = 1163$ and $3d_{5/2} = 1135$ eV, expected being 1166 and 1136 eV for $\text{Eu}(\text{III})$ respectively¹¹ and $\text{Tb}(\text{III})$ $3d_{3/2} = 1177$ and $3d_{5/2} = 1141$ eV, expected being 1176 and 1141 eV for $\text{Tb}(\text{III})$ respectively.¹²

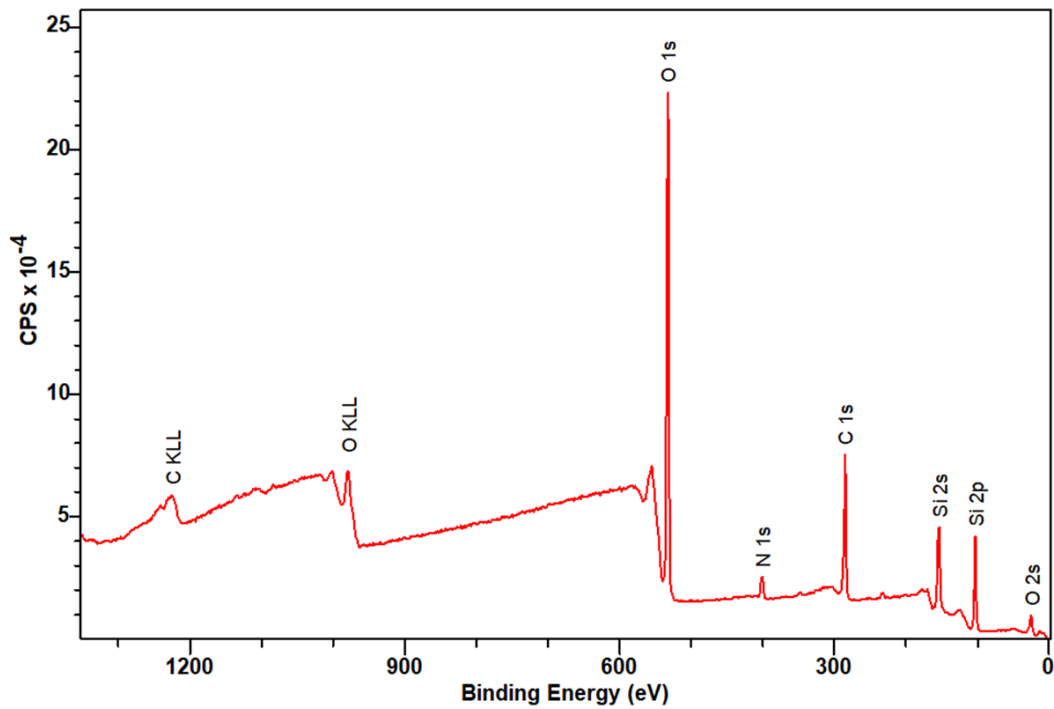


Figure S105. Survey scan XPS spectrum of $\text{Eu}(1)_3:\text{Tb}(1)_3:\text{Dy}(1)_3:\text{Sm}(1)_3$ (1:1:1:1) monolayer LB film.

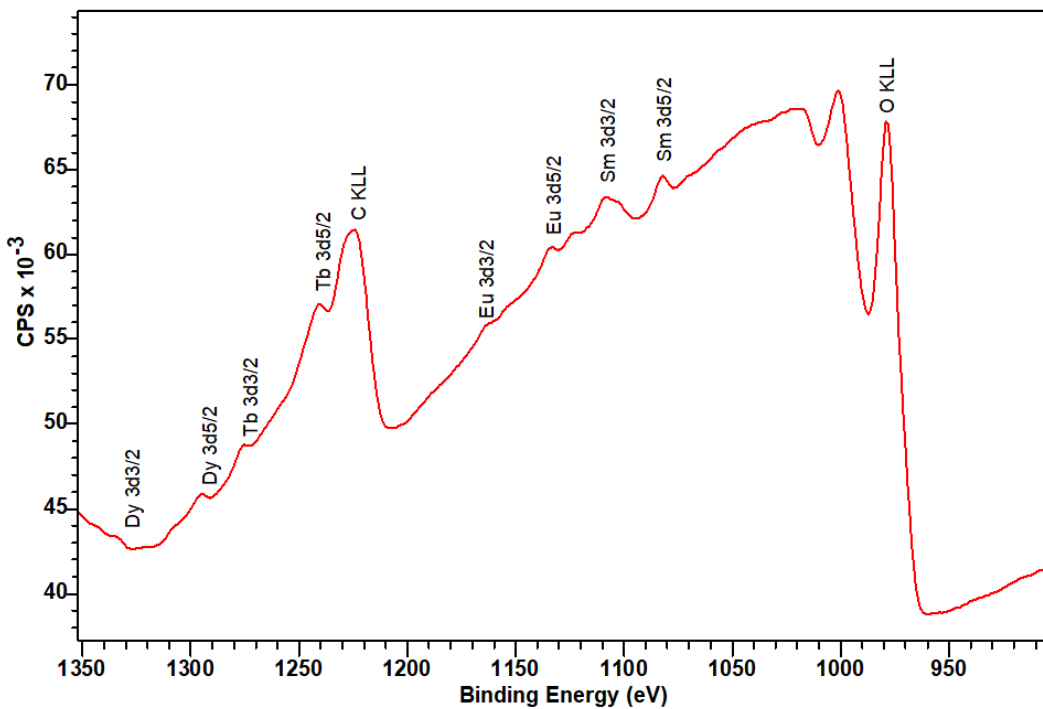


Figure S106. Enclosed window scan of $\text{Eu}(1)_3:\text{Tb}(1)_3:\text{Dy}(1)_3:\text{Sm}(1)_3$ (1:1:1:1) monolayer LB film (a total of 10 scans). With $\text{Eu(III)} 3d_{3/2} = 1164$ and $3d_{5/2} = 1134$ eV, expected being 1136 and 1166 eV for Eu(III) respectively¹¹, $\text{Tb(III)} 3d_{3/2} = 1175$ and $3d_{5/2} = 1141$ eV, expected being 1176 and 1141 eV for Tb(III) respectively, $\text{Dy(III)} 3d_{3/2} = 1334$ and $3d_{5/2} = 1295$ eV, expected being 1333 and 1296 eV for Dy(III) respectively^{12,13} and with $\text{Sm(III)} 3d_{3/2} = 1108$ and $3d_{5/2} = 1082$ eV, expected being 1108 and 1281 eV for Sm(III) respectively.¹²

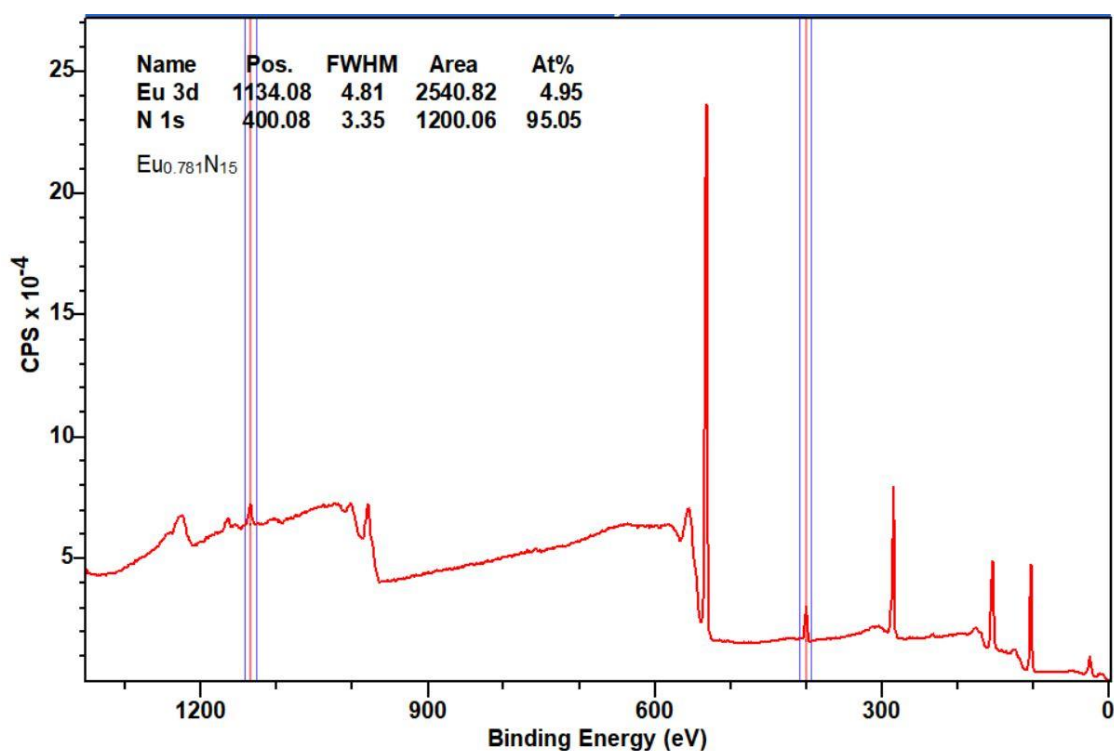


Figure S107. Survey scan XPS spectrum of Eu(1)₃ monolayer LB film, with ratios of N to Eu³⁺ compared, showing a close to 1:15 Eu³⁺:N ratio as expected for the 1:3 metal to ligand complex Eu(C₂₆H₄₀N₅O₉)₃.

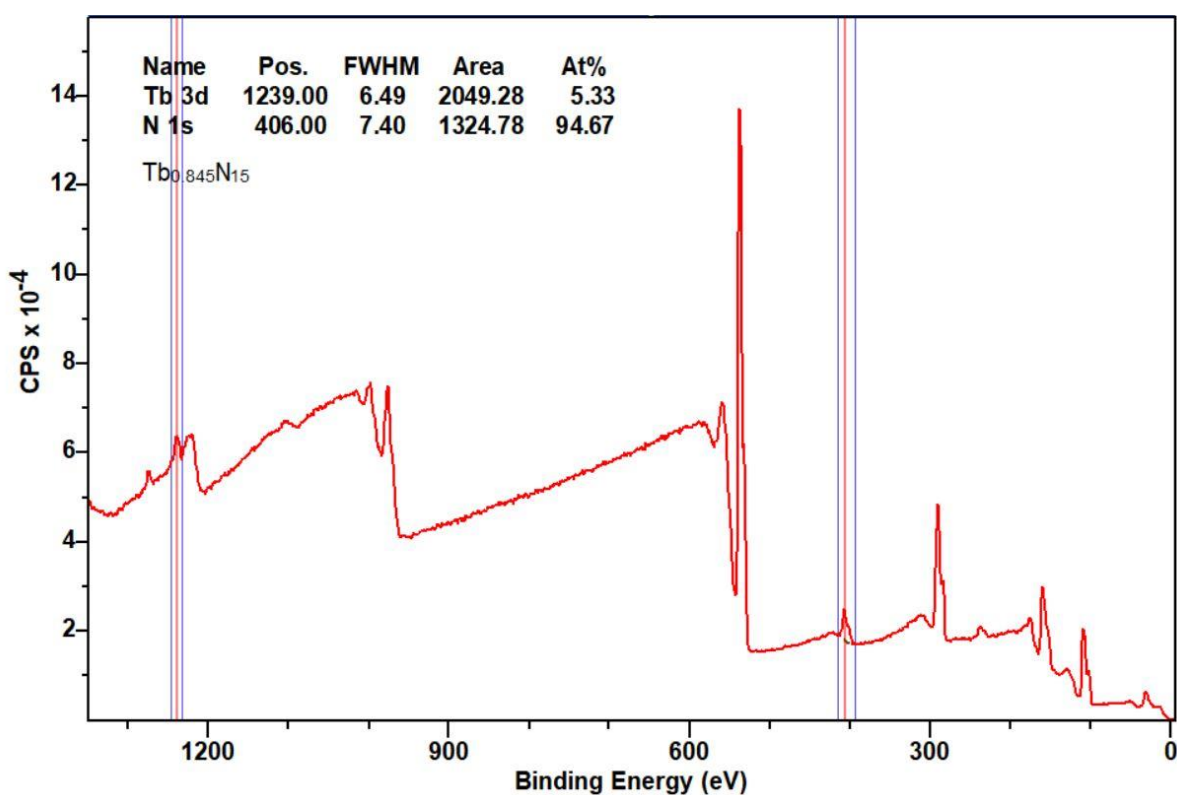


Figure S108. Survey scan XPS spectrum of Tb(1)₃ monolayer LB film, with ratios of N to Tb³⁺ compared, showing a close to 1:15 Tb³⁺:N ratio, as expected for the 1:3 metal to ligand complex Tb(C₂₆H₄₀N₅O₉)₃.

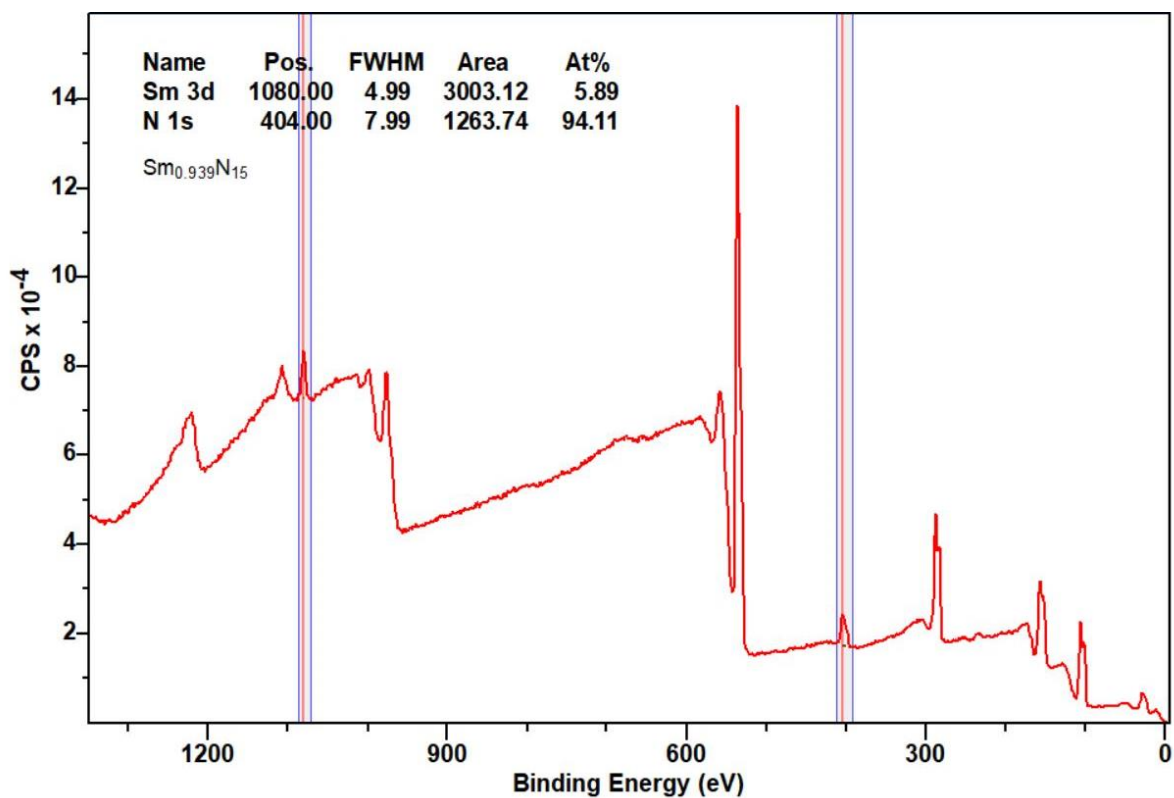


Figure S109. Survey scan XPS spectrum of $\text{Sm}(\mathbf{1})_3$ monolayer LB film, with ratios of N to Sm^{3+} compared, showing a close to 1:15 Tb^{3+} :N ratio, as expected for the 1:3 metal to ligand complex $\text{Sm}(\text{C}_{26}\text{H}_{40}\text{N}_5\text{O}_9)_3$.

Reference

1. Coles, S.J.; Gale, P.A. *Chem. Sci.* 2012, **3**, 683-689.
2. Sheldrick, G. *Sect. A.* 2008, **64**, 112-122.
3. Dolomanov, O.V.; Bourhis, L.J.; Gildea, R.J.; Howard, J.A.K.; Puschmann, H. *J. Appl. Crystallogr* 2009, **42**, 339-341.
4. Rafi, A.A.; Ibrahim, I.; Córdova, A.. *Sci Rep.* 2020, **10**, (1), 20547.
5. J. D. Crowley, P. H. Bandeen and L. R. Hanton, *Polyhedron*, 2010, **29**, 70-83.
6. LED ColourCalculator (7.77), OSRAM SYLVANIA
7. Crosby, G. A.; Demas, J. N., *J. Phys. Chemn.* 1971, **75**, 991-1024.
8. Chauvin, A. S.; Gummy, F.; Imbert, D.; Bünzli, J. C. G. *Spectroscop Lett.* 2004, **37**, 517-532.
9. Erratum. *Spectroscop Lett.* 2007, **40**, 193-193
10. *ReactLab™ EQUILIBRIA*, Jplus consulting multivariate analytical technologies.
11. Myhre, K.; Meyer, H.; Du, M. *Surf. Sci. Spectra.* 2016, **23**, (2), 102-111.
12. J. F. Moulder and J. Chastain, *Handbook of X-ray Photoelectron Spectroscopy: A Reference Book of Standard Spectra for Identification and Interpretation of XPS Data*, Physical Electronics Division, Perkin-Elmer Corporation, 1992.
13. A. Kurachi, M. Matsumiya, K. Tsunashima and S. Kodama, *J. Appl. Electrochem.*, 2012, **42**, 961-968.